

UC Irvine

UC Irvine Previously Published Works

Title

The contribution of global aviation to anthropogenic climate forcing for 2000 to 2018

Permalink

<https://escholarship.org/uc/item/7gh3p3z1>

Authors

Lee, DS
Fahey, DW
Skowron, A
et al.

Publication Date

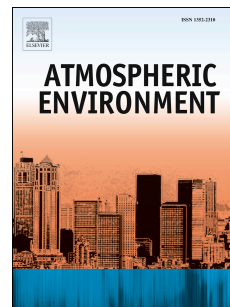
2021

DOI

10.1016/j.atmosenv.2020.117834

Peer reviewed

Journal Pre-proof



The contribution of global aviation to anthropogenic climate forcing for 2000 to 2018

D.S. Lee, D.W. Fahey, A. Skowron, M.R. Allen, U. Burkhardt, Q. Chen, S.J. Doherty, S. Freeman, P.M. Forster, J. Fuglestedt, A. Gettelman, R.R. De León, L.L. Lim, M.T. Lund, R.J. Millar, B. Owen, J.E. Penner, G. Pitari, M.J. Prather, R. Sausen, L.J. Wilcox

PII: S1352-2310(20)30568-9

DOI: <https://doi.org/10.1016/j.atmosenv.2020.117834>

Reference: AEA 117834

To appear in: *Atmospheric Environment*

Received Date: 9 February 2020

Revised Date: 2 July 2020

Accepted Date: 30 July 2020

Please cite this article as: Lee, D.S., Fahey, D.W., Skowron, A., Allen, M.R., Burkhardt, U., Chen, Q., Doherty, S.J., Freeman, S., Forster, P.M., Fuglestedt, J., Gettelman, A., De León, R.R., Lim, L.L., Lund, M.T., Millar, R.J., Owen, B., Penner, J.E., Pitari, G., Prather, M.J., Sausen, R., Wilcox, L.J., The contribution of global aviation to anthropogenic climate forcing for 2000 to 2018, *Atmospheric Environment* (2020), doi: <https://doi.org/10.1016/j.atmosenv.2020.117834>.

This is a PDF file of an article that has undergone enhancements after acceptance, such as the addition of a cover page and metadata, and formatting for readability, but it is not yet the definitive version of record. This version will undergo additional copyediting, typesetting and review before it is published in its final form, but we are providing this version to give early visibility of the article. Please note that, during the production process, errors may be discovered which could affect the content, and all legal disclaimers that apply to the journal pertain.

© 2020 Published by Elsevier Ltd.

Author Contributions

D. S. Lee, D. W. Fahey

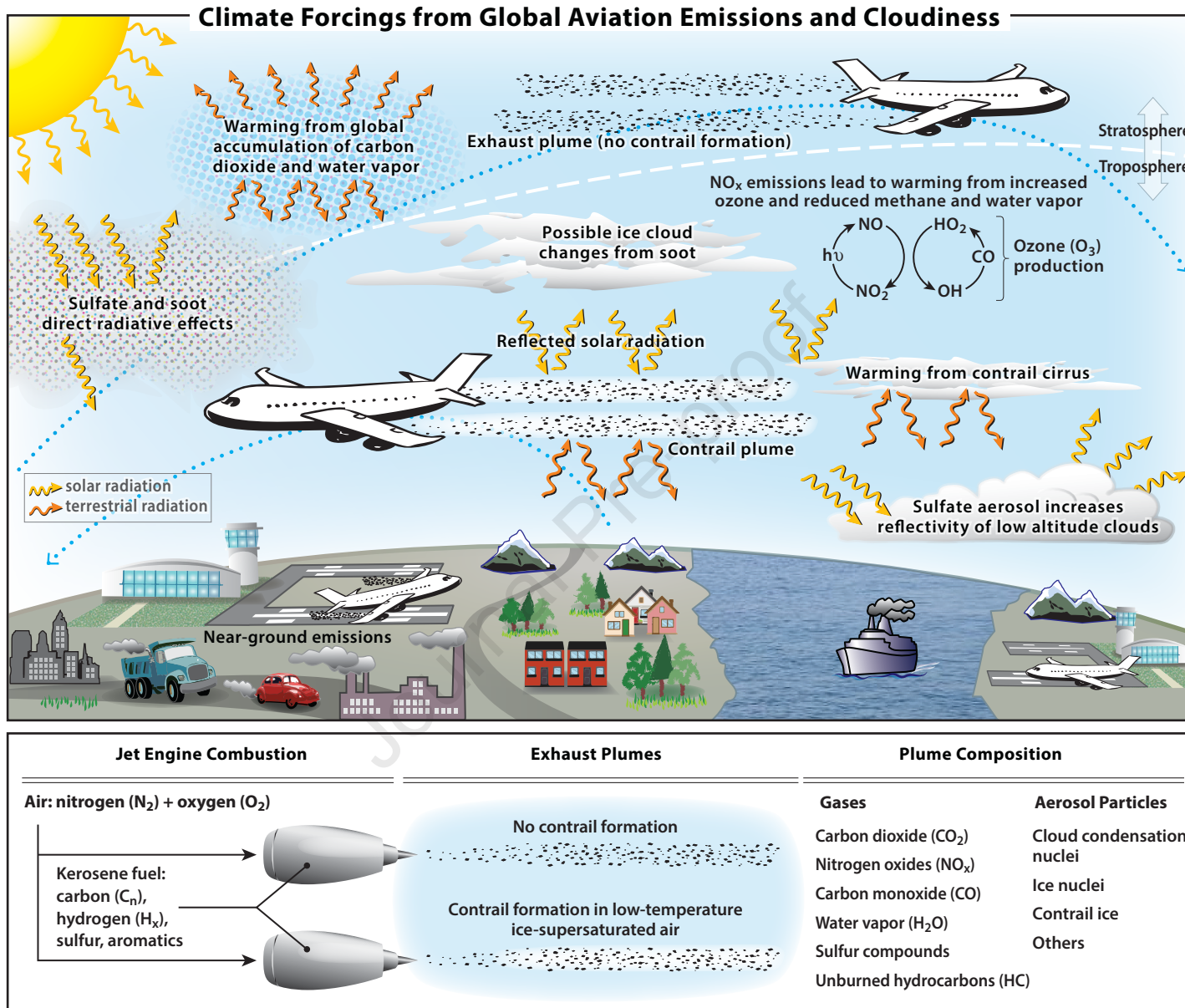
Role: Investigation, Methodology, Writing–review & editing, Data curation; Formal analysis, Project administration, Supervision

A. Skowron

Role: Investigation, Methodology, Writing–review & editing, Data curation, Formal analysis; Software

M. R. Allen, U. Burkhardt, Q. Chen, S. J. Doherty, S. Freeman, P.M. Forster, J. Fuglestedt, A. Gettelman, R. R. De León, L. L. Lim, M. T. Lund, R. J. Millar, B. Owen, J. E. Penner, G. Pitari, M. J. Prather, R. Sausen, L. J. Wilcox

Role: Writing–review & editing, Investigation, Methodology, Writing–original draft, Data curation; Formal analysis;



1 July 2020 Revised

1 The contribution of global aviation to anthropogenic climate forcing for 2000 to
2 2018

3
4 D. S. Lee^{a,1}, D. W. Fahey^b, A. Skowron^a, M. R. Allen^{c,n}, U. Burkhardt^d, Q. Chen^e, S. J. Doherty^f, S.
5 Freeman^a, P.M. Forster^g, J. Fuglested^h, A. Gettelmanⁱ, R. R. De León^a, L. L. Lim^a, M. T. Lund^h, R. J.
6 Millar^{c,o}, B. Owen^a, J. E. Penner^j, G. Pitari^l, M. J. Prather^k, R. Sausen^d, L. J. Wilcox^m

7
8 ^aFaculty of Science and Engineering, Manchester Metropolitan University, John Dalton Building, Chester Street,
9 Manchester M1 5GD, United Kingdom;

10 ^bNOAA Chemical Sciences Laboratory (CSL), Boulder, CO USA;

11 ^cSchool of Geography and the Environment, University of Oxford, Oxford, UK;

12 ^dDeutsches Zentrum für Luft- und Raumfahrt (DLR), Institut für Physik der Atmosphäre, Oberpfaffenhofen,
13 Germany;

14 ^eState Key Joint Laboratory of Environmental Simulation and Pollution Control, College of Environmental Sciences
15 and Engineering, Peking University, Beijing 100871, China;

16 ^fCooperative Institute for Research in Environmental Sciences (CIRES), University of Colorado, Boulder, CO,
17 USA;

18 ^gSchool of Earth and Environment, University of Leeds, Leeds LS2 9JT, United Kingdom;

19 ^hCICERO—Center for International Climate Research—Oslo, PO Box 1129, Blindern, 0318 Oslo, Norway;

20 ⁱNational Center for Atmospheric Research, Boulder, CO, USA;

21 ^jDepartment of Climate and Space Sciences and Engineering, University of Michigan, 2455 Hayward St., Ann
22 Arbor, MI 48109-2143, USA;

23 ^kDepartment of Earth System Science, University of California, Irvine, 3329 Croul Hall, CA 92697-3100, USA;

24 ^lDepartment of Physical and Chemical Sciences, Università dell'Aquila, Via Vetoio, 67100 L'Aquila, Italy;

25 ^mNational Centre for Atmospheric Science, Department of Meteorology, University of Reading, Earley Gate,
26 Reading RG6 6BB, UK;

27 ⁿ also at the Department of Physics, University of Oxford, Oxford, UK;

28 ^o also at the Committee on Climate Change, 151 Buckingham Palace Road, London, SW1W 9SZ, UK.

29
30 ¹To whom correspondence should be addressed. Email: d.s.lee@mmu.ac.uk Tel: +44 161 247 3663

31

32 **Highlights**

- 33 • Global aviation warms Earth's surface through both CO₂ and net non-CO₂ contributions.
- 34 • Global aviation contributes a few percent to anthropogenic radiative forcing.
- 35 • Non-CO₂ impacts comprise about 2/3 of the net radiative forcing.
- 36 • Comprehensive and quantitative calculations of aviation effects are presented.
- 37 • Data are made available to analyze past, present and future aviation climate forcing.

39 **Abstract**

40 Global aviation operations contribute to anthropogenic climate change via a complex set of processes that
41 lead to a net surface warming. Of importance are aviation emissions of carbon dioxide (CO₂), nitrogen
42 oxides (NO_x), water vapor, soot and sulfate aerosols, and increased cloudiness due to contrail formation.
43 Aviation grew strongly over the past decades (1960–2018) in terms of activity, with revenue passenger
44 kilometers increasing from 109 to 8269 billion km yr⁻¹, and in terms of climate change impacts, with CO₂
45 emissions increasing by a factor of 6.8 to 1034 Tg CO₂ yr⁻¹. Over the period 2013–2018, the growth rates
46 in both terms show a marked increase. Here, we present a new comprehensive and quantitative approach
47 for evaluating aviation climate forcing terms. Both radiative forcing (RF) and effective radiative forcing
48 (ERF) terms and their sums are calculated for the years 2000 to 2018. Contrail cirrus, consisting of linear
49 contrails and the cirrus cloudiness arising from them, yields the largest positive net (warming) ERF term
50 followed by CO₂ and NO_x emissions. The formation and emission of sulfate aerosol yields a negative
51 (cooling) term. The mean contrail cirrus ERF/RF ratio of 0.42 indicates that contrail cirrus is less
52 effective in surface warming than other terms. For 2018 the net aviation ERF is +100.9 milliwatts (mW)
53 m⁻² (5–95% likelihood range of (55, 145)) with major contributions from contrail cirrus (57.4 mW m⁻²),
54 CO₂ (34.3 mW m⁻²), and NO_x (17.5 mW m⁻²). Non-CO₂ terms sum to yield a net positive (warming) ERF
55 that accounts for more than half (66%) of the aviation net ERF in 2018. Using normalization to aviation
56 fuel use, the contribution of global aviation in 2011 was calculated to be 3.5 (4.0, 3.4) % of the net
57 anthropogenic ERF of 2290 (1130, 3330) mW m⁻². Uncertainty distributions (5%, 95%) show that non-
58 CO₂ forcing terms contribute about 8 times more than CO₂ to the uncertainty in the aviation net ERF in
59 2018. The best estimates of the ERFs from aviation aerosol-cloud interactions for soot and sulfate remain
60 undetermined. CO₂-warming-equivalent emissions based on global warming potentials (GWP* method)
61 indicate that aviation emissions are currently warming the climate at approximately three times the rate of
62 that associated with aviation CO₂ emissions alone. CO₂ and NO_x aviation emissions and cloud effects
63 remain a continued focus of anthropogenic climate change research and policy discussions.

64 **Key words:** | aviation | contrail cirrus | climate | radiative forcing | CO₂ | NO_x |

65 **Dedication:** This paper is dedicated to the memory of Professor Ivar S. A. Isaksen of the University of
66 Oslo, whose scientific excellence, friendship, and mentorship is sorely missed.

68 **1. Introduction**

69 Aviation is one of the most important global economic activities in the modern world. Aviation emissions
70 of CO₂ and non-CO₂ aviation effects result in changes to the climate system (**Figure 1**). Both aviation
71 CO₂ and the sum of quantified non-CO₂ contributions lead to surface warming. The largest contribution to
72 anthropogenic climate change across all economic sectors comes from the increase in CO₂ concentration,
73 which is the primary cause of observed global warming in recent decades (IPCC, 2013; 2018). Aviation
74 contributions involve a range of atmospheric physical processes, including plume dynamics, chemical
75 transformations, microphysics, radiation, and transport. Aggregating these processes to calculate changes
76 in a greenhouse gas component or a cloud radiative effect is a complex challenge for contemporary

1 July 2020 Revised

77 atmospheric modeling systems. Given the dependence of aviation on burning fossil fuel, its significant
78 CO₂ and non-CO₂ effects, and the projected fleet growth, it is vital to understand the scale of aviation's
79 impact on present-day climate forcing.

80 Historically, estimating aviation non-CO₂ effects has been particularly challenging. The primary
81 (quantified) non-CO₂ effects result from the emissions of NO_x, along with water vapor and soot that can
82 result in contrail formation. Aviation aerosols are small particles composed of soot (black and organic
83 carbon (BC/OC)) and sulfur (S) and nitrogen (N) compounds. The largest positive (warming) climate
84 forcings adding to that of CO₂ are those from contrail cirrus and from NO_x-driven changes in the chemical
85 composition of the atmosphere (Lee et al., 2009 (L09)). L09 estimated that in 2005, aviation CO₂
86 radiative forcing (RF (Wm⁻²)) was 1.59% of total anthropogenic CO₂ RF and that the sum of aviation CO₂
87 and non-CO₂ effects contributed about 5% of the overall net anthropogenic forcing.

88 Understanding of aviation's impacts on the climate system has improved over the decade since the last
89 comprehensive evaluation (L09), but remains incomplete. Published studies of aviation contributions to
90 climate change generally focus on one or a few ERF terms. For example, about 20 studies are cited here
91 that quantify the contribution from global NO_x emissions. In contrast, only a few studies have addressed
92 the net RF from global aviation (IPCC, 1999; Sausen et al., 2005; L09). A more recent study updated
93 some aviation terms without providing a net RF (Brasseur et al., 2016). Here, a comprehensive analysis of
94 individual aviation ERFs is undertaken in order to provide an overall ERF for global aviation, along with
95 the associated uncertainties, which is an analysis unavailable elsewhere. This step updates and improves
96 the analysis of L09. Best estimates of individual aviation ERF terms are derived here for the first time and
97 combined to provide a net ERF for global aviation. Quantifying the terms required new analyses of CO₂
98 and NO_x ERFs and recalibration of other individual ERFs accounting for factors not previously applied in
99 a common framework.

100 In L09, the net RF was calculated with and without the full contrail cirrus term but including an estimate
101 for linear contrails. The exclusion was based on the lack of a best estimate derived from existing studies.
102 At that time radiative forcing estimates were limited to linear or line-shaped contrails since the modelling
103 approaches required scaling contrail formation frequency to observed coverage and only satellite
104 observations of linear contrails existed (Burkhardt et al., 2010). The contrail cirrus term requires the
105 simulation of the whole contrail cirrus life cycle, starting from persistent linear contrails which spread and
106 often become later indistinguishable from natural cirrus. Persistent contrail formation requires ice-
107 supersaturated conditions along a flight track, which are variable in space and time in the troposphere and
108 tropopause region (Irvine et al., 2013). Estimating the RF from contrail cirrus requires knowledge of
109 complex microphysical processes, radiative transfer, and the interaction with background cloudiness
110 (Burkhardt et al., 2010). Contrail cirrus forcing dominates that of persistent linear contrails with the latter
111 on the order of 10% of the combined forcing (Burkhardt and Kärcher, 2011). In the present study, we
112 present a best estimate and uncertainty based on the results from global climate models employing
113 process-based contrail cirrus parameterizations.

114 Emissions of NO_x from aviation lead to photochemical changes that increase global ozone (O₃) formation
115 while decreasing the lifetime and abundance of methane (CH₄). The changes result in positive and
116 negative (cooling) RF contributions, respectively. Since L09, improved understanding and modeling
117 capabilities have emerged, as well as additional RF terms in response to NO_x emissions, namely a longer-
118 term decrease in background O₃ and a reduction in H₂O in the stratosphere in response to decreased CH₄.
119 Here, model results are used to calculate the additional RF terms, and to incorporate the updated CH₄
120 forcing as assessed by Etminan et al. (2016) and the equilibrium-to-transient corrections for the CH₄ term
121 (see A4). Finally, aviation-specific efficacies (Appendix C) of the individual NO_x components are used to
122 estimate a net NO_x ERF for the first time.

123 L09 includes best estimates for the RFs resulting from the aerosol-radiation interactions (previously
124 called direct effects) of soot and sulfate aerosols from aviation. However, no best estimates of RFs from
125 aerosol-cloud interactions (previously called indirect effects) were available in 2009. Subsequent studies
126 discussed here have yet to provide a basis for best estimates of ERFs from aviation aerosol-cloud
127 interactions that may be significant.

128 The primary motivations for the present study are to provide an updated, comprehensive evaluation of
129 aviation climate forcings in terms of RF and ERF based on new calculations and the normalization of
130 values from published modeling studies, and to combine the resulting best estimates via a Monte-Carlo
131 analysis to yield a best estimate for the net ERF for global aviation for the years 2000 to 2018. The three
132 years 2018, 2011, and 2005 are notable because the year 2018 is the latest year for which air traffic and
133 fuel use datasets are available, 2011 is the most recent year evaluated for net anthropogenic climate
134 forcing by the IPCC (IPCC, 2013), and 2005 is the year evaluated in the latest comprehensive aviation
135 and climate evaluation (L09). By normalizing the calculations across these years, more specific and self-
136 consistent comparisons can be made of the changes in aviation contributions over time. The normalization
137 step requires addressing in each study, for example, the choice of air traffic inventory, the integration of
138 emissions along flight tracks, and the assumed jet-engine emission indices. The new best estimates of
139 aviation ERF, for example, show that the 2018 value is about 48% larger than the updated 2005 value.

140 In general, previous global aviation climate assessments have made different assumptions concerning
141 emissions, cloudiness effects, and aviation operations (e.g., IPCC, 1999). Here, our self-consistent set of
142 component and net aviation ERFs for 2000 to 2018 allows historical and scenario projections of aviation
143 climate impacts to be assessed in context with other sectors, such as maritime shipping, ground
144 transportation and energy generation. This updated understanding is especially important given the
145 potential role of international aviation in meeting the goals of the Paris Agreement (Section 2) on limiting
146 future temperature increases.

147 The remaining sections address global aviation growth statistics (Section 2); a brief summary of methods
148 used in the analysis (Section 3); results for the ERF estimates of CO₂, NO_x, water vapor, contrail cirrus,
149 and aerosol-radiation and aerosol-cloud interactions with soot and sulfate (Section 4); results for the net
150 ERF of global aviation (Section 5); emission metrics (Section 6); and aviation CO₂ vs non-CO₂ forcings
151 (Section 7). The appendices contain additional detailed information on trends in aviation emissions (App.
152 A); aviation CO₂ radiative forcing calculations (App. B); radiative forcing, efficacy and ERF definitions
153 (App. C); aviation NO_x RF calculations (App. D); contrail cirrus RF scaling factors and uncertainty (App.
154 E); and emission equivalency metric calculations (App. F). A Supplemental Data (SD) file is provided
155 containing the interactive spreadsheet used to calculate RFs and ERFs for each aviation term.

156 2. Global aviation growth

157 Global aviation fuel use and CO₂ emissions have increased in the last four decades with large growth
158 occurring in Asia and other developing regions due to the rapid expansion of civil aviation (**Figure 2** and
159 Appendix A). Looking forward, this pattern of growth is expected to be maintained—for example, of the
160 1229 orders of Airbus and 1031 orders of Boeing in 2017, 20.3% and 37.5%, respectively, are for airlines
161 in the Asia region (Airbus, 2017; Boeing, 2018). Airbus projects 41% of orders over the next two decades
162 to be from the Asia-Pacific region (Airbus, 2017). The uncertainty in this expectation has increased due to
163 the slowdown in aviation operations in the early months of 2020 due to the COVID-19 pandemic (Le
164 Quéré et al., 2020). Annual aviation emissions in 2020 are now expected to be below recent projections
165 that are based on historical growth.

166 A striking feature of **Figure 2a** is the sustained multi-decade growth in CO₂ emissions; the average rate
167 for the period 1960–2018 is 15 Tg CO₂ yr⁻¹. The growth rate for 2013 through 2018 is much larger (44 Tg
168 CO₂ yr⁻¹). The annually averaged growth rate over the period 1970 to 2012 is 2.2% yr⁻¹ and for 2013 to
169 2018 is 5% yr⁻¹ (increase of 27%). In 2018, global aviation CO₂ emissions exceeded 1000 million tonnes

170 per year for the first time (see methodology for scaling 2016 IEA data in Appendix A). The cumulative
171 emissions of global aviation (1940 to 2018) are 32.6 billion (10^9) tonnes of CO₂, of which approximately
172 50% were emitted in the last 20 years. Current (2018) CO₂ emissions from aviation represent
173 approximately 2.4% of anthropogenic emissions of CO₂ (including land use change) (**Figure 2c**).

174 Aviation has grown strongly over time (**Figure 2b**) in terms of available seat kilometers (ASK, a measure
175 of capacity) and revenue passenger kilometers (RPK, a measure of transport work). Fuel usage and hence
176 CO₂ emissions have grown at a lesser rate than RPK, reflecting increases in aircraft efficiency derived
177 from changes in technology, larger average aircraft sizes and increased passenger load factor. Aviation
178 transport efficiency has improved by approximately eightfold since 1960, to 125 gCO₂ (RPK)⁻¹.

179 At present and for some considerable time into the future, aviation growth is likely to be largely
180 dependent upon the combustion of kerosene fossil fuel (Jet A-1/A) (OECD, 2012), resulting in emission
181 of CO₂. Renewable biofuels partially offset fossil fuel emissions but these have yet to be produced in
182 sufficient quantities to offset growth of fossil fuel use. Furthermore, considerable uncertainties remain
183 regarding the life-cycle emissions of biofuels, which determine the reductions in net CO₂ emissions (e.g.,
184 Hari et al., 2015). There are current regulations regarding aviation emissions of CO₂, NO_x, and soot mass
185 and number based on decisions by the International Civil Aviation Organization (ICAO). Under the 2016
186 Paris climate agreement, nations are committing to limiting future increases in global temperatures with
187 Nationally Determined Contributions (NDCs) (UNFCCC). Whereas domestic aviation CO₂ emissions are
188 included in the NDCs, CO₂ emissions from international aviation are not mentioned in the agreement. It
189 remains open as to whether emissions from international aviation or global emissions beyond greenhouse
190 gases (e.g., short-lived (non-CO₂) climate forcers) will be included in future international agreements.

191 **3. Methods**

192 The methodologies used to calculate ERF and RF for individual aviation terms are described in this
193 section, and results of these calculations are given in Section 4. Common to the methodologies is a
194 comprehensive multi-page spreadsheet (see SD) that begins with a user's guide. The spreadsheet pages
195 include those for contrail cirrus, CO₂, NO_x, H₂O, and sulfate and soot aerosol, along with CO₂-equivalent
196 metrics, ERF probability distributions, ERF time series, and estimates of forcings from aerosol-cloud
197 effects. The spreadsheet displays the results of aviation forcings provided by individual published studies.
198 ERF and RF values were calculated for 2018 and other years based on the normalized values of ERF or
199 RF per unit emission or distance, choice of appropriate emission indices, and times series data on fuel use
200 and distance travelled. In the case of the contrail cirrus forcing, the flight-track distance was chosen as the
201 proxy over fuel usage. Annual global emissions are derived from fuel burn by multiplying by the average
202 emission indices (**Table 1**). The combined and normalized results are used to create sets of RF and ERF
203 aviation terms for the years 2000 to 2018. In addition to facilitating the present study, the spreadsheet also
204 provides a quantitative framework for follow-on analyses.

205 Calculations of radiative forcing are expanded here beyond the approach in L09 to include ERF values in
206 addition to the traditional RF values (**Tables 2 and 3 and Figure 3**). The distinction between ERF and
207 RF is presented in Appendix C. ERF is the preferred metric for comparing the expected impacts of
208 climate forcing terms (Myhre et al., 2013). Its use derives from the stronger correlation between ERF and
209 the change in the equilibrium global-mean surface temperature for some forcing agents than for the
210 corresponding RF. ERF is calculated as the change in net top-of-the-atmosphere (TOA) downward
211 radiative flux after allowing for rapid adjustments in atmospheric temperatures, water vapor and clouds
212 with globally-averaged sea surface and/or land surface temperatures unchanged. ERF is preferred over RF
213 estimates because the imposed forcing and rapid responses to the forcing cannot always be separately
214 evaluated, especially for aerosols. In general, the largest differences between ERF and RF are expected
215 for aerosol-cloud interactions and contrail cirrus (Myhre et al., 2013; Boucher et al., 2013). In calculating
216 ERF values for 2000-2018, the ERF/RF ratio is assumed to be constant with time.

217 Most of the results for the non-CO₂ terms have associated statistics from which the median was chosen as
218 the best estimate, including the net aviation ERF and RF, and the net non-CO₂ ERF and RF. For CO₂ and
219 contrail cirrus, for which the sample sizes are small (3, in both cases), the mean was used as the best
220 estimate. The best estimates of the non-CO₂ terms except contrail cirrus have associated uncertainties
221 expressed as 5% and 95% confidence intervals calculated from 5, 95% percentile statistics. The
222 uncertainty distributions for all forcing terms other than CO₂ and contrail cirrus are lognormal and that for
223 net NO_x has a discrete probability distribution function (PDF). The uncertainties for the ERF and RF of
224 CO₂ were taken from IPCC (2013) and fitted with a Monte Carlo analysis with a normal distribution (see
225 Section 5). The uncertainties for contrail cirrus were estimated partly from expert judgement of the
226 underlying processes, as described in Appendix E, again fitted with a Monte Carlo analysis with a normal
227 distribution.

228 4. Calculations of ERFs for aviation terms

229 4.1. CO₂.

230 The time series of aviation CO₂ emissions is shown in **Figure 2** as derived from combined kerosene and
231 avgas usage (UKDS, 2016). Calculating CO₂ concentrations from emissions requires use of a global
232 carbon-cycle model, which has a range of complexity from a comprehensive Earth system model (ESM)
233 to a simple climate model (SCM), with the latter being based on a box model or impulse response
234 function (IRF) model. Three SCMs were used here: LinClim, an IRF model based on Sausen and
235 Schumann (2000) (Appendix B); the Finite-amplitude Impulse Response (FaIR) model (Millar et al.,
236 2017); and the CICERO-SCM (Fuglestedt and Berntsen, 1999; Skeie et al., 2017). The performance of
237 LinClim and CICERO-SCM with respect to aviation emissions is documented in the multi-model
238 comparison of Khodayari et al. (2013). The CO₂ concentrations attributable to aviation in 2018 based on
239 LinClim, CICERO-SCM and FaIR are 2.9, 2.4 and 2.4 ppm, respectively, with concentrations nearly
240 doubling in the last 20 years (see SD spreadsheet). The ERF/RF ratio for CO₂ is assumed to be unity. The
241 resulting CO₂ ERFs, as derived from global concentrations using standard IPCC expressions (IPCC,
242 2001), are 38.6, 32.0 and 32.4 mW m⁻², respectively. With only three model estimates, the average of 34.3
243 mW m⁻² (5 and 95% percentiles of 29 and 40 mW m⁻²), is chosen as the CO₂ RF best estimate.

244 4.2. NO_x

245 The photochemical effects of aviation NO_x emissions on the atmospheric abundances of O₃, CH₄, carbon
246 monoxide (CO) and reactive hydrogen (HO_x) are well established (Fuglestedt et al., 1999). Earlier
247 studies assessed the short-term increase of O₃ and the longer-term reduction in CH₄ lifetime and
248 abundance, which yield positive and negative RFs, respectively (IPCC, 1999; Sausen et al., 2005). L09
249 introduced the concept of the ‘net NO_x’ effect by combining the two components, extending and updating
250 the study of Sausen et al. (2005). Later studies expanded the analysis of NO_x effects to include the long-
251 term decreases in both O₃ and stratospheric water vapor (SWV) resulting from the CH₄ reduction. Both
252 effects yield negative RFs (Holmes et al., 2011; Myhre et al., 2011). In the present study, an ensemble of
253 20 NO_x studies is assessed to provide NO_x forcing best estimates based on a wide range of global
254 atmospheric chemistry/climate models and a broad range of present-day aviation emission inventories
255 (details in Appendix D and SD spreadsheet). Results from 6 of the studies were adopted from Holmes et
256 al. (2011).

257 The study ensemble represents various model methodologies in calculating and treating both the short-
258 term and the long-term NO_x components. In order to avoid gaps and additional uncertainties, standardized
259 ERFs were developed that estimated disparate elements (e.g., CH₄ mediated decreases in SWV and long-
260 term O₃). Moreover, most of the studies were based upon a parameterization of the CH₄ response that
261 assumed a full equilibrium response. In order to calculate the transient response for a specific year more
262 accurately, a correction factor is needed (Myhre et al., 2011). Here, the CH₄ responses for individual
263 years were calculated (see Appendix D) using the difference between two simulations with differing

1 July 2020 Revised

264 aviation NO_x emissions. A number of transient and equilibrium simulations were conducted with a 2D
265 chemical-transport model to find that the requirement for a correction factor is well supported and that the
266 2018 value is 0.79 (see Transient vs. equilibrium in Appendix D and Appendix Table D.2). In addition, a
267 scaling factor (1.23) is applied to derived CH_4 ERF numbers to account for the effect of shortwave CH_4
268 forcing, following Etminan et al. (2016) (see Appendix D). The existence and nature of correlations
269 between the NO_x RF components were also explored (see Correlations in Appendix D and Appendix
270 Figure D.1) since the degree of correlation between short-term O_3 and CH_4 terms was a source of
271 uncertainty in the calculation of the net- NO_x forcing in L09. The work of Holmes et al. (2011) supports
272 the prior assumption of correlation, which is greatly expanded here. Regardless of inter-model
273 differences, significant correlations are observed; for example, a significant negative correlation ($p = -0.7$)
274 exists between the short-term and the long-term NO_x RF components.

275 The normalized sensitivity results for net NO_x in units of $\text{mW m}^{-2} (\text{Tg (N) yr}^{-1})^{-1}$ for the individual
276 modeling studies are shown in **Figure 4** along with statistical parameters (see Ensemble values in
277 Appendix D). Given the diversity of studies conducted over nearly two decades, the standard deviations
278 of the distributions are reasonably small. In contrast, the sign of the net- NO_x RF obtained from summing
279 over the 4 component values varies from positive to negative. The spread in NO_x RF values is caused by
280 various factors (e.g., emissions inventories, experimental design or inter-model differences) and is
281 particularly sensitive to the NO_x distribution in the model background troposphere (Holmes et al., 2011).
282 The NO_x efficacies are 1.37 for the short-term ozone increases and 1.18 for methane decreases (Ponater et
283 al., 2006). The efficacies do not equal the ERF/RF ratios, in general (Ponater et al., 2020; Appendix C);
284 nonetheless, in the present study, we assume the efficacies and the ERF/RF ratios are equal, in the
285 absence of better information. The factor of 1.18 was similarly adopted for the CH_4 -mediated decreases in
286 long-term ozone and SWV. It is noted that these ratios are from one study and that, in general, the ratio of
287 ERF to RF for CH_4 and tropospheric O_3 are currently the subject of some debate (Smith et al., 2018; Xie
288 et al., 2016; Richardson et al., 2019). Given the strength of the net effect of the ERF adjustment on the net
289 NO_x forcing (more than doubling over its stratosphere-adjusted RF), these ratios warrant further study.

290 The net- NO_x ERF sensitivity of $5.5 \pm 8.1 \text{ mW m}^{-2} (\text{Tg (N) yr}^{-1})^{-1}$ yields a 2018 best estimate of 17.5 (0.6,
291 28.5) mW m^{-2} . This best estimate includes the correction factor for non-steady state conditions as well as
292 the revised formulation of CH_4 RF (Appendix D).

293 Other potential short-term effects from NO_x emissions involve the direct formation of nitrate aerosol and
294 indirect enhancement of sulfate aerosol. These effects, addressed in a few modelling studies, are
295 associated with large uncertainties (Righi et al., 2013; Pitari et al., 2017; Unger, 2011). The effects of
296 NO_x on aerosol abundances are not further considered here owing to the limited number of studies and the
297 large associated uncertainties.

298 *4.3. Water vapor emissions.*

299 A large fraction of annual aircraft emissions from the global fleet occurs in the stratosphere, primarily in
300 the northern hemisphere (Forster et al., 2003). The accumulation of water vapor emissions perturbs the
301 low background humidity in the lower stratosphere and changes the water vapor radiative balance.
302 Calculating the water vapor RF is complicated by the sensitivity to the vertical and horizontal distribution
303 of emissions, seasonal changes in tropopause heights, and short stratospheric residence times. Some
304 earlier studies do not include the water vapor effect.

305 The water vapor effects were explored in detail (see SD) using results from nine studies: IPCC (1999),
306 Marquart et al. 2001, Gauss et al. (2003), Ponater et al. (2006), Frömming et al. (2012), Wilcox et al.
307 (2012), Lim et al. (2015), Pitari et al. (2015) and Brasseur et al. (2016). The reported RFs from these
308 studies vary from 0.4 mW m^{-2} (Wilcox et al., 2012) through 1.5 mW m^{-2} (Frömming et al. 2012, Lim et
309 al., 2015) to 3.0 mW m^{-2} (IPCC, 1999). The differences are attributed to the different transport models
310 used, with some contribution from the different meteorologies in different studies. Normalizing to the

1 July 2020 Revised

311 same emissions and averaging these reported estimates yields a water vapor sensitivity of $0.0052 \pm$
312 $0.0026 \text{ mW m}^{-2} (\text{Tg} (\text{H}_2\text{O}) \text{ yr}^{-1})^{-1}$. Scaling this value linearly to emissions of 382 Tg H_2O yields an ERF
313 best estimate of 2.0 (0.8, 3.2) mW m^{-2} for 2018, which is well within the uncertainty range of the 2005
314 L09 value of 2.8 (0.39, 20.3) mW m^{-2} . The ERF/RF ratio for stratospheric water increases is assumed to
315 be unity. We have greater confidence in the new estimate and its smaller uncertainty since it is based on
316 detailed physical studies, rather than a scaling of the earlier IPCC (1999) estimate. The new best estimate
317 is also in good agreement with the earlier results of Gauss et al. (2003) and Ponater et al. (2006), after
318 scaling their results to account for emissions differences.

319 4.4. Contrail cirrus.

320 The aviation fleet increases global cloudiness through the formation of persistent contrails when the
321 ambient atmosphere is supersaturated with respect to ice (IPCC, 1999). Contrail cirrus, consisting of
322 linear contrails and the cirrus cloudiness arising from them, have cooling (short-wave) and warming
323 (long-wave) effects, with the effect at night being exclusively warming. In past assessments (e.g., IPCC,
324 1999; L09), a best estimate was only available for the RF of linear persistent contrails, in part because of
325 the difficulty of quantifying the cloudiness contribution of aging and spreading contrails (Minnis et al.,
326 2013). The ERF of contrail cirrus was estimated for 2011 as 50 (20, 150) mW m^{-2} by Boucher et al.
327 (2013). Results of a recent assessment of contrail cirrus and other aviation effects are included here,
328 although the study did not propose new best estimates (Brasseur et al., 2016).

329 A persistent contrail requires ice-supersaturated conditions along the flight track. Contrail cirrus life
330 cycles are dependent on the temporal and spatial scales of the ice supersaturated areas, which are highly
331 variable in the troposphere and tropopause region (e.g., Lamquin et al., 2012; Irvine et al., 2013; Bier et
332 al., 2017). Estimating the impact of contrail cirrus on upper tropospheric cloudiness requires the
333 simulation of complex microphysical processes, contrail spreading, overlap with natural clouds, radiative
334 transfer, and the interaction with background cloudiness (Burkhardt et al., 2010). We present new best
335 estimates based on the results of global climate models employing process-based contrail cirrus
336 parameterizations (Appendix E). Due to the small number of independent estimates the uncertainty must
337 be estimated from the sensitivities of the respective processes and the uncertainty in the underlying
338 parameters and fields.

339 Here, we consider RF and ERF estimates from global climate models (Burkhardt and Kärcher, 2011;
340 Bock and Burkhardt, 2016; Chen and Gettelman, 2013; Schumann et al., 2015; Bickel et al., 2019) to
341 ultimately produce an ERF best estimate. For the present study, the Chen and Gettelman study was
342 repeated with lower prescribed initial ice-crystal diameters, thereby bringing assumptions in line with
343 measurements (e.g., Schumann et al., 2017a). Since the RF estimates differ regarding the air traffic
344 inventory, the measure of air traffic distance (i.e., taking only surface-projected or overall flight distances
345 into account) and the temporal resolution of the air traffic data, the estimates were homogenized using
346 known sensitivities (Bock and Burkhardt, 2016) (see Appendix E). Furthermore, the estimates were
347 corrected to account for the underestimation of the contrail cirrus RF, as calculated by climate models that
348 use frequency bands, relative to more detailed line-by-line radiative transfer calculations (Myhre et al.,
349 2009). The Chen and Gettelman (2013) study is closer to a calculation of an ERF, since it accounts for
350 fast feedbacks on natural clouds, which Bickel et al. (2019) show in their model explains most of the
351 differences between an ERF and an RF calculation. Bickel et al. (2019) presents an explicit calculation of
352 the contrail cirrus ERF and uses the same basic model formulation of Bock and Burkhardt, so the ERF
353 calculation was not used here directly but rather the estimation of the ERF/RF ratio was used.

354 The RF best estimate for 2011 was calculated here for comparison to the most recent IPCC estimate
355 (Boucher et al., 2013). With each study weighted equally, the resulting 2011 RF best estimate for contrail
356 cirrus (excluding any adjustments) is approximately 86 (25, 146) mW m^{-2} (see **Table 3**). The IPCC best
357 estimate of 50 (20, 150) mW m^{-2} (including the natural cloud feedback) was derived from scaling and

1 July 2020 Revised

358 averaging two studies. IPCC assigned a large uncertainty and low confidence to reflect important aspects
359 with incomplete knowledge (e.g., spreading rate, optical depth, and radiative transfer). The RF best
360 estimate derived here for 2018 is 111 (33, 189) mW m⁻². The uncertainties in the present study are
361 reduced due to the development of process-based approaches simulating contrail cirrus in recent years.
362 The uncertainty in the new RF estimate, excluding the uncertainty in the ERF/RF scaling of individual RF
363 values, is ±70%, a value substantially lower than the factor of three stated in IPCC.

364 The ±70% uncertainty was derived differently than for the NO_x forcing due to the smaller number of
365 available studies. Instead, the uncertainty was derived from the combined uncertainties associated with
366 the processes involved (see Appendix E). The processes fall into two groups: those connected with the
367 upper tropospheric water budget and the contrail cirrus scheme itself, and those associated with the
368 change in radiative transfer due to the presence of contrail cirrus. We considered uncertainty in upper
369 tropospheric ice-supersaturation frequencies and their simulation in global models and the uncertainty of
370 ice-crystal numbers due to uncertainty in soot-number emissions, ice nucleation within the plume, and
371 loss processes in the contrail's vortex phase. Finally, an important uncertainty comes from the adjustment
372 of natural clouds (Burkhardt and Kärcher, 2011). There is also a small uncertainty associated with the
373 contrail cirrus life cycle, which affects the difference in nighttime and daytime contrail cirrus cover
374 (Stuber et al., 2006) based on work analyzing the diurnal cycle (Chen and Gettelman, 2013; Newinger
375 and Burkhardt, 2012).

376 Uncertainty connected with the radiative response to contrail cirrus is largely due to the differences in the
377 radiation schemes across climate models and the approximations made therein (Myhre et al., 2009;
378 Gounou and Hogan, 2007); the background cloud field and its vertical overlap with contrail cirrus; and
379 assumptions about the homogeneity of the contrail cirrus field. Furthermore, the presence of very small
380 ice crystals (<5µm) (Bock and Burkhardt, 2016) and unknown ice-crystal habits (Markowicz and Witek,
381 2011) add to the uncertainty.

382 Our best estimate of the contrail cirrus uncertainty does not include the impact of contrails forming within
383 natural clouds, which was recently shown to be observable from space (Tesche et al., 2016), or the change
384 in radiative transfer due to soot cores in contrail cirrus ice crystals (Liou et al., 2013), which decreases the
385 albedo at solar wavelengths and increases the top of atmosphere net RF. Both effects are very likely to
386 lead on average to an increase in contrail cirrus RF, causing our best estimate to be conservative. The
387 estimated uncertainty relates to the average contrail cirrus RF. In specific synoptic situations,
388 uncertainties may be much larger and correlated with each other.

389 In contrast to other aviation forcing terms, the average ERF/RF ratio for contrail cirrus is estimated to be
390 0.42, much less than unity. The associated uncertainty is thought to be very large and dependent on
391 prevailing aviation traffic and its geographic distribution. The low ERF/RF value is largely due to the
392 reduction in natural cloudiness caused by increased contrail cirrus similar to the reduction in natural cirrus
393 cloudiness as reported by Burkhardt and Kärcher (2011). The ERF/RF value is the average of three global
394 climate model studies: two that estimated climate efficacies of 31% and 59% (Ponater et al., 2005; Rap et
395 al., 2010) and a third that gave a direct estimate of the ERF of contrail cirrus that is 35% of the
396 corresponding RF (Bickel et al., 2019). These studies conclude that efficacies equal to that of CO₂
397 overstate the role of cirrus changes due to aviation on global mean surface temperatures. The average
398 ERF/RF ratio was applied to the homogenized estimates of RF, while the RF of Chen and Gettelman
399 (2013) was interpreted as an ERF (see above). Weighting each study equally, the resulting ERF for
400 contrail cirrus is 57 (17, 98) mW m⁻² for 2018. It is important to note that the uncertainty does not include
401 any contribution coming from the ERF/RF estimate. Despite the large ERF/RF adjustment, this ERF term
402 is the largest for global aviation in 2018 and is comparable in magnitude to the CO₂ term in the
403 normalized results for 2000 to 2018 (**Figure 6**). While comparable in magnitude, these ERFs have
404 different implications for future climate change (Section 6).

405 4.5. Aerosol-radiation interaction.

406 Aircraft engines directly emit soot, defined as mixture of BC and OC, and precursors for sulfate (SO_4^{2-})
407 and nitrate (NO_3^-) aerosol along flight tracks. Soot aerosol is formed from the condensation of unburnt
408 aromatic compounds in the combustor (e.g. Ebbinghaus and Wiesen, 2001) and sulfate aerosol from the
409 oxidation of sulfur in the fuel (Dstn 91-91, 2015). Most of the sulfur is emitted as SO_2 , whilst a small
410 fraction (~3%) is emitted as oxidized H_2SO_4 (Petzold et al., 2005). Most of the sulfate aerosol is produced
411 after emission from sulfur precursor compounds by oxidation in the ambient atmosphere. Both aerosol
412 types create RFs from aerosol-radiation interactions: soot absorbs short-wave radiation leading to net
413 warming and sulfate aerosol scatters incoming short-wave radiation leading to net cooling (IPCC, 1999).
414 As figures of merit, year 2000 global aviation emissions increase aerosol mass for both soot and sulfate
415 by a few percent and aerosol number by 10–30% near air traffic flight corridors in the northern
416 extratropics (Righi et al., 2013).

417 Past calculations of aerosol-radiation RF values using a variety of global aerosol models have yielded
418 values of a few mW m^{-2} and with large uncertainties (e.g., Righi et al., 2013; Gettelman and Chen, 2013;
419 L09). In the present study, 10 estimates across 8 models were used to evaluate soot and sulfate aerosol
420 normalized RFs (IPCC, 1999; Sausen et al., 2005; Fuglestedt et al., 2008; Balkanski et al., 2010;
421 Gettelmann and Chen, 2013; Unger et al., 2013; Pitari et al., 2015; Brasseur et al., 2016) (see SD
422 spreadsheet). Averaging the normalized values yields a 2018 best estimate of the soot aerosol-radiation
423 RF of 0.9 (0.1, 4.0) mW m^{-2} for 0.0093 Tg soot emitted. The corresponding best estimate for sulfate
424 aerosol is -7.4 (-19, -3) mW m^{-2} for 0.37 Tg SO_2 emitted. The uncertainties are derived from the standard
425 deviation of the model values. The ERF/RF ratios for soot and sulfate are assumed to be unity in the
426 absence of any estimates of this ratio.

427 4.6 Aerosol-cloud interaction.

428 Aerosol-cloud interactions are those processes by which aerosols influence cloud formation. For example,
429 cloud droplets and ice crystals nucleate on aerosol particles. Thus, aerosol-cloud interactions involving
430 aviation aerosol potentially result in an ERF. Aviation soot and sulfate particles are the predominant
431 primary and secondary aerosol from aircraft. The uncertainties in evaluating the aerosol-cloud
432 interactions of aviation soot and sulfate preclude best estimates of ERF contributions. Given the potential
433 importance of these ERF terms, placeholders are included in **Figure 3**. Furthermore, to promote progress
434 towards future best estimates, the results of relevant modeling studies were compiled and normalized to
435 global aviation fuel usages in 2005, 2011, 2018, to a soot emission index, and to a fuel S content of 600
436 pm (except in the cases of low fuel-S content tests) (see **Figure 5** and spreadsheet). As noted in the
437 caption of **Figure 5**, some earlier wide-ranging values for the soot aerosol-cloud interaction have been
438 superseded by a more recent study (Penner et al., 2018).

439 4.6.1 Sulfate aerosol.

440 Aviation sulfate aerosol primarily affects liquid clouds in the background atmosphere. Sulfate aerosol is
441 very efficient as a cloud condensation nuclei (CCN) for liquid clouds, and for promoting homogeneous
442 freezing of solution particles at cold temperatures, thus nucleating ice clouds. Two integrated model
443 simulations (Kapadia et al., 2016; Gettelman and Chen, 2013) found large impacts on liquid clouds from
444 aviation sulfate aerosol that is transported to liquid clouds at lower altitudes over oceans, which have low
445 albedo. The reported RF values in these studies, when scaled appropriately, are -37 to -76 mW m^{-2} in
446 2018, excluding a low fuel-sulfur case. Note that the study of Righi et al. (2013) that yields an RF of -213
447 mW m^{-2} in 2018 includes sulfate aerosol-cloud interactions but cannot be directly compared with Kapadia
448 et al. (2016) and Gettelman and Chen (2013), since the former treats the combined effects of sulfate,
449 nitrate and particulate organic matter (POM) rather than isolating the effects of sulfate as done in the
450 latter studies. While these RF estimates do not support a best estimate at present, they do suggest that the
451 sign of the sulfate aerosol-cloud effect on low-level clouds is likely to be negative (i.e., a cooling), similar

1 July 2020 Revised

452 to the ERF for the aerosol-cloud interactions of other anthropogenic sources of sulfate aerosol (IPCC,
453 2013).

454 Sulfate aerosol-cloud interaction forcing estimates are highly dependent on the sensitivity (or
455 susceptibility) of the cloud radiative field to aerosol perturbations, which is dependent on uncertain model
456 processes and the model background aerosol state. Clouds that form with small CCN number
457 concentrations in the background atmosphere are more sensitive to CCN perturbations. Forcing by these
458 cloud effects are largely concentrated near flight corridors over oceans because the high albedo contrast
459 between the ocean surface and clouds increases forcing sensitivity to CCN perturbations.

460 A large uncertainty was also reported for the magnitude of the aerosol-cloud ERF from all anthropogenic
461 activities, estimated for 2011 to be -450 (-1200 , 0.0) mW m^{-2} (Myhre et al., 2013). A more recent estimate
462 of the aerosol-cloud RF from all anthropogenic activities has a 68% confidence interval of -650 to -1600
463 mW m^{-2} (Bellouin et al., 2019). In general, aerosol-cloud interactions contribute the largest uncertainty in
464 calculations of anthropogenic ERF (IPCC, 2013).

465 4.6.2 Soot.

466 The magnitude and the sign of the global RF from aviation soot effects on background cloudiness remain
467 highly uncertain. The uncertainties center on the difficulties in accurately simulating homogeneous and
468 heterogeneous ice nucleation in the background atmosphere, variations in the treatment of updraft
469 velocities during cirrus formation, and the lack of knowledge of the ice nucleating (IN) ability of aviation
470 soot particles during their atmospheric lifetime (Zhou and Penner, 2014; Penner et al., 2018).

471 Two studies find moderate effects of soot aerosol on ice clouds, depending on the ice nucleating
472 efficiency and the size distribution. RF values of about 11 to 13 mW m^{-2} (normalized to 2018 emissions)
473 are calculated in some studies for moderate ice-nucleating efficiencies (Pitari et al., 2015, Gettelman and
474 Chen, 2013).

475 In sensitivity tests, if soot processed within contrails is assumed to be an efficient IN particle, then the RF
476 may be negative by up to -330 mW m^{-2} due to reductions in ice crystal number in regions dominated by
477 homogeneous freezing (Penner et al., 2018; see Figure 5). The RF could be significantly smaller (less
478 negative) if additional ice-forming particles, such as secondary organic aerosol (SOA), are already present
479 in the background atmosphere (Penner et al., 2018; Gettelman and Chen, 2013). In addition, increases in
480 ice crystal numbers occur when the background atmosphere has much lower sulfate or haze-forming
481 aerosol number concentrations and is dominated by heterogeneous freezing, causing forcings near zero or
482 even positive (Zhou and Penner, 2014). Other studies predict decreases in cirrus number for smaller
483 numbers of larger soot particles (Hendricks et al., 2011), resulting in a slight warming (Gettelman and
484 Chen, 2013).

485 A dominant uncertainty for the aerosol-cloud effect from soot is the IN properties of aviation soot aerosol.
486 Some laboratory studies indicate soot particles are not efficient ice nuclei (DeMott et al., 1999), while
487 other studies indicate higher efficiencies (Möhler et al., 2005; Hoose and Möhler, 2012). The possibility
488 that contrail-processed soot particles would show enhanced IN activity after sublimation in the
489 background atmosphere was addressed in the laboratory (Mahrt et al., 2020). The effect was limited to
490 large soot particles, suggesting that the impact of aviation soot on cloudiness may be overestimated in
491 previous studies that assume soot processed through contrails and not covered by a sulfate coating is an
492 efficient IN (Penner et al., 2018).

493 Another source of uncertainty is soot number concentrations. For individual engines, the soot number can
494 vary by two orders of magnitude (Agarwal et al., 2019). Soot number concentrations from aviation vary
495 with the assumed size of the particles emitted as well as the mass emissions. Soot emissions from aircraft
496 are set as a regulatory parameter for the landing/take-off (LTO) cycle by ICAO and are measured in terms
497 of mass. Robust conversion factors from mass to number have recently been developed for the ICAO-

1 July 2020 Revised

498 LTO cycle (Agarwal et al., 2019) but have not yet been made for cruise, although other methodologies
499 exist (Teoh et al., 2019).

500 5. Calculated net aviation ERF and RF values

501 ERF and RF values for the terms associated with global aviation emissions and cloudiness are given in
502 **Tables 2 and 3**, respectively, for the years 2018, 2011, and 2005, along with uncertainties, sensitivities to
503 emissions and the ERF/RF ratio for selected terms. ERF values are shown for all years in **Figure 6**. All
504 ERF and RF values are available in the analysis spreadsheet (SD). Through normalization and scaling, all
505 2000 to 2018 values are self-consistent. The sensitivity of each term to emission magnitudes or flight
506 track distances is derived in the normalization process. ERF best estimates and uncertainties (95%
507 confidence limits) are highlighted for year 2018 in **Figure 3** along with their assessed confidence levels.
508 No best estimates are included for sulfate and soot aerosol-cloud interactions because of the substantial
509 uncertainties noted above. However, placeholder spaces are included in both the **Tables 2 and 3** and
510 **Figure 3** to indicate the potential importance of these terms and to flag the associated knowledge gaps for
511 consideration in future research and assessment activities. The confidence levels and their justifications
512 shown in **Figure 3** are obtained by employing the methodology of Mastrandrea et al. (2011), which is
513 based on evidence and agreement in accordance with IPCC guidance (**Table 4**).

514 In **Figure 3**, contrail cirrus formation yields the largest positive (warming) ERF term, followed by CO₂
515 and NO_x emissions. For the 1940 to 2018 period, the net aviation ERF is +100.9 mW m⁻² (5–95%
516 likelihood range of (55, 145)) with major contributions from contrail cirrus (57.4 mW m⁻²), CO₂ (34.3
517 mW m⁻²), and NO_x (17.5 mW m⁻²). The aerosol and water vapor terms represent minor contributions. The
518 formation and emission of sulfate aerosol yields the only significant negative (cooling) term. Non-CO₂
519 terms sum to yield a positive (warming) ERF that accounts for 66% of the aviation net ERF in 2018 (66.6
520 (21, 111) mW m⁻²). The application of ERF/RF ratios more than halves the RF value of contrail cirrus
521 while approximately doubling the NO_x value. ERF/RF ratios were not included in the L09 analysis.
522 Uncertainty distributions (5%, 95%) show that non-CO₂ forcing terms contribute about 8 times more than
523 CO₂ to the uncertainty in the aviation net ERF in 2018. The best estimates of the ERFs from aviation
524 aerosol-cloud interactions remain undetermined.

525 The time series of ERF values for individual terms is shown in **Figure 6** for the 2000–2018 period.
526 Through normalization and scaling the terms are self-consistent over this period. The increase in all of the
527 terms with time is consistent with the growth of aviation fuel burn and CO₂ emissions over the same
528 period (**Figure 2**). Note that net ERF values shown for each year are not linear sums over the component
529 terms due to the separate probability distributions associated with each component term in the sum, and
530 instead are calculated with a Monte Carlo sampling method described below.

531 A comparison of updated RF estimates with L09 values for 2005 is given in **Table 3**. The large increase
532 in the contrail cirrus RF between 2005 and 2018 results in part because the 2005 value only includes
533 linear contrails. In L09, only an estimate of 2005 contrail cirrus was provided rather than a best estimate.
534 The present study now includes a process-based model estimate of the contrail cirrus term (Section 4.4).
535 The NO_x treatment in L09 did not include the negative forcing contributions of the long-term O₃ decrease
536 or the SWV decrease, the updated treatment of CH₄ of Etminan et al. (2016), nor an equilibrium-to-
537 transient correction. As a result, the updated RF values for NO_x are approximately a factor of 2 smaller.
538 Incorporating all the updated information in the RF calculations of the NO_x and contrail cirrus terms
539 yields an approximately 30% increase in the net aviation RF for 2005, from 78.0 to 95.2 mW m⁻². In the
540 ERF evaluation for 2005 the net aviation forcing is reduced from 95.2 to 66.9 mW m⁻² because the
541 ERF/RF ratios for NO_x and contrail cirrus are different than unity.

542 In seeking comparison of net aviation ERF with net anthropogenic ERF, we note that IPCC (Myhre et al.,
543 2013) provides a value for 1750–2011 of 2290 (1130, 3330) mW m⁻². The percentage contributions of
544 aviation to the net ERF in 2011 are 3.5% (4.0, 3.4%) and 1.59% (1.65, 1.56%) for the sum of all terms

545 and the CO₂ term alone, respectively. The 2005 and 2018 percentages are likely the same because the
546 fraction of aviation CO₂ emissions of total anthropogenic CO₂ emissions has averaged 2.1% (± 0.15) for
547 the last two decades (see **Figure 2**). Normalized relative probabilities of CO₂ and non-CO₂ ERFs for 2018
548 as derived from the Monte Carlo simulations show that non-CO₂ uncertainties are the predominant
549 contribution to the uncertainty in the aviation net ERF (**Figure 7**). IPCC also separately estimated the
550 contrail cirrus term for 2011 as 50 (20, 150) mW m⁻² as discussed above, which compares well with the
551 updated value of 44.1 (13, 75) mW m⁻².

552 The determination of net aviation ERFs and their uncertainties shown in **Figure 3** and accompanying
553 tables required a Monte Carlo approach to summing over terms with discrete probability distributions. A
554 similar method was employed in L09. PDFs of each term were constructed from the respective individual
555 studies as normal, lognormal or discrete distributions (see SD spreadsheet). Monte Carlo samplings (one
556 million random points) of the individual forcing PDFs were then used to combine terms to yield net ERFs
557 and the uncertainties (95% likelihood range) for the sum of all terms and for only non-CO₂ terms (**Figure**
558 **7**). The forcing terms are generally assumed to be independent (uncorrelated) with the notable exception
559 of the NO_x component terms which have strong paired correlations as shown in Appendix Figure D.1.
560 Only the short-term O₃ and CH₄ terms were included in L09 and a 100% correlation was assumed, in part,
561 because the assumption of uncorrelated effects was deemed less acceptable. A subsequent study showed
562 that these terms are indeed strongly correlated ($R^2 = 0.79$) (Holmes et al., 2011), similar to the present
563 results in Appendix Figure D.1. The Holmes et al. (2011) study further concluded that the assumption of
564 100% correlation in this case would lead to an underestimate of uncertainty in the NO_x RF. Another
565 correlation of forcing terms not considered here may be the dependence of the soot direct effect and
566 contrail properties on the soot number index since ice nucleation at the time of contrail formation depends
567 on the soot number index (e.g., Kärcher, 2018).

568 **6. Emission equivalency metrics**

569 Using the best estimate ERFs, we calculate updated aviation-specific Global Warming Potential (GWP)
570 and Global Temperature change Potential (GTP) values, presented for 20-, 50-, and 100-year time
571 horizons in **Table 5**. These metrics assign so-called ‘CO₂-emission equivalences’ for non-CO₂ emissions
572 via ratios of time-integrated ERF and changes in future temperatures, respectively. The choice of metric
573 depends upon the particular underlying application (Fuglestedt et al., 2010) such that there is no
574 uniquely ‘correct’ metric or time horizon, and alternative metrics are available. GWP and GTP are the
575 most commonly applied metrics and the values calculated here allow a comparison with previous
576 estimations (e.g., Lee et al., 2010; Lund et al. 2017). In calculating the GWPs and GTPs, the CO₂ IRF
577 from Joos et al. (2013) is used and the climate response IRF from Boucher and Reddy (2008) for the
578 GTPs (see Appendix F for further details about the metrics calculations).

579 GWPs and GTPs for contrail cirrus and for water vapor reported here are similar to, albeit slightly smaller
580 than, corresponding results previously reported, while soot and sulfate numbers are larger in magnitude
581 (positive and negative) than previous estimates (Fuglestedt et al. 2010; Lund et al. 2017). The
582 Fuglestedt et al. (2010) estimates for soot are based on RF due to soot emissions from all sources, not
583 just aviation, which yields a lower radiative efficiency (i.e., forcing per unit emission) than in the present
584 study. Also given in **Table 5** are CO₂-equivalent aviation emissions, along with ratios of total CO₂-
585 equivalent emissions to CO₂ emissions. Such ratios are sometimes used as ‘multipliers’ to illustrate the
586 additional climate impact from aviation non-CO₂ terms over those from CO₂ emissions alone. Here,
587 estimated multipliers for 2018 range from 1.0 to 4.0 depending on the choice of time horizon and
588 emission metric. This is broadly consistent with what has been reported and used previously (Lee et al.,
589 2010). The broad range emphasizes the challenges associated with developing comparisons of emission
590 equivalences for short- and long-lived climate forcers within a common framework and how such
591 considerations strongly depend on the chosen perspective.

592 One of the significant uncertainties in calculating GWPs and GTPs is the treatment of climate-carbon (C-
 593 cycle) feedbacks in the modeling framework. The efficiency of carbon sinks reduces with increasing
 594 warming (Ciais et al., 2013) and this climate feedback is implicitly included in the Absolute GWP of CO₂
 595 through the IRF used (Joos et al., 2013). However, Myhre et al. (2013) highlighted that this introduces an
 596 inconsistency since the numerators for the GWP and GTP do not include such a climate carbon feedback.
 597 One of the studies that have proposed ways of addressing this inconsistency is Gasser et al. (2017). They
 598 show that when the C-cycle feedback is consistently accounted for, the non-CO₂ emission metrics
 599 increase, but less so than initially suggested by Myhre et al. (2013). They also find that removing the C-
 600 cycle feedback from both numerator and denominator give similar metric values as including it in both
 601 places. Using the CO₂ IRF without the C-cycle feedback provided by Gasser et al. (2017), we calculate a
 602 second set of aviation emission metrics (Table F.1), showing that the changes to the GWP100 and
 603 GTP100 values from those given in Table 5 are rather small.

604 In response to the challenges related to comparing short-lived and long-lived forcing components, a
 605 number of new ‘flow-based’ methods have been introduced representing both short-lived and long-lived
 606 climate forcers explicitly as ‘warming-equivalent’ emissions that have approximately the same impact on
 607 the global average surface temperature over multi-decade to century timescales (Lauder et al., 2012; Allen
 608 et al., 2016; 2018; Cain et al., 2019; Collins et al., 2019). A simple version of these methods, known as
 609 GWP*, defines the average annual rate of CO₂-warming-equivalent emissions ($E_{CO_2e}^*$) over a period of Δt
 610 years arising from a particular component of RF or ERF by (Cain et al., 2019):

$$611 \quad E_{CO_2e}^* = [(1 - \alpha)H/AGWP_H] \Delta F / \Delta t + [\alpha/AGWP_H] \bar{F}, \quad (1)$$

612 where ΔF is the ERF change and \bar{F} the average ERF arising from that component over that period,
 613 $AGWP_H$ is the Absolute GWP of CO₂ (Wm⁻² kg⁻¹ year) over time-horizon H and α is a small coefficient
 614 depending on the previous history of that RF component. This equation gives the rate of CO₂ emission
 615 that would, alone, create the same rate of global temperature increase as the combined effect of aviation
 616 climate forcings. For historically small and/or rapidly changing RF components, α may be neglected, and
 617 hence to a good approximation, total CO₂-warming-equivalent emissions over this period ($\Delta t E_{CO_2e}^*$) are
 618 approximated by an increase in forcing, ΔF , multiplied by $H/AGWP_H$ (see Appendix A.6), which is about
 619 1000 GtCO₂ per W/m² for H in the range 20 to 100 years (Myhre et al, 2013; IPCC, 2018, Figure SPM.1,
 620 caption). This result follows from the definition of AGWP: since all GWP calculations assume a
 621 linearization, the $AGWP_H$ is equivalent to the forcing change resulting from the emission of H tonnes of
 622 CO₂ spread over H years (Shine et al, 2005), so $AGWP_H/H$ is the forcing change per tonne of CO₂. Under
 623 the historical profile of increasing global annual aviation-related emissions and associated ERFs, CO₂-
 624 warming-equivalent emissions based on GWP* indicate that aviation emissions are currently warming the
 625 climate around three times faster than that associated with aviation CO₂ emissions alone (**Table 5**).

626 It is important to note that, unlike the conventional GWP and GTP metrics given in **Table 5**, the ratio
 627 between total CO₂-warming-equivalent emissions from all forcing agents and those from CO₂ alone will
 628 change substantially if future aviation emissions deviate from their current growth trajectory (calculated
 629 here over the period 2000–2018). If annual global aviation emissions were to stabilize, this ratio declines
 630 towards unity, as $\Delta F / \Delta t$ would decline to zero. This does not indicate, however, that the non-CO₂ effects
 631 do not have a warming affect. This human-induced warming still represents a mitigation potential.
 632 Warming-equivalent emissions capture the fact that constant emission of short-lived climate forcers
 633 maintain an approximately constant level of warming, whilst constant emissions of long-lived climate
 634 forcers, such as CO₂, continue to accumulate in the atmosphere resulting in a constantly increasing level
 635 of associated warming. Hence warming-equivalent emissions show that the widely-used assumption of a
 636 constant ‘multiplier’, assuming that net warming due to aviation is a constant ratio of warming due to
 637 aviation CO₂ emissions alone, only applies in a situation in which aviation emissions are rising
 638 exponentially such that the rate of change of non-CO₂ RF is approximately proportional to the rate of CO₂
 639 emissions (assuming non-CO₂ RF is proportional to CO₂ emissions, and noting that the rate of change any

640 quantity is proportional to that quantity only when both are growing exponentially). In contrast, under a
641 future hypothetical trajectory of decreasing aviation emissions, this GWP* based multiplier could fall
642 below unity, as a steadily falling rate of emission of (positive) short-lived climate forcers has the same
643 effect on global temperature as active removal of CO₂ from the atmosphere. The GWP* based ‘multiplier’
644 calculated here (which depends on the ratio of the increase in net aviation warming to the increase in
645 warming due to aviation CO₂ emissions alone over the recent past), should not be applied to future
646 scenarios that deviate substantially from the current trend of increasing aviation-related emissions. The
647 broad range of values for a ‘multiplier’ presented here is an illustration of the limitations of using a
648 constant multiplier in the assessment of climate impacts of aviation, and a reminder that the choice of
649 metric for such a multiplier involves subjective choices.

650 7. Aviation CO₂ vs non-CO₂ forcings

651 Since IPCC (1999), the comparison of aviation CO₂ RF with the non-CO₂ RFs has been a major scientific
652 topic, as well as a discussion point amongst policy makers and civil society (ICAO, 2019). Aviation as a
653 sector is not unique in having significant non-CO₂ forcings; the same is true of agriculture with significant
654 CH₄ and N₂O emissions, or maritime shipping with net-negative current-day RF despite CO₂ emissions of
655 a similar magnitude to those from aviation (Fuglesvedt et al., 2009). However, unlike direct emissions of
656 the greenhouse gases N₂O and CH₄ from the agricultural sector, aviation non-CO₂ forcings are not
657 covered by the former Kyoto Protocol. It is unclear whether future developments of the Paris Agreement
658 or ICAO negotiations to mitigate climate change, in general, will include short-lived indirect greenhouse
659 gases like NO_x and CO, aerosol-cloud effects, or other aviation non-CO₂ effects. Aviation is not
660 mentioned explicitly in the text of the Paris Agreement, but according to its Article 4, total global
661 greenhouse-gas emissions need to be reduced rapidly to achieve a balance between anthropogenic
662 emissions by sources and removals by sinks of greenhouse gases in the second half of this century.

663 The IPCC concludes: “*Reaching and sustaining net-zero global anthropogenic CO₂ emissions and*
664 *declining net non-CO₂ radiative forcing would halt anthropogenic global warming on multi-decadal time*
665 *scales.*” (IPCC, 2018, bullet A2.2, SPM). Crucially, both conditions would need to be met to halt global
666 warming. Hence, to halt aviation’s contribution to global warming, the aviation sector would need to
667 achieve net-zero CO₂ emissions and declining non-CO₂ radiative forcing (unless balanced by net negative
668 emissions from another sector): neither condition is sufficient alone. Some combination of reductions in
669 CO₂ emissions and non-CO₂ forcings might halt further warming temporarily, but only for a few years: it
670 would not be possible to offset continued warming from CO₂ by varying non-CO₂ radiative forcing, or
671 *vice versa*, over multi-decade timescales.

672 That aviation’s non-CO₂ forcings are not included in global climate policy has resulted in studies as to
673 whether they could be incorporated into existing policies, such as the European Emissions Trading
674 Scheme, using an appropriate overall emissions ‘multiplier’; however, scientific uncertainty has so far
675 precluded this (Faber et al., 2008). In addition, as noted above, the multiplier is highly dependent on the
676 future emissions scenario (Section 6). Alternatively, proposals have been made to reduce aviation’s non-
677 CO₂ forcings by, for example, avoiding contrail formation by re-routing aircraft (Matthes et al., 2017), or
678 optimizing flight times to avoid the more positive (warming) fractional forcings (e.g., by avoiding night
679 flights, Stuber et al., 2006). There is a developing body of literature on this topic (e.g., Newinger and
680 Burkhardt, 2012; Yin et al., 2018). Similarly, studies have assessed whether changes in cruise altitudes
681 could mitigate NO_x impacts (e.g. Frömming et al., 2012). The potential impacts of changes in technology
682 have also been examined to reduce the non-CO₂ forcings such as lowering the emission index for NO_x
683 (Freeman et al., 2018) or soot particle number emissions (Moore et al., 2017) to reduce net NO_x and
684 contrail cirrus forcings, respectively (Burkhardt et al., 2018).

685 Avoidance of contrail formation through re-routing can incur a fuel penalty and therefore additional CO₂
686 emissions during a flight, and changes in combustor technology to minimize NO_x generally increases

1 July 2020 Revised

687 marginal fuel burn and CO₂ emission. Both methods invoke the usage of climate metrics such as those
688 calculated and presented in Section 6 to evaluate whether there is a net climate benefit or disbenefit over
689 a defined period. In examining such mitigation scenarios involving tradeoffs (e.g. Teoh et al., 2020), the
690 perceived success or otherwise of the outcome will be a function of the user's choice of metric and time
691 horizon. A limitation noted for the GWP is that it has an 'artificial memory' over longer time horizons,
692 since the integrated-RF nature of the metric accumulates 'signal' over time that the climate system has
693 'forgotten' (Fuglestedt et al., 2010). The GTP, being an 'end point' metric that captures the temperature
694 response, overcomes this limitation of the GWP but is not yet in usage within current climate policy.

695 Changes to aviation operations or technology that result in a reduction of a non-CO₂ forcing with the
696 added consequence of increased CO₂ emissions can result in net reductions of forcing on short timescales
697 while increasing the net forcing on longer timescales (e.g., Freeman et al., 2018). In a case study of
698 contrail avoidance through routing changes, Teoh et al. (2019) found that the resultant small increase in
699 CO₂ emissions still reduces the net forcing over a timescale of 100 years. In such 'tradeoff cases' the
700 balance between non-CO₂ and CO₂ forcings have to be weighted carefully, since CO₂ accumulates in the
701 atmosphere and a fraction has millennial timescales (Archer and Brovkin, 2008; IPCC, 2007). Prior to the
702 COVID-19 pandemic, global aviation traffic and emissions were projected to grow to 2050 (Fleming and
703 Lepinay, 2019). As the COVID-19 pandemic diminishes, aviation traffic is likely to recover to meet
704 projected rates on varying timescales (IATA, 2020), with continued growth further increasing CO₂
705 emissions. Thus, reducing CO₂ aviation emissions will remain a continued focus in reducing future
706 anthropogenic climate change, along with aviation non-CO₂ forcings. The latter increase the current-day
707 impact on global average temperatures by a factor of around 3 (using GWP*) above that due to CO₂
708 alone.

709 **Author Contributions**

710 **D. S. Lee, D. W. Fahey**

711 Role: Investigation, Methodology, Writing–review & editing, Data curation; Formal analysis, Project
712 administration, Supervision

713 **A. Skowron**

714 Role: Investigation, Methodology, Writing–review & editing, Data curation, Formal analysis;
715 Software

716 **M. R. Allen, U. Burkhardt, Q. Chen, S. J. Doherty, S. Freeman, P.M. Forster, J. Fuglestedt, A.
717 Gettelman, R. R. De León, L. L. Lim, M. T. Lund, R. J. Millar, B. Owen, J. E. Penner, G. Pitari,
718 M. J. Prather, R. Sausen, L. J. Wilcox**

719 Role: Writing–review & editing, Investigation, Methodology, Writing–original draft, Data curation;
720 Formal analysis;

721 **Declaration of competing interest**

722 The authors declare that they have no known competing financial interests or personal relationships that
723 could have appeared to influence the work reported in this paper.

724 **Acknowledgements**

725 We gratefully acknowledge discussions with many colleagues during the preparation of this paper, in
726 particular Andreas Bier and Bernd Kärcher. We acknowledge help with graphical displays from Beth
727 Tully (Figure 1) and Chelsea R. Thompson (Figures 5, 6 and 7).

728 **Funding**

1 July 2020 Revised

729 DSL, AS, RRdL, LL, BO acknowledge support from the UK Department for Transport. PMF
730 acknowledges support of the European Union's Horizon 2020 Research and Innovation Programme under
731 grant agreement number 820829 (CONSTRAIN) by the UK National Environment Research Council
732 (NERC) SMURPHS project (NE/N006038/1). MRA acknowledges support from the EU H2020 grant
733 agreement number 821205 (FORCeS) and the Oxford Martin Programme on Climate Pollutants. MTL
734 and JSF acknowledges support from the Norwegian Research Council (RCN) grant number 300718
735 (AVIATE), for which DSL and RS have a collaboration agreement. JEP acknowledges support from the
736 National Science Foundation (NSF 1540954).

737 **Data Availability**

738 Supplementary data to this article is a spreadsheet that can be found online at: <https://doi.org/xxxxx>.

739

740 **References**

- 741 Airbus, Global Market Forecast 2017–2036 (Airbus, France 2017).
- 742 Allen, M. R. J. S. Fuglestedt, K. P. Shine, A. Reisinger, R. T. Pierrehumbert, and P. M. Forster, New use
743 of global warming potentials to compare cumulative and short-lived climate pollutants. *Nature Climate*
744 *Change* 6 (8), 773–776, <https://doi.org/10.1038/nclimate2998> (2016).
- 745 Allen, M. R. K. P. Shine, J. S. Fuglestedt, R. J. Millar, M. Cain, D. J. Frame, A. H. Macey, A solution to
746 the misrepresentations of CO₂-equivalent emissions of short-lived climate pollutants under ambitious
747 mitigation. *npj Climate and Atmospheric Science* 1:16; <https://doi.org/10.1038/s41612-018-0026-8>
748 (2018).
- 749 Agarwal, A., R. L. Speth, T. M. Fritz, S. D. Jacob, T. Rindlisbacher, R. Iovinelli, B. Owen, R. C. Miake-
750 Lye, J. S. Sabnis, S. R. H. Barrett, SCOPE11 method for estimating aircraft black carbon mass and
751 particle number emissions. *Environmental Science and Technology* 53, 1364–1373,
752 <https://doi.org/10.1021/acs.est.8b04060>, (2019).
- 753 Alfsen, K. H. and T. Berntsen, T., An Efficient and Accurate Carbon Cycle Model for Use in Simple
754 Climate Models. CICERO, Oslo, Norway, <https://core.ac.uk/reader/52082516>
- 755 Archer, D. and V. Brovkin, The millennial atmospheric lifetime of anthropogenic CO₂. *Climatic Change*
756 90, 283–297, <https://doi.org/10.1007/s10584-008-9413-1> (2008).
- 757 Balkanski, Y., G. Myhre, M. Gauss, G. Rädcl, E. J. Highwood, K. P. Shine, Direct radiative effect of
758 aerosols emitted by transport: from road, shipping and aviation. *Atmospheric Chemistry and Physics*
759 10(10), 4477–4489, <https://doi.org/10.5194/acp-10-4477-2010> (2010).
- 760 Barrett, S., M. Prather, J. Penner, H. Selkirk, S. Balasubramanian, A. Doppelheuer, G. Fleming, M. Gupta,
761 R. Halthore, J. Hileman, M. Jacobson, S. Kuhn, S. Lukachko, R. Miake-Lye, A. Petzold, C. Roof, M.
762 Schaefer, U. Schumann, I. Waitz, R. Wayson R., Guidance on the use of AEDT gridded aircraft emissions
763 in atmospheric models. Massachusetts Institute for Technology, Laboratory for Aviation and the
764 Environment, LAE-2010-008-N. (2010)
765 <http://citeseerx.ist.psu.edu/viewdoc/download?doi=10.1.1.719.2090&rep=rep1&type=pdf>
- 766 Bellouin, N., J. Quaas, E. Gryspeerdt, S. Kinne, P. Stier, D. Watson-Parris, O. Boucher, K.S. Carslaw, M.
767 Christensen, A.-L. Daniau, J.-L. Dufresne, G. Feingold, Bounding global aerosol radiative forcing of
768 climate change. *Reviews of Geophysics* 58, e2019RG000660, <https://doi.org/10.1029/2019RG000660>
769 (2019).
- 770 Bickel, M., M. Ponater, L. Bock, U. Burkhardt, S Reineke, Estimating the effective radiative forcing of
771 contrail cirrus, *Journal of Climate*, 33, 1991–2005, <https://doi.org/10.1175/JCLI-D-19-0467.1> (2020).

1 July 2020 Revised

- 772 Bier, A., U. Burkhardt, L. Bock, Synoptic control of contrail cirrus life cycles and their modification due
773 to reduced soot number emissions. *Journal of Geophysical Research Atmospheres* 122 (21), 11,584-
774 11,603 <https://doi.org/10.1002/2017JD027011> (2017).
- 775 Bier, A. and A. U. Burkhardt, Variability in contrail ice nucleation and its dependence on soot number
776 emissions. *Journal of Geophysical Research Atmospheres* 124, 3384–3400,
777 <https://doi.org/10.1029/2018JD029155> (2019).
- 778 Bock, L. and U. Burkhardt, Reassessing properties and radiative forcing of contrail cirrus using a climate
779 model. *Journal of Geophysical Research Atmospheres* 121, 9717–9736,
780 <https://doi.org/10.1002/2016JD025112> (2016).
- 781 Boeing, Orders and Deliveries for January 2018, <http://www.boeing.com/commercial/#/orders-deliveries>
782 (2018).
- 783 Boucher, O. and M. S. Reddy, Climate trade-off between black carbon and carbon dioxide emissions.
784 *Energy Policy* 36, 193–200, <https://doi.org/10.1016/j.enpol.2007.08.039> (2008).
- 785 Brasseur, G. P., M. Gupta, B. E. Anderson, S. Balasubramanian, S. Barrett, D. Duda, G. Fleming, P. M.
786 Forster, J. Fuglestedt, et al., Impact of Aviation on Climate: FAA’s Aviation Climate Change Research
787 Initiative (ACCRI) Phase II. *Bulletin of the American Meteorological Society* 97, 561–583,
788 <https://doi.org/10.1175/BAMS-D-13-00089.1> (2016).
- 789 Burkhardt, U., B. Kärcher, U. Schumann, Global Modelling of the contrail and contrail cirrus climate
790 impact. *Bulletin of the American Meteorological Society* 91, 479-484,
791 <https://doi.org/10.1175/2009BAMS2656.1> (2010).
- 792 Burkhardt, U. and B. Kärcher, Global radiative forcing from contrail cirrus. *Nature Climate Change* 1,
793 54–58, <https://doi.org/10.1038/nclimate1068> (2011).
- 794 Burkhardt, U., L. Bock, A. Bier, Mitigating the contrail cirrus climate impact by reducing aircraft soot
795 number emissions. *npj Climate and Atmospheric Science* 1:37, [https://doi.org/10.1038/s41612-018-0046-](https://doi.org/10.1038/s41612-018-0046-4)
796 4 (2018).
- 797 Cain, M., J. Lynch, M. R. Allen, J. S. Fuglestedt, D. J. Frame, A. H. Macey, Improved calculation of
798 warming-equivalent emissions for short-lived climate pollutants. *npj Climate and Atmospheric Science*,
799 2:29, <https://doi.org/10.1038/s41612-019-0086-4> (2019).
- 800 Carlin, B., Q. Fu, U. Lohmann, G. Mace, K. Sassen, J. Comstock, High-cloud horizontal inhomogeneity
801 and solar albedo bias. *Journal of Climate* 15, 2321–2339, [https://doi.org/10.1175/1520-](https://doi.org/10.1175/1520-0442(2002)015<2321:HCHIAS>2.0.CO;2)
802 0442(2002)015<2321:HCHIAS>2.0.CO;2 (2002).
- 803 Chen, C.-C., A. Gettelman, C. Craig, P. Minnis, D. P. Duda, Global contrail coverage simulated by
804 CAM5 with the inventory of 2006 global aircraft emissions. *Journal of Advances in Modeling Earth*
805 *Systems* 4, 04003. <https://doi.org/10.1029/2011MS000105> (2012).
- 806 Chen, C.-C. and A. Gettelman, Simulated radiative forcing from contrails and contrail cirrus. *Atmospheric*
807 *Chemistry and Physics*, 13, 12525–12536, <https://doi.org/10.5194/acp-13-12525-2013> (2013).
- 808 Ciais, P., Sabine, C., Bala, G., Bopp, L., Brovkin, V., Canadell, J., Chhabra, A., DeFries, R., Galloway, J.,
809 Heimann, M., Jones, C., Le Quéré, C., Myneni, R. B., Piao, S., and Thornton, P. Carbon and Other
810 Biogeochemical Cycles, in: Climate Change 2013: The Physical Science Basis. Contribution of Working
811 Group I to the Fifth Assessment Report of the Intergovernmental Panel on Climate Change, edited by:
812 Stocker, T. F., Qin, D., Plattner, G.-K., Tignor, M., Allen, S. K., Boschung, J., Nauels, A., Xia, Y., Bex,
813 V., and Midgley, P. M., Cambridge University Press, Cambridge, UK and New York, NY, USA (2013)

1 July 2020 Revised

- 814 Clarke, L., J. Edmonds, H. Jacoby, H. Pitcher, J. Reilly, R. Richels, “Scenarios of Greenhouse Gas
815 Emissions and Atmospheric Concentrations”. Sub-report 2.1A of Synthesis and Assessment Product 2.1
816 by the U.S. Climate Change Science Program and the Subcommittee on Global Change Research
817 (Department of Energy, Office of Biological & Environmental Research, Washington, 7 DC. 2007) pp.
818 54, https://globalchange.mit.edu/sites/default/files/CCSP_SAP2-1a-FullReport.pdf.
- 819 Collins, W. J., D. J. Frame, J. S. Fuglestedt, K. P. Shine, Stable climate metrics for emissions of short
820 and long-lived species – combining steps and pulses. *Environmental Research Letters* 15(2), 024018,
821 <https://doi.org/10.1088/1748-9326/ab6039> (2019).
- 822 Creutzig, F., P. Jöcjem, O. Y. Edelenbosch, L. Mattauach, D. P. van Vuuren, D. McCollum, J. Minx,
823 Transport: a roadblock to climate change mitigation? *Science* 350, 911–912,
824 <https://doi.org/10.1126/science.aac8033> (2015).
- 825 Dalsøren, S. B., C. L. Myhre, G. Myhre, A. J. Gomez-Pelaez, O. A. Søvde, I. S. A. Isaksen, R. F. Weiss,
826 C. M. Harth, Atmospheric methane evolution the last 40 years. *Atmospheric Chemistry and Physics* 16,
827 3099–3126, <https://doi.org/10.5194/acp-16-3099-2016> (2016).
- 828 DeMott, P. J., Y. Chen, S. M. Kreidenweis, D. C. Rogers, D. E. Sherman, Ice formation by black carbon
829 particles. *Geophysical Research Letters* 26, 2429–2432, <https://doi.org/10.1029/1999GL900580> (1999).
- 830 Derwent, R. G., W. J. Collins, C. E. Johnson, D. S. Stevenson, Transient behaviour of tropospheric ozone
831 precursors in a global 3-D CTM and their indirect greenhouse effects. *Climatic Change* 49, 463–487,
832 <https://doi.org/10.1023/A:1010648913655> (2001).
- 833 Dstan 91-91 “Turbine fuel, kerosene type, Jat A-1. Ministry of Defence, Defence Standard 91-91”, Issue
834 7, Amendment 3. Defence Equipment and Support (UK Defence Standardization, Glasgow, UK, 2015).
- 835 Ebbinghaus, A. and P. Wiesen, Aircraft fuels and their effects upon engine emissions. *Air and Space*
836 *Europe* 3, 101-103, [https://doi.org/10.1016/S1290-0958\(01\)90026-7](https://doi.org/10.1016/S1290-0958(01)90026-7) (2001).
- 837 Etminan, M., G. Myhre, E. J. Highwood, K. P. Shine, Radiative forcing of carbon dioxide, methane, and
838 nitrous oxide: A significant revision of the methane radiative forcing. *Geophysical Research Letters* 43,
839 12,614–12,623 <https://doi.org/10.1002/2016GL071930> (2016).
- 840 Faber, J., D. Greenwood, D. S. Lee, M. Mann, P. M. de Leon, D. Nelissen, B. Owen, M. Ralph, J. Tilston,
841 A. van Velzen, G. van de Vreede, “Lower NO_x at higher altitudes: policies to reduce the climate impact of
842 aviation NO_x emissions”. (CE-Delft, 08.7536.32, Delft, The Netherlands, 2008).
- 843 Fleming, G. and U. Ziegler, Environmental trends in aviation to 2050. In ‘ICAO Environmental Report,
844 2016’, International Civil Aviation Organization, Montreal. (2016) [https://www.icao.int/environmental-](https://www.icao.int/environmental-protection/Documents/EnvironmentalReports/2019/ENVReport2019_pg17-23.pdf)
845 [protection/Documents/EnvironmentalReports/2019/ENVReport2019_pg17-23.pdf](https://www.icao.int/environmental-protection/Documents/EnvironmentalReports/2019/ENVReport2019_pg17-23.pdf)
- 846 Fleming, G. and I. de Lepinay, “Environmental trends in aviation to 2050”, in ICAO Environmental
847 Report, 2019 Destination Green the Next Chapter, (ICAO Montreal, 2019),
848 [https://www.icao.int/environmental-](https://www.icao.int/environmental-protection/Documents/EnvironmentalReports/2019/ENVReport2019_pg17-23.pdf)
849 [protection/Documents/EnvironmentalReports/2019/ENVReport2019_pg17-23.pdf](https://www.icao.int/environmental-protection/Documents/EnvironmentalReports/2019/ENVReport2019_pg17-23.pdf) (2019)
- 850 Forster, P.M.d.F. and K. P. Shine, Radiative forcing and temperature trends from stratospheric ozone
851 changes. *Journal of Geophysical Research* 102, 10841–10855, <https://doi.org/10.1029/96JD03510>
852 (1997).
- 853 Forster, C., A. Stohl, P. James, V. Thouret, The residence times of aircraft emissions in the stratosphere
854 using a mean emission inventory and emissions along actual flight tracks. *Journal of Geophysical*
855 *Research Atmospheres* 108, 8524, <https://doi.org/10.1029/2002JD002515> (2003).

1 July 2020 Revised

- 856 Freeman, S., D. S. Lee, L. L. Lim, A. Skowron, R. R. De León, Trading off aircraft fuel burn and NO_x
857 emissions for optimal climate policy. *Environmental Science and Technology* 52, 2498–2505,
858 <https://doi.org/10.1021/acs.est.7b05719> (2018).
- 859 Friedlingstein, P., P. Cox, R. Betts, L. Bopp, W. von Bloh, V. Brovkin, P. Cadule, S. Doney, M. Eby, I.
860 Fung, G. Bala, J. John, C. Jones, F. Joos, T. Kato, M. Kawamiya, W. Knorr, K. Lindsay, H. D. Matthews,
861 T. Raddatz, P. Rayner, C. Reick, E. Roeckner, K.-G. Schnitzler, R. Schnur, K. Strassmann, A. J. Weaver,
862 C. Yoshikawa and N. Zeng, Climate-carbon cycle feedback analysis: Results from the C⁴MIP model
863 intercomparison, *Journal of Climate* 19, 3337–3353, <https://doi.org/10.1175/JCLI3800.1> (2006)
- 864 Frömming, C., M. Ponater, K. Dahlmann, V. Grewe, D. S. Lee, R. Sausen, Aviation-induced radiative
865 forcing and surface temperature change in dependency of the emission altitude. *Journal of Geophysical*
866 *Research Atmospheres* 117, 9717–9736, <https://doi.org/10.1029/2012JD018204> (2012).
- 867 Fuglestad, J. S. and T. Berntsen, “A simple model for scenario studies of changes in climate, Version
868 1.0”, (CICERO, Oslo, Norway, 1999) pp. 59, <https://cicero.oslo.no/no/publications/internal/326>.
- 869 Fuglestad, J. S., T. K. Berntsen, I. S. A. Isaksen, H. T. Mao, X. Z. Liang, W. C. Wang, Climatic forcing
870 of nitrogen oxides through changes in tropospheric ozone and methane; global 3D model studies.
871 *Atmospheric Environment* 33, 961–977 (1999).
- 872 Fuglestad, J., T. Berntsen, G. Myhre, K. Rypdal, R. B. Skeie Climate forcing from the transport sectors.
873 *Proceedings of the National Academy of Sciences U.S.A.* 105(2), 454-458,
874 <https://doi.org/10.1073/pnas.0702958104> (2008).
- 875 Fuglestad, J. S., T. Berntsen, V. Eyring, I. Isaksen, D. S. Lee, R. Sausen, Shipping emissions: from
876 cooling to warming of climate—and reducing impacts on health. *Environmental Science and Technology*
877 43, 9057–9062, <https://doi.org/10.1021/es901944r> (2009).
- 878 Fuglestad, J. S., K. P. Shine, T. Berntsen, J. Cook, D. S. Lee, A. Stenke, R. B. Skeie, G. J. M. Velders,
879 I. A. Waitz, Transport impacts on atmosphere and climate: Metrics. *Atmospheric Environment* 44, 4648–
880 4677, <https://doi.org/10.1016/j.atmosenv.2009.04.044> (2010).
- 881 Fuglestad, J., J. Rogelj, R. J. Millar, M. Allen, O. Boucher, M. Cain, P. M. Forster, E. Kriegler, D.
882 Shindell, Implications of possible interpretations of ‘greenhouse gas balance’ in the Paris Agreement.
883 *Philosophical Transactions of the Royal Society A* 376: 20160445.
884 <http://dx.doi.org/10.1098/rsta.2016.0445> (2018).
- 885 Gauss, M., I. S. A. Isaksen, S. Wong, W. C. Wang, Impact of H₂O emissions from cryoplanes and
886 kerosene aircraft on the atmosphere, *Journal of Geophysical Research Atmospheres* 108 (D10), 4304,
887 <https://doi.org/10.1029/2002JD002623> (2003).
- 888 Gettelman, A. and C. Chen, The climate impact of aviation aerosols. *Geophysical Research Letters* 40,
889 2785–2789, <https://doi.org/10.1002/grl.50520> (2013).
- 890 Gounou, A. and R. J. Hogan, A sensitivity study of the effect of horizontal photon transport on the
891 radiative forcing of contrails. *Journal of the Atmospheric Sciences* 64, 1706–1716,
892 <https://doi.org/10.1175/JAS3915.1> (2007).
- 893 Gottschaldt, K., C. Voigt, P. Jöckel, M. Righi, R. Deckert, S. Dietmüller, Global sensitivity of aviation
894 NO_x effects to the HNO₃-forming channel of the HO₂ + NO reaction. *Atmospheric Chemistry and Physics*
895 13, 3003–3025, <https://doi.org/10.5194/acp-13-3003-2013> (2013).
- 896 Grewe, V., and A. Stenke, AirClim: an efficient tool for climate evaluation of aircraft technology.
897 *Atmospheric Chemistry and Physics* 8, 4621–4639, <https://doi.org/10.5194/acp-8-4621-2008> (2008).

1 July 2020 Revised

- 898 Hansen, J., M. Sato, R. Ruedy, Radiative forcing and climate response. *Journal of Geophysical Research*
899 *Atmospheres* 102 (D6), 6831–6864, <https://doi.org/10.1029/96JD03436> (1997).
- 900 Hansen, J., and L. Nazarenko Soot climate forcing via snow and ice albedos. *Proceedings of the National*
901 *Academy of Sciences U.S.A.* 101, 423–428, <https://doi.org/10.1073/pnas.2237157100> (2004).
- 902 Hansen, J., M. Sato, R. Ruedy, L. Nazarenko, A. Lacis, G. A. Schmidt, G. Russell, I. Aleinov, M. Bauer,
903 S. Bauer, N. Bell, B. Cairns, V. Canuto, M. Chandler, Y. Cheng, A. Del Genio, G. Faluvegi, E. Fleming,
904 A. Friend, T. Hall, C. Jackman, M. Kelley, N. Kiang, D. Koch, J. Lean, J. Lerner, K. Lo, S. Menon, R.
905 Miller, P. Minnis, T. Novakov, V. Oinas, Ja. Perlwitz, Ju. Perlwitz, D. Rind, A. Romanou, D. Shindell, P.
906 Stone, S. Sun, N. Tausnev, D. Thresher, B. Wielicki, T. Wong, M. Yao, S. Zhang, Efficacy of climate
907 forcings. *Journal of Geophysical Research Atmospheres* 110, D18104.
908 <https://doi.org/10.1029/2005JD005776> (2005).
- 909 Hari, T. K., Z. Yaakob, N. Binitha, Aviation biofuel from renewable resources: routes, opportunities and
910 challenges. *Renewable and Sustainable Energy Reviews* 42, 1234–1244
911 <https://doi.org/10.1016/j.rser.2014.10.095> (2015).
- 912 Hasselmann K., S. Hasselmann, R. Giering, V. Ocana, H. von Storch, Sensitivity study of optimal CO₂
913 emission paths using a Simplified Structural Integrated Assessment Model (SIAM). *Climatic Change* 37,
914 345–386, <https://doi.org/10.1023/A:1005339625015> (1997).
- 915 Hendricks, J., B. Kärcher, U. Lohmann, Effects of ice nuclei on cirrus clouds in a global climate model.
916 *Journal of Geophysical Research Atmospheres* 116, 2156–2202, <https://doi.org/10.1029/2010JD015302>
917 (2011).
- 918 Hodnebrog, Ø., T. K. Berntsen, O. Dessens, M. Gauss, V. Grewe, I. S. A. Isaksen, B. Koffi, G. Myhre, D.
919 Olivié, M. J. Prather, J. A. Pyle, F. Stordal, S. Szopa, Q. Tang P. van Velthoven, J. E. Williams, K.
920 Ødemark, Future impact of non-land based traffic emissions on atmospheric ozone and OH – an
921 optimistic scenario and a possible mitigation strategy. *Atmospheric Chemistry and Physics* 11, 11,293–
922 11,317, <https://doi.org/10.5194/acp-11-11293-2011> (2011).
- 923 Hodnebrog, Ø., T. K. Berntsen, O. Dessens, M. Gauss, V. Grewe, I. S. A. Isaksen, B. Koffi, G. Myhre, D.
924 Olivié, M. J. Prather, F. Stordal, S. Szopa, Q. Tang, P. van Velthoven, J. E. Williams, Future impact of
925 traffic emissions on atmospheric ozone and OH based on two scenarios. *Atmospheric Chemistry and*
926 *Physics* 12, 12,211–12,225, <https://doi.org/10.5194/acp-12-12211-2012> (2012).
- 927 Holmes, C. D., Q. Tang, M. J. Prather, Uncertainties in climate assessment for the case of aviation
928 NO. *Proceedings of the National Academy of Science U.S.A.* 108(27), 10997–11002,
929 <https://doi.org/10.1073/pnas.1101458108> (2011).
- 930 Holmes, C. D., M. J. Prather, O. A. Søvde, G. Myhre, Future methane, hydroxyl, and their uncertainties:
931 key climate and emission parameters for future predictions. *Atmospheric Chemistry and Physics* 13, 285–
932 302, <https://doi.org/10.5194/acp-13-285-2013> (2013).
- 933 Hoor, P., J. Borken-Kleefeld, D. Caro, O. Dessens, O. Endresen, M. Gauss, V. Grewe, D. Hauglustaine, I.
934 S. A. Isaksen, P. Jöckel, J. Lelieveld, G. Myhre, E. Meijer, D. Olivié, M. Prather, C. Schnadt-Poberaj, K.
935 P. Shine, J. Staehelin, Q. Tang, J. van Aardenne, P. van Velthoven, R. Sausen, The impact of traffic
936 emissions on atmospheric ozone and OH: results from QUANTIFY. *Atmospheric Chemistry and Physics*
937 9, 3113–3136, <https://doi.org/10.5194/acp-9-3113-2009> (2009).
- 938 Hoose, C. and O. Möhler, Heterogeneous ice nucleation on atmospheric aerosols: a review of results from
939 laboratory experiments. *Atmospheric Chemistry and Physics* 12, 9817–9854, <https://doi.org/10.5194/acp-12-9817-2012> (2012).

1 July 2020 Revised

- 941 Hough, A. M., The development of a two-dimensional global tropospheric model – 1. The model
942 transport. *Atmospheric Environment* 23, 1235–1261, [https://doi.org/10.1016/0004-6981\(89\)90150-9](https://doi.org/10.1016/0004-6981(89)90150-9)
943 (1989).
- 944 Hough, A. M., Development of a two-dimensional global tropospheric model: model chemistry. *Journal*
945 *of Geophysical Research Atmospheres* 96, 7325–7362, <https://doi.org/10.1029/90JD01327> (1991).
- 946 Irvine, E. A., B. J. Hoskins, K. P. Shine, A Lagrangian analysis of ice-supersaturated air over the North
947 Atlantic. *Journal of Geophysical Research Atmospheres* 119, 90–100,
948 <https://doi.org/10.1002/2013JD020251> (2013).
- 949 IATA, Economic Performance of the Airline Industry.
950 [https://www.iata.org/contentassets/f88f0ceb28b64b7e9b46de44b917b98f/iata-economic-performance-of-](https://www.iata.org/contentassets/f88f0ceb28b64b7e9b46de44b917b98f/iata-economic-performance-of-the-industry-end-year-2018-report.pdf)
951 [the-industry-end-year-2018-report.pdf](https://www.iata.org/contentassets/f88f0ceb28b64b7e9b46de44b917b98f/iata-economic-performance-of-the-industry-end-year-2018-report.pdf) (2019).
- 952 IATA, Outlook for air travel in the next 5 years, [https://www.iata.org/en/iata-](https://www.iata.org/en/iata-repository/publications/economic-reports/covid-19-outlook-for-air-travel-in-the-next-5-years/)
953 [repository/publications/economic-reports/covid-19-outlook-for-air-travel-in-the-next-5-years/](https://www.iata.org/en/iata-repository/publications/economic-reports/covid-19-outlook-for-air-travel-in-the-next-5-years/) (2020)
- 954 ICAO (2018) ICAO Carbon Emissions Calculator Methodology, version 11, June 2018,
955 ([https://www.icao.int/environmental-](https://www.icao.int/environmental-protection/CarbonOffset/Documents/Methodology%20ICAO%20Carbon%20Calculator_v11-2018.pdf)
956 [protection/CarbonOffset/Documents/Methodology%20ICAO%20Carbon%20Calculator_v11-2018.pdf](https://www.icao.int/environmental-protection/CarbonOffset/Documents/Methodology%20ICAO%20Carbon%20Calculator_v11-2018.pdf))
957 accessed 19-05-2020.
- 958 ICAO, ‘Destination Green the Next Chapter’, ICAO Environmental Report, Montreal,
959 [https://www.icao.int/environmental-protection/Documents/ICAO-ENV-Report2019-F1-WEB%20\(1\).pdf](https://www.icao.int/environmental-protection/Documents/ICAO-ENV-Report2019-F1-WEB%20(1).pdf)
960 (2019).
- 961 IEA, International Energy Agency. International Energy Agency Oil Information, 1960-2017. [data
962 collection]. 12th Edition. UK Data Service. SN: 5187, <http://doi.org/10.5257/iea/oil/2019-1> (2019).
- 963 IPCC (1999), “*Aviation and the Global Atmosphere*”, Intergovernmental Panel on Climate Change
964 Special Report, J. E. Penner, D. H. Lister, D. J. Griggs, D. J. Dokken, M. McFarland, Eds. (Cambridge
965 University Press, Cambridge, UK, 1999) [https://www.ipcc.ch/report/aviation-and-the-global-atmosphere-](https://www.ipcc.ch/report/aviation-and-the-global-atmosphere-2/)
966 [2/](https://www.ipcc.ch/report/aviation-and-the-global-atmosphere-2/).
- 967 IPCC (2001) “Climate Change 2001: The Scientific Basis. Contribution of Working Group I to the Third
968 Assessment Report of the Intergovernmental Panel on Climate Change”. J.T. Houghton, Y. Ding, D.J.
969 Griggs, M. Noguer, P.J. van der Linden, X. Dai, K. Maskell and C.A. Johnson (eds). Cambridge
970 University Press, UK. https://www.ipcc.ch/site/assets/uploads/2018/07/WG1_TAR_FM.pdf
- 971 IPCC (2007), “Climate change 2007. “Mitigation of climate change”, in: Contribution of Working Group
972 III to the Fourth Assessment Report of the Intergovernmental Panel on Climate Change”, B. Metz, O. R.
973 Davidson, P. R. Bosch, R. Dave, L. A. Meyer, eds (Cambridge University Press, UK)
974 <https://www.ipcc.ch/report/ar4/wg3/>
- 975 IPCC (2013) “Climate Change 2013: The Physical Science Basis, Contribution of Working Group I to the
976 Fifth Assessment Report of the Intergovernmental Panel on Climate Change”, T. F. Stocker, D. Qin, G. -
977 K. Plattner, M. Tignor, S. K. Allen, J. Boschung, A. Nauels, Y. Xia, V. Bex, P. M. Midgley, Eds.
978 (Cambridge University Press, Cambridge, United Kingdom and New York, NY, USA, 2013).
979 <https://www.ipcc.ch/report/ar5/wg1/>
- 980 IPCC (2018) “Global Warming of 1.5°C. An IPCC Special Report on the impacts of global warming of
981 1.5°C above pre-industrial levels and related global greenhouse gas emission pathways, in the context of
982 strengthening the global response to the threat of climate change, sustainable development, and efforts to
983 eradicate poverty”, Masson-Delmotte, V., P. Zhai, H.-O. Pörtner, D. Roberts, J. Skea, P.R. Shukla, A.
984 Pirani, W. Moufouma-Okia, C. Péan, R. Pidcock, S. Connors, J.B.R. Matthews, Y. Chen, X. Zhou, M.I.

1 July 2020 Revised

- 985 Gomis, E. Lonnoy, T. Maycock, M. Tignor, and T. Waterfield (eds), (2018).
986 <https://www.ipcc.ch/sr15/download/>
- 987 Joos, F., M. Bruno, R. Fink, T. F. Stocker, U. Siegenthaler, C. LeQuéré, J. L. Sarmiento, J.L., An efficient
988 and accurate representation of complex oceanic and biospheric models for anthropogenic carbon uptake.
989 *Tellus* 48B, 397e417, <https://doi.org/10.1034/j.1600-0889.1996.t01-2-00006.x> (1996)
- 990 Joos, F., R. Roth, J. S. Fuglestedt, G. P. Peters, I. G. Enting, W. von Bloh, V. Brovkin, E. J. Burke, M.
991 Eby, N. R. Edwards, T. Friedrich, T. L. Frolicher, P. R. Halloran, P. B. Holden, C. Jones, T. Kleinen, F. T.
992 Mackenzie, K. Matsumoto, M. Meinshausen, G.-K. Plattner, A. Reisinger, J. Segschneider, G. Shaffer,
993 M. Steinacher, K. Strassmann, K. Tanaka, A. Timmermann, A. J. Weaver, Carbon dioxide and climate
994 impulse response functions for the computation of greenhouse gas metrics: a multi-model analysis.
995 *Atmospheric Chemistry and Physics* 13, 2793–2825, <https://doi.org/10.5194/acp-13-2793-2013> (2013).
- 996 Kapadia, Z. Z., D. V. Spracklen, S. R. Arnold, D. J. Borman, G. W. Mann, K. J. Pringle, S. A. Monks, C.
997 L. Reddington, F. Benduhn, A. Rap, C. E. Scott, E. W. Butt, M. Yoshioka, Impacts of aviation fuel sulfur
998 content on climate and human health. *Atmospheric Chemistry and Physics* 16, 10521–10541,
999 <https://doi.org/10.5194/acp-16-10521-2016> (2016).
- 1000 Kärcher, B., U. Burkhardt, A. Bier, L. Bock, I. J. Ford, The microphysical pathway to contrail formation.
1001 *Journal of Geophysical Research Atmospheres* 120, 7893–7927, <https://doi.org/10.1002/2015JD023491>
1002 (2015).
- 1003 Kärcher, B. Formation and radiative forcing of contrail cirrus. *Nature Communications* 9:1824,
1004 <https://doi.org/10.1038/s41467-018-04068-0> (2018).
- 1005 Khodayari, A., D. J. Wuebbles, S. Olsen, J. S. Fuglestedt, T. Berntsen, M. T. Lund, I. Waitz, P. Wolfe,
1006 P. M. Forster, M. Meinshausen, D. S. Lee, L. L. Lim, Intercomparison of the capabilities of simplified
1007 climate models to project the effects of aviation CO₂ on climate. *Atmospheric Environment* 75, 321–328,
1008 <https://doi.org/10.1016/j.atmosenv.2013.03.055> (2013).
- 1009 Khodayari, A., S. C. Olsen, D. J. Wuebbles, Evaluation of aviation NO_x-induced radiative forcings for
1010 2005 and 2050. *Atmospheric Environment* 91, 95–103, <https://doi.org/10.1016/j.atmosenv.2014.03.044>
1011 (2014a).
- 1012 Khodayari, A., S. Tilmes, S. C. Olsen, D. B. Phoenix, D. J. Wuebbles, J.-F. Lamarque, C.-C. Chen,
1013 Aviation 2006 NO_x-induced effects on atmospheric ozone and HO_x in Community Earth System Model
1014 (CESM). *Atmospheric Chemistry and Physics* 14, 9925–9939, <https://doi.org/10.5194/acp-14-9925-2014>
1015 (2014b).
- 1016 Köhler, M. O., G. Rädcl, O. Dessens, K. P. Shine, H. L. Rogers, O. Wild, J. A. Pyle, Impact of
1017 perturbation of nitrogen oxide emissions from global aviation *Journal of Geophysical Research*
1018 *Atmospheres* 113, D11305, <https://doi.org/10.1029/2007JD009140> (2008).
- 1019 Köhler, M. O., G. Rädcl, K. P. Shine, H. L. Rogers, J. A. Pyle, Latitudinal variation of the effect of
1020 aviation NO_x emissions on atmospheric ozone and methane and related climate metrics. *Atmospheric*
1021 *Environment* 64, 1–9, <https://doi.org/10.1016/j.atmosenv.2012.09.013> (2013).
- 1022 Lamarque, J.-F., T. C. Bond, V. Eyring, C. Granier, A. Heil, Z. Klimont, D. Lee, C. Liou, A. Mieville,
1023 B. Owen, M. G. Schultz, D. Shindell, S. J. Smith, E. Stehfest, J. van Aardenne, O. R. Cooper, M.
1024 Kainuma, N. Mahowald, J. R. McConnell, V. Naik, K. Riahi, D. P. van Vuuren, Historical (1850–2000)
1025 gridded anthropogenic and biomass burning emissions of reactive gases and aerosols: methodology and
1026 application. *Atmospheric Chemistry and Physics* 10, 7017–7039, [https://doi.org/10.5194/acp-10-7017-](https://doi.org/10.5194/acp-10-7017-2010)
1027 2010 (2010).

1 July 2020 Revised

- 1028 Lamquin, N., C. J. Stubenrauch, K. Gierens, U. Burkhardt, H. Smit, A global climatology of upper
1029 tropospheric ice supersaturation occurrence inferred from the Atmospheric Infrared Sounder calibrated by
1030 MOZAIC. *Atmospheric Chemistry and Physics* 12, 381–405, <https://doi.org/10.5194/acp-12-381-2012>
1031 (2012).
- 1032 Lauder, A. R., I. G. Enting, J. O. Carter, N. Clisby, A. L. Cowie, B. K. Henry, M. R. Raupach, Offsetting
1033 methane emissions — An alternative to emission equivalence metrics. *International Journal of*
1034 *Greenhouse Gas Control* 12, 419–429, <https://doi.org/10.1016/j.ijggc.2012.11.028> (2012).
- 1035 Lee, D. S., D. Fahey, P. M. Forster, P. J. Newton, R. C. N. Wit, L. L. Lim, B. Owen, R. Sausen, Aviation
1036 and global climate change in the 21st century. *Atmospheric Environment* 43, 3520–3537
1037 <https://doi.org/10.1016/j.atmosenv.2009.04.024> (2009).
- 1038 Lee, D. S., G. Pitari, V. Grewe, K. Gierens, J. E. Penner, A. Petzold, M. Prather, U. Schumann, A. Bais,
1039 T. Berntsen, D. Iachetti, L. L. Lim, R. Sausen, Transport impacts on atmosphere and climate: Aviation.
1040 *Atmospheric Environment* 44, 4678–4734, <https://doi.org/10.1016/j.atmosenv.2009.06.005> (2010).
- 1041 Le Quéré, C. and 76 others, Global carbon budget 2018. *Earth System Science Data* 10, 2141–2194,
1042 <https://doi.org/10.5194/essd-10-2141-2018> (2018).
- 1043 Le Quéré, C., R. B. Jackson, M. W. Jones, A. J. P. Smith, S. Abernethy, R. M. Andrew, A. J. De-Goll, D.
1044 R. Willis, Y. Shan, J. G. Canadell, P. Friedlingstein, F. Creutzig and G. P. Peters, Temporary reduction in
1045 daily global CO₂ emissions during the COVID-19 forced confinement, *Nature Climate Change*,
1046 <https://doi.org/10.1038/s41558-020-0797-x> (2020).
- 1047 Lim, L. L., D. S. Lee, B. Owen, A. Skowron, S. Matthes, U. Burkhardt, S. Dietmuller, G. Pitari, G. Di
1048 Genova, D. Iachetti, I. Isaksen, O. A. Søvde, REACT4C: Simplified mitigation study. TAC-4
1049 Proceedings, June 22nd to 25th, 2015, Bad Kohlgrub, 181–185,
1050 https://www.pa.op.dlr.de/tac/2015/Proceedings_of_TAC4_conference_final.pdf (2015).
- 1051 Liou, K. N., Y. Takano, Q. Yue, P. Yang, On the radiative forcing of contrail cirrus contaminated by
1052 black carbon. *Geophysical Research Letters* 40, 778–784, <https://doi.org/10.1002/GRL.50110> (2013).
- 1053 Lund, M. T., B. Aamaas, T. Berntsen, L. Bock, U. Burkhardt, J. S. Fuglestedt, K. P. Shine, Emission
1054 metrics for quantifying regional climate impacts of aviation. *Earth System Dynamics* 8, 547–563,
1055 <https://doi.org/10.5194/esd-8-547-2017> (2017).
- 1056 Mahrt, F., K. Kilchhofer, C. Marcolli, P. Grönquist, R. O. David, M. Rösch, U. Lohmann, Z. A. Kanji,
1057 The impact of cloud processing on the ice nucleation abilities of soot particles at cirrus temperatures.
1058 *Journal of Geophysical Research* 125, e2019JD030922, <https://doi.org/10.1029/2019JD030922> (2020).
- 1059 Maier-Reimer, E. and K. Hasselmann, Transport and storage of CO₂ in the ocean—An inorganic ocean-
1060 circulation carbon cycle model. *Climate Dynamics* 2, 63–90, <https://doi.org/10.1007/BF01054491> (1987).
- 1061 Matthes, M., V. Grewe, K. Dahlmann, C. Frömming, E. Irvine, L. Lim, F. Linke, B. Lührs, B. Owen, K.
1062 Shine, S. Stromatas, H. Yamashita, F. Yin, A concept for multi-criteria environmental assessment of
1063 aircraft trajectories. *Aerospace* 4 42, <https://doi.org/10.3390/aerospace4030042> (2017).
- 1064 Markowicz, K. M. and M. L. Witek, Simulations of contrail optical properties and radiative forcing for
1065 various crystal shapes. *Journal of Applied Meteorology and Climatology* 50, 1740–1755,
1066 <https://doi.org/10.1175/2011JAMC2618.1> (2011).
- 1067 Marquart, S., R. Sausen, M. Ponater, V. Grewe, Estimate of the climate impact of the cryoplanes,
1068 *Aerospace Science and Technology*, 5, 73–84, [https://doi.org/10.1016/S1270-9638\(00\)01084-1](https://doi.org/10.1016/S1270-9638(00)01084-1) (2001).
- 1069 Mastrandrea, M. D., K. J. Mach, G. K. Plattner, O. Edenhofer, T. F. Stocker, C. B. Field, K. L. Ebi, P. R.
1070 Matschoss, The IPCC AR5 guidance note on consistent treatment of uncertainties: a common approach

1 July 2020 Revised

- 1071 across the working groups. *Climatic Change* 108, 675–691, <https://doi.org/10.1007/s10584-011-0178-6>
1072 (2011).
- 1073 Meinshausen, M., S. J. Smith, K. Calvin, J. S. Daniel, M. L. T. Kainuma, J. -F. Lamarque, K. Matsumoto,
1074 S. A. Montzka, S. C. B. Raper, K. Riahi, A. Thomson, G. J. M. Velders, D. P. P. van Vuuren, The RCP
1075 greenhouse gas concentrations and their extensions from 1765 to 2300. *Climatic Change* 109, 213–241,
1076 <https://doi.org/10.1007/s10584-011-0156-z> (2011).
- 1077 Millar, R. J., Z. R. Nicholls, P. Friedlingstein, M. R. Allen, A modified impulse-response representation
1078 of the global near-surface air temperature and atmospheric concentration response to carbon dioxide
1079 emissions. *Atmospheric Chemistry and Physics*. 17, 7213–7228, [https://doi.org/10.5194/acp-17-7213-](https://doi.org/10.5194/acp-17-7213-2017)
1080 2017 (2017).
- 1081 Miller, M., P. Brook and C. Eyers, Reduction of Sulphur limits in aviation fuel standards (SULPHUR).
1082 EASA research project EASA.2008/C11, European Aviation Safety Agency. (2010)
1083 [https://www.easa.europa.eu/sites/default/files/dfu/2009-SULPHUR-](https://www.easa.europa.eu/sites/default/files/dfu/2009-SULPHUR-Reduction%20of%20sulphur%20limits%20in%20aviation%20fuel%20standards-Final%20Report.pdf)
1084 [Reduction%20of%20sulphur%20limits%20in%20aviation%20fuel%20standards-Final%20Report.pdf](https://www.easa.europa.eu/sites/default/files/dfu/2009-SULPHUR-Reduction%20of%20sulphur%20limits%20in%20aviation%20fuel%20standards-Final%20Report.pdf)
- 1085 Minnis, P., S. T. Bedka, D. P. Duda, K. M. Bedka, T. Chee, J. K. Ayers, R. Palikonda, D. A.
1086 Spangenberg, K. V. Khlopenkov, R. Boeke, Linear contrail and contrail cirrus properties determined from
1087 satellite data. *Geophysical Research Letters*, 40, 3220–3226, <https://doi.org/10.1002/grl.50569> (2013).
- 1088 Möhler, O., S. Büttner, C. Linke, M. Schnaiter, H. Saathof, O. Stetzer, R. Wagner, M. Krämer, A.
1089 Mangold, V. Ebert, U. Schurath, Effect of sulfuric acid coating on heterogenous ice nucleation by soot
1090 aerosol particles. *Journal of Geophysical Research* 110 (D11), <https://doi.org/10.1029/2004JD005169>
1091 (2005).
- 1092 Montzka, S. A., C. M. Spivakovsky, J. H. Butler, J. W. Elkins, L. T. Lock, D. J. Mondeel, New
1093 observational constraints for atmospheric hydroxyl on global and hemispherical scales. *Science* 288, 500–
1094 503, <https://doi.org/10.1126/science.288.5465.500> (2000).
- 1095 Moore, R. H., K. L. Thornhill, B. Weinzierl, D. Sauer, E. D'Ascoli, J. Kim, et al., Biofuel blending
1096 reduces particle emissions from aircraft engines at cruise conditions. *Nature*, 543, 411–415,
1097 <https://doi.org/10.1038/nature21420> (2017)
- 1098 Myhre, G., J. S. Nilsen, L. Gulstad, K. P. Shine, B. Rognerud, I. S. A. Isaksen, Radiative forcing due to
1099 stratospheric water vapor from CH₄ oxidation. *Geophysical Research Letters* 34, L01807,
1100 <https://doi.org/10.1029/2006GL027472> (2007).
- 1101 Myhre, G., M. Kvalevåg, G. Rädcl, J. Cook, K. P. Shine, H. Clark, F. Karcher, K. Markowicz, A. Kardas,
1102 P. Wolkenberg, Y. Balkanski, M. Ponater, P. Forster, A. Rap, R. R. de Leon, Intercomparison of
1103 radiative forcing calculations of stratospheric water vapour and contrails. *Meteorologische Zeitschrift* 18,
1104 585–596, <https://doi.org/10.1127/0941-2948/2009/0411> (2009).
- 1105 Myhre, G., K. P. Shine, G. Rädcl, M. Gauss, I. S. A. Isaksen, Q. Tang, M. J. Prather, J. E. Williams, P.
1106 van Velthoven, O. Dessens, B. Koffi, S. Szopa, P. Hoor, V. Grewe, J. Borken-Kleefeld, T. K. Berntsen, J.
1107 S. Fuglestvedt, Radiative forcing due to changes in ozone and methane caused by the transport sector.
1108 *Atmospheric Environment* 45, 387–394, <https://doi.org/10.1016/j.atmosenv.2010.10.001> (2011).
- 1109 Myhre, G., D. Shindell, F. -M Breon, W. Collins, J. Fuglestvedt, J. Huang, D. Koch, J. -F. Lamarque, D.
1110 Lee., B. Mendoza, T. Nakajima, A. Robock, G. Stephens, T. Takemura, H. Zhang, “Anthropogenic and
1111 Natural Radiative Forcing” in *Climate Change 2013: the Physical Science Basis, Contribution of*
1112 *Working Group I to the Fifth Assessment Report of the Intergovernmental Panel on Climate Change,*
1113 (Cambridge University Press, 2013). <https://www.ipcc.ch/report/ar5/wg1/>

1 July 2020 Revised

- 1114 Newinger, C. and U. Burkhardt, Sensitivity of contrail cirrus radiative forcing to air traffic scheduling.
1115 *Journal of Geophysical Research Atmospheres* 117, D10205, <https://doi.org/10.1029/2011JD016736>
1116 (2012).
- 1117 OECD, Green growth and the future of aviation. Paper prepared for the 27th Round Table on Sustainable
1118 Development held at OECD Headquarters 23-24 January 2012 (OECD 2012). [https://www.oecd.org/sd-](https://www.oecd.org/sd-roundtable/papersandpublications/49482790.pdf)
1119 [roundtable/papersandpublications/49482790.pdf](https://www.oecd.org/sd-roundtable/papersandpublications/49482790.pdf)
- 1120 Olivié, D. J. L., D. Cariolle, H. Teyssèdre, D. Salas, A. Voltaire, H. Clark, D. Saint-Martin, M. Michou,
1121 F. Karcher, Y. Balkanski, M. Gauss, O. Dessens, B. Koffi, R. Sausen, Modeling the climate impact of
1122 road transport, maritime shipping and aviation over the period 1860–2100 with an AOGCM. *Atmospheric*
1123 *Chemistry and Physics* 12, 1449–1480, <https://doi.org/10.5194/acp-12-1449-2012> (2012).
- 1124 Olsen, S. C., G. P. Brasseur, D. J. Wuebbles, S. R. H. Barrett, H. Dang, S. D. Eastham, M. Z. Jacobson,
1125 A. Khodayari, H. Selkirk, A. Sokolov, N. Unger, Comparison of model estimates of the effects of
1126 aviation emissions on atmospheric ozone and methane. *Geophysical Research Letters* 40, 6004–6009,
1127 <https://doi.org/10.1002/2013GL057660> (2013).
- 1128 Penner, J.E., Y. Chen, M. Wang, and X. Liu, Possible influence of anthropogenic aerosols on cirrus
1129 clouds and anthropogenic forcing. *Atmospheric Chemistry and Physics*, 9, 879–96,
1130 <https://doi.org/10.5194/acp-9-879-2009> (2009).
- 1131 Penner, J. E., C. Zhou, A. Garnier, D. L. Mitchell, Anthropogenic aerosol indirect effects in cirrus clouds.
1132 *Journal of Geophysical Research Atmospheres*, 123, 11,652–11,677,
1133 <https://doi.org/10.1029/2018JD029204> (2018).
- 1134 Petzold, A., M. Gysel, X. Vancassel, R. Hitzenberger, H. Puxbaum, S. Vrochticky, E. Weingartner, U.
1135 Baltensperger, P. Mirabel, On the effects of organic matter and sulphur-containing compounds on the
1136 CCN activation of combustion particles. *Atmospheric Chemistry and Physics* 5, 3187–3203,
1137 <https://doi.org/10.5194/acp-5-3187-2005> (2005).
- 1138 Pitari, G., D. Iachetti, G. Genova, N. De Luca, O. A. Søvde, Ø. Hodnebrog, D. S. Lee, L. L. Lim, Impact
1139 of coupled NO_x/aerosol aircraft emissions on ozone photochemistry and radiative forcing. *Atmosphere* 6,
1140 751–782, <https://doi.org/10.3390/atmos6060751> (2015).
- 1141 Pitari, G., I. Cionni, G. Di Genova, O. A. Søvde, L. Lim, Radiative forcing from aircraft emissions of
1142 NO_x: model calculations with CH₄ surface flux boundary condition. *Meteorologische Zeitschrift* 26(6),
1143 663-687, <https://doi.org/10.1127/metz/2016/0776> (2017).
- 1144 Pomroy, H. R. and J. A. Illingworth, Ice cloud inhomogeneity: Quantifying bias in emissivity from radar
1145 observations. *Geophysical Research Letters* 27, 2101–2104, <https://doi.org/10.1029/1999GL011149>
1146 (2000).
- 1147 Ponater, M., S. Marquart, R. Sausen, U. Schumann, On contrail climate sensitivity. *Geophysical Research*
1148 *Letters* 32, L10706, <https://doi.org/10.1029/2005GL022580> (2005).
- 1149 Ponater, M., S. Pechtl, R. Sausen, U. Schumann, G. Hüttig, Potential of the cryoplane technology to
1150 reduce aircraft climate impact: a state-of-the-art assessment. *Atmospheric Environment* 40, 6928-6944,
1151 <https://doi.org/10.1016/j.atmosenv.2006.06.036> (2006).
- 1152 Ponater, M., M. Bickel, L. Bock, and U. Burkhardt, Towards determining the efficacy of contrail cirrus.
1153 In Matthes, S. and A. Blum, Making Aviation Environmentally Sustainable, 3rd ECATS Conference,
1154 Book of Abstracts, Volume 1. ISBN 978-1-910029-58-9. 51-44 (2020). ([http://www.ecats-](http://www.ecats-network.eu/uploads/2020/06/ECATS_Main_BookOfAbstracts_Vol1_final.pdf)
1155 [network.eu/uploads/2020/06/ECATS_Main_BookOfAbstracts_Vol1_final.pdf](http://www.ecats-network.eu/uploads/2020/06/ECATS_Main_BookOfAbstracts_Vol1_final.pdf))

1 July 2020 Revised

- 1156 Prather, M. J., Lifetimes and eigenstates in atmospheric chemistry. *Geophysical Research Letters* 21,
1157 801–804, <https://doi.org/10.1029/94GL00840> (1994).
- 1158 Prather, M., D. Ehhalt, F. Dentener, R. Derwent, E. Dlugokencky E, “Atmospheric chemistry and
1159 greenhouse gases”, in *Climate Change 2001: The Scientific Basis, Contribution of Working Group I to*
1160 *the Third Assessment Report of the Intergovernmental Panel on Climate Change*, J. T. Houghton ed.
1161 (Cambridge University Press, Cambridge, United Kingdom and New York, NY, USA, 2001) pp. 239–
1162 287. <https://www.ipcc.ch/site/assets/uploads/2018/03/TAR-04.pdf>
- 1163 Prather, M. J., C. D. Holmes, J. Hsu, Reactive greenhouse gas scenarios: Systematic exploration of
1164 uncertainties and the role of atmospheric chemistry, *Geophysical Research Letters*, 39, L09803,
1165 <https://doi.org/10.1029/2012GL051440> (2012).
- 1166 Rap, A., P. M. Forster, J. M. Haywood, A. Jones, O. Boucher, Estimating the climate impact of linear
1167 contrails using the UK Met Office climate model. *Geophysical Research Letters* 37, L20703,
1168 <https://doi.org/10.1029/2010GL045161> (2010).
- 1169 Revelle, R. and H. E. Suess, Carbon dioxide exchange between atmosphere and ocean and the question of
1170 an increase of atmospheric CO₂ during the past decades, *Tellus*, 9, 18–27, [https://doi.org/10.1111/j.2153-](https://doi.org/10.1111/j.2153-3490.1957.tb01849.x)
1171 [3490.1957.tb01849.x](https://doi.org/10.1111/j.2153-3490.1957.tb01849.x) (1957).
- 1172 Richardson, T. B., P.M. Forster, C. J. Smith, A. C. Maycock, T. Wood, T. Andrews, O. Boucher, G.
1173 Faluvegi, D. Fläschner, Ø. Hodnegrog, M. Kasoar, A. Kirkevåg, J.-F. Lamarque, J. Mülmenstädt, G.
1174 Myhre, D. Olivíe, R. W. Portmann, B. H. Samset, D. Shawki, D. Shindell, P. Stier, T. Takemura, A.
1175 Voulgarakis, D. Watson-Parris, Efficacy of climate forcings in PDRMIP models. *Journal of Geophysical*
1176 *Research: Atmospheres* 124, <https://doi.org/10.1029/2019JD030581>
- 1177 Righi, M., J. Hendricks, R. Sausen, The global impact of the transport sectors on atmospheric aerosol:
1178 simulations for year 2000 emissions. *Atmospheric Chemistry and Physics* 13, 9939–9970,
1179 <https://doi.org/10.5194/acp-13-9939-2013> (2013).
- 1180 Sander, S. P., R. R. Friedl, A. R. Ravishankara, D. M. Golden, C. E. Kolb, M. J. Kurylo, M. J. Molina, G.
1181 K. Moortgat, B. J. Finlayson-Pitts, “Chemical Kinetics and Photochemical Data for Use in Atmospheric
1182 Studies”, (JPL Publ. 06-2, No. 15, 2006). https://jpldataeval.jpl.nasa.gov/pdf/JPL_02-25_rev02.pdf
- 1183 Sausen R. and U. Schumann, Estimates of the climate response to aircraft CO₂ and NO_x emissions
1184 scenarios. *Climatic Change* 44, 27–58 (2000).
- 1185 Sausen, R. I. Isaksen, V. Grewe, D. Hauglustaine, D. S. Lee, G. Myhre, M. O. Köhler, G. Pitari, U.
1186 Schumann, F. Stordal, C. Zerefos, Aviation radiative forcing in 2000: An update on IPCC (1999).
1187 *Meteorologische Zeitschrift* 14, 555–561, <https://doi.org/10.1127/0941-2948/2005/0049> (2005).
- 1188 Schumann, U., J. E. Penner, Y. Chen, C. Zhou, K. Graf, Dehydration effects from contrails in a coupled
1189 contrail-climate model. *Atmospheric Chemistry and Physics* 15, 11179–11199,
1190 <https://doi.org/10.5194/acp-15-11179-2015> (2015).
- 1191 Schumann, U., R. Baumann, D. Baumgardner, S. T. Bedka, D. P. Duda, V. Freudenthaler, J.-F. Gayet, A.
1192 J. Heymsfield, P. Minnis, M. Quante, E. Raschke, H. Schlager, M. Vázquez-Navarro, C. Voigt, Z. Wang,
1193 Properties of individual contrails: a compilation of observations and some comparisons. *Atmospheric*
1194 *Chemistry and Physics* 17, 403–438, <https://doi.org/10.5194/acp-17-403-2017> (2017a).
- 1195 Schumann, U., C. Kiemle, H. Schlager, R. Weigel, S. Bormann, F. D’Amato, M. Krämer, R. Matthey, A.
1196 Protat, C. Voigt, C. M. Volk, Long-lived contrails and convective cirrus above the tropical tropopause.
1197 *Atmospheric Chemistry and Physics* 17, 2311–2346, <https://doi.org/10.5194/acp-17-2311-2017> (2017b).

1 July 2020 Revised

- 1198 Shine, K. P., J.S. Fuglestedt, K. Hailemariam, N. Stuber, Alternatives to the global warming potential
1199 for comparing climate impacts of emissions of greenhouse gases. *Climatic Change* 68, 281–302,
1200 <https://doi.org/10.1007/s10584-005-1146-9> (2005).
- 1201
- 1202 Skeie, R. B., J. Fuglestedt, T. Berntsen, G. P. Peters, R. Andrew, M. Allen, S. Kallbekken, Perspective
1203 has a strong effect on the calculation of historical contributions to global warming. *Environmental*
1204 *Research Letters* 12, 024022, <https://doi.org/10.1088/1748-9326/aa5b0a> (2017).
- 1205 Skowron, A., D. S. Lee, J. Hurley, “Aviation NO_x Global Warming Potential”, in 2nd International
1206 Conference on Transport, Atmosphere and Climate, 25-28 June 2009, Aachen/Maastricht,
1207 Germany/Netherlands, <https://www.pa.op.dlr.de/tac/2009/proceedings/FB2010-10.pdf> (2009).
- 1208 Skowron, A., D. S. Lee, R. R. de León, The assessment of the impact of aviation NO_x on ozone and other
1209 radiative forcing responses—The importance of representing cruise altitudes accurately. *Atmospheric*
1210 *Environment* 74, 159–168, <https://doi.org/10.1016/j.atmosenv.2013.03.034> (2013).
- 1211 Skowron, A., D. S. Lee, R. R. de León, Variation of radiative forcings and global warming potentials
1212 from regional aviation NO_x emissions. *Atmospheric Environment* 104, 69–78,
1213 <https://doi.org/10.1016/j.atmosenv.2014.12.043> (2015).
- 1214 Søvde, O. A., S. Matthes, A. Skowron, D. Iachetti, L. Lim, B. Owen, Ø. Hodnebrog, G. Di Genova, G.
1215 Pitari, D. S. Lee, G. Myhre, I. S. A. Isaksen, Aircraft emission mitigation by changing route altitude: A
1216 multi-model estimate of aircraft NO_x emission impact on O₃ photochemistry. *Atmospheric Environment*
1217 95, 468–479, <https://doi.org/10.1016/j.atmosenv.2014.06.049> (2014).
- 1218 Smith, C. J., R. J. Kramer, G. Myhre, P. M. Forster, B. J. Soden, T. Andrews, O. Boucher, G. Faluvegi,
1219 D. Fläschner, Ø. Hodnebrog, M. Kasoar, V. Kharin, A. Kirkevåg, J.-F. Lamarque, J. Mülmenstädt, D.
1220 Olivié, T. Richardson, B. H. Samset, D. Shindell, P. Stier, T. Takemura, A. Voulgarakis, D. Watson-
1221 Parris, Understanding rapid adjustments to diverse forcing agents. *Geophysical Research Letters* 45,
1222 doi:10.1029/2018GL079826 (2018)
- 1223 Stevenson, D. S., C. E. Johnson, W. J. Collins, R. G. Derwent, K. P. Shine, J. M. Edwards, Evolution of
1224 tropospheric ozone radiative forcing. *Geophysical Research Letters* 25, 3819–3822,
1225 <https://doi.org/10.1029/1998GL900037> (1998).
- 1226 Stevenson, D. S., R. M. Doherty, M. G. Sanderson, W. J. Collins, C. E. Johnson, R. G. Derwent,
1227 Radiative forcing from aircraft NO_x emissions: mechanisms and seasonal dependence *Journal of*
1228 *Geophysical Research Atmospheres* 109, D17307, <https://doi.org/10.1029/2004JD004759> (2004).
- 1229 Stordal, F., M. Gauss, G. Myhre, E. Mancini, D. A. Hauglustaine, M. O. Köhler, T. Berntsen, E. J. G.
1230 Stordal, D. Iachetti, G. Pitari, I. S. A. Isaksen, TRADEOFFs in climate effects through aircraft routing:
1231 forcing due to radiatively active gases. *Atmospheric Chemistry and Physics Discussions* 6, 10733–10771
1232 (2006).
- 1233 Stuber, N., M. Ponater, R. Sausen, Why radiative forcing might fail as a predictor of climate change.
1234 *Climate Dynamics* 24, 497–510 doi:10.1007/s00382-004-0497-7 (2005).
- 1235 Stuber, N., P. Forster, G. Rädcl, K. Shine, The importance of the diurnal and annual cycle of air traffic for
1236 contrail radiative forcing. *Nature* 441, 864–867, <https://doi.org/10.1038/nature04877> (2006).
- 1237 Teoh, R., M. E. J. Stettler, A. Majumdar, U. Schumann, B. Graves, A. M. Boies, A methodology to relate
1238 black carbon particle number and mass emissions. *Journal of Aerosol Science* 132, 44–59,
1239 <https://doi.org/10.1016/j.jaerosci.2019.03.00> (2019).

1 July 2020 Revised

- 1240 Teoh, R., Schumann, U., Majumdar, A., Stettler, M. E. J., Mitigating the climate forcing of aircraft
1241 contrails by small-scale diversions and technology adoption. *Environmental Science and Technology*, 54
1242 2941–2950, doi: 10.1021/acs.est.9b05608.
- 1243 Tesche, M., P. Achtert, P. Glantz, K. J. Noone, Aviation effects on already-existing cirrus clouds. *Nature*
1244 *Communications* 7, 12016, <https://doi.org/10.1038/ncomms12016> (2016).
- 1245 UKDS (2016) http://stats.ukdataservice.ac.uk/index.aspx?r=349678&DataSetCode=IEA_COAL_BA,
1246 2016.
- 1247 UNFCCC, <https://unfccc.int/nationally-determined-contributions-ndcs>
- 1248 Unger, N., T. C. Bond, J. S. Wang, D. M. Koch, S. Menon, D. T. Shindell, S. Bauer, Attribution of
1249 climate forcing to economic sectors. *Proceedings of the National Academy of Sciences U.S.A.* 107, 3382–
1250 3387, <https://doi.org/10.1073/pnas.0906548107> (2010).
- 1251 Unger, N., Global climate impact of civil aviation for standard and desulfurized jet fuel. *Geophysical*
1252 *Research Letters* 38, 1–6, <https://doi.org/10.1029/2011GL049289> (2011).
- 1253 Unger, N., Y. Zhao, H. Dang, Mid-21st century chemical forcing of climate by the civil aviation sector.
1254 *Geophysical Research Letters* 40, 641–645, <https://doi.org/10.1002/grl.50161> (2013).
- 1255 Unterstrasser, S., Large-eddy simulation study of contrail microphysics and geometry during the vortex
1256 phase and consequences on contrail-to-cirrus transition. *Journal of Geophysical Research Atmospheres*
1257 119, 7537–7555, <https://doi.org/10.1002/2013JD021418> (2014).
- 1258 Voulgarakis, A., V. Naik, J.-F. Lamarque, D. T. Shindell, P. J. Young, M. J. Prather, O. Wild, R. D. Field,
1259 D. Bergmann, P. Cameron-Smith, I. Cionni, W. J. Collins, S. B. Dalsøren, R. M. Doherty, V. Eyring, G.
1260 Faluvegi, G. A. Folberth, L. W. Horowitz, B. Josse, I. A. McKenzie, T. Nagashima, D. A. Plummer, M.
1261 Righi, S. T. Rumbold, D. S. Stevenson, S. A. Strode, K. Sudo, S. Szopa, G. Zeng, Analysis of present-day
1262 and future OH and methane lifetime in the ACCMIP simulations. *Atmospheric Chemistry and Physics* 13,
1263 2563–2587, <https://doi.org/10.5194/acp-13-2563-2013> (2013).
- 1264 Wilcox, L., K. P. Shine, B. J. Hoskins, Radiative forcing due to aviation water vapour emissions.
1265 *Atmospheric Environment* 63, 1–13, <https://doi.org/10.1016/j.atmosenv.2012.08.072> (2012).
- 1266 Wild, O., M. J. Prather, H. Akimoto, Indirect long-term global radiative cooling from NO_x emissions.
1267 *Geophysical Research Letters* 28, 1719–1722, <https://doi.org/10.1029/2000GL012573> (2001).
- 1268 Xie B., H. Zhang, Z. Wang, S. Zhao, Q. Fu, A modelling study of effective radiative forcing and climate
1269 response due to tropospheric ozone. *Advances in Atmospheric Sciences* 33, 819–828 doi: 10.1007/s00376-
1270 016-5193-0
- 1271 Yin, F., V. Grewe, C. Frömming, H. Yamashita, Impact on flight trajectory characteristics when avoiding
1272 the formation of persistent contrails for transatlantic routes. *Transportation Research Part D: Transport*
1273 *and Environment* 65, 466–484, <https://doi.org/10.1016/j.trd.2018.09.017> (2018).
- 1274 Zhou, C. and J. E. Penner, Aircraft soot indirect effect on large-scale cirrus clouds: Is the indirect forcing
1275 by aircraft soot positive or negative? *Journal of Geophysical Research Atmospheres* 119, 11,303–11,320,
1276 <https://doi.org/10.1002/2014JD021914> (2014).
- 1277

1 July 2020 Revised

1278 **Table 1.** Emission indices used in ERF and RF calculations

Emission	Emission index	Reference	Notes
CO ₂	3.16 kg/kg fuel	ICAO (2018)	
NO _x	15.14 g/kg fuel	Fleming and Ziegler (2016)	2018, 2011
	14.12 g/kg fuel	Barrett et al. (2010)	2005
Water vapor	1.231 kg/kg fuel	Barrett et al. (2010)	
Soot	0.03 g/kg fuel	Barrett et al. (2010)	
	2×10^{14} particles/kg fuel ^a		
Sulphur (SO ₂)	1.2 g/kg fuel	Miller et al. (2010)	Assumed S content of 600 ppm

1279 ^a Assumes mean particle size in the range of 11–79 nm diameter.

1280

1 July 2020 Revised

1281

1282

1283

Table 2. Best estimates and high/low limits of the 90% likelihood ranges for aviation ERF components derived in this study

ERF (mW m ⁻²)	2018 ^a	2011 ^a	2005 ^a	Sensitivity to emissions	ERF/RF
Contrail cirrus	57.4 (17, 98)	44.1 (13, 75)	34.8 (10, 59)	9.36 x 10 ⁻¹⁰ mW m ⁻² km ⁻¹	0.42
CO ₂	34.3 (28, 40)	29.0 (24, 34)	25.0 (21, 29)		1.0
Short-term O ₃ increase	49.3 (32, 76)	37.3 (24, 58)	33.0 (21, 51)	34.4 ± 9.9 mW m ⁻² (Tg (N) yr ⁻¹) ⁻¹	1.37
Long-term O ₃ decrease	-10.6 (-20, -7.4)	-7.9 (-15, -5.5)	-6.7 (-13, -4.7)	-9.3 ± 3.4 mW m ⁻² (Tg (N) yr ⁻¹) ⁻¹	1.18
CH ₄ decrease	-21.2 (-40, -15)	-15.8 (-30, -11)	-13.4 (-25, -9.4)	-18.7 ± 6.9 mW m ⁻² (Tg (N) yr ⁻¹) ⁻¹	1.18
Stratospheric water vapor decrease	-3.2 (-6.0 -2.2)	-2.4 (-4.4, -1.7)	-2.0 (-3.8, -1.4)	-2.8 ± 1.0 mW m ⁻² (Tg (N) yr ⁻¹) ⁻¹	1.18
Net NO _x	17.5 (0.6, 29)	13.6 (0.9, 22)	12.9 (1.9, 20)	5.5 ± 8.1 mW m ⁻² (Tg (N) yr ⁻¹) ⁻¹	
Stratospheric H ₂ O increase	2.0 (0.8, 3.2)	1.5 (0.6, 2.4)	1.4 (0.6, 2.3)	0.0052 ± 0.0026 mW m ⁻² (Tg (H ₂ O) yr ⁻¹) ⁻¹	---
Soot (aerosol-radiation)	0.94 (0.1, 4.0)	0.71 (0.1, 3.0)	0.67 (0.1, 2.8)	100.7 ± 165.5 mW m ⁻² (Tg (BC) yr ⁻¹) ⁻¹	---
Sulfate (aerosol-radiation)	-7.4 (-19, -2.6)	-5.6 (-14, -1.9)	-5.3 (-13, -1.8)	-19.9 ± 16.0 mW m ⁻² (Tg (SO ₂) yr ⁻¹) ⁻¹	---
Sulfate and soot (aerosol-cloud)	----	----	----	----	---
Net ERF (only non-CO ₂ terms)	66.6 (21, 111)	51.4 (16, 85)	41.9 (14, 69)	----	---
Net aviation ERF	100.9 (55, 145)	80.4 (45, 114)	66.9 (38, 95)	----	---
Net anthropogenic ERF in 2011	----	2290 (1130, 3330) ^b	----	----	---

1284

1285

1286

1287

^a The uncertainty distributions for all forcing terms are lognormal except for CO₂ and contrail cirrus (normal) and Net NO_x (discrete pdf).

^b Boucher et al., 2013. IPCC also separately estimated the contrail cirrus term for 2011 as 50 (20, 150) mW m⁻².

1 July 2020 Revised

1288 **Table 3.** Best estimates and low/high limits of the 95% likelihood ranges for aviation RF components
 1289 derived in this study ^a

RF (mW m ⁻²)	2018 ^b	2011 ^b	2005 ^b	L09 2005 values	Sensitivity to emissions (this work)
Contrail cirrus	111.4 (33, 189)	85.6 (25, 146)	67.5 (20, 115)	(11.8 ^c)	1.82 x 10 ⁻⁹ mW m ⁻² km ⁻¹
CO ₂	34.3 (31, 38)	29.0 (26, 32)	25.0 (23, 27)	28.0	
Short-term O ₃ increase	36.0 (23, 56)	27.3 (17, 42)	24.0 (15, 37)	26.3	25.1 ± 7.3 mW m ⁻² (Tg (N) yr ⁻¹) ⁻¹
Long-term O ₃ decrease	-9.0 (-17, -6.3)	-6.7 (-13, -4.7)	-5.7 (-11, -4.0)	----	-7.9 ± 2.9 mW m ⁻² (Tg (N) yr ⁻¹) ⁻¹
CH ₄ decrease	-17.9 (-34, -13)	-13.4 (-25, -9.3)	-11.4 (-21, -7.9)	-12.5	-15.8 ± 5.9 mW m ⁻² (Tg (N) yr ⁻¹) ⁻¹
Stratospheric water vapor decrease	-2.7 (-5.0, -1.9)	-2.0 (-3.8, -1.4)	-1.7 (-3.2, -1.2)	----	-2.4 ± 0.9 mW m ⁻² (Tg (N) yr ⁻¹) ⁻¹
Net NO _x	8.2 (-4.8, 16)	6.5 (-3.3, 12)	6.6 (1.9, 12)	13.8 ^d	1.0 ± 6.6 mW m ⁻² (Tg (N) yr ⁻¹) ⁻¹
Stratospheric H ₂ O increase	2.0 (0.8, 3.2)	1.5 (0.6, 2.4)	1.4 (0.6, 2.3)	2.8	0.0052 ± 0.0026 mW m ⁻² (Tg (H ₂ O) yr ⁻¹) ⁻¹
Soot (aerosol-radiation)	0.94 (0.1, 4.0)	0.71 (0.1, 3.0)	0.67 (0.1, 2.8)	3.4	100.7 ± 165.5 mW m ⁻² (Tg (BC) yr ⁻¹) ⁻¹
Sulfate (aerosol-radiation)	-7.4 (-19, -2.6)	-5.6 (-14, -1.9)	-5.3 (-13, -1.8)	-4.8	-19.9 ± 16.0 mW m ⁻² (Tg (SO ₂) yr ⁻¹) ⁻¹
Sulfate and soot (aerosol-cloud)	----	----	----	----	----
Net RF (only non-CO ₂ terms)	114.8 (35, 194)	88.4 (27, 149)	70.3 (22, 119)	----	----
Net aviation RF	149.1 (70, 229)	117.4 (56, 179)	95.2 (47, 144)	78.0	----

1290 ^a ERF values are shown in **Table 2**.

1291 ^b The uncertainty distributions for all forcing terms are lognormal except for CO₂ and contrail cirrus (normal) and Net
 1292 NO_x (discrete pdf).

1293 ^c Linear contrails only; excludes the increase in cirrus cloudiness due to aged spreading contrails.

1294 ^d Excludes updated CH₄ RF evaluation of Etminan et al. (2016) and equilibrium-to-transient correction.

1295

1 July 2020 Revised

1296 **Table 4a.** Confidence levels for the ERF estimates in **Figure 3**

Terms	Evidence	Agreement	Conf. level	Basis for uncertainty estimates	Understanding change since L09
Contrail cirrus formation in high-humidity regions	Limited	Medium	Low*	Robust evidence for the phenomenon. Large remaining uncertainties in magnitude in part due to incomplete representation of key processes	The inclusion of contrail cirrus processes in global climate models.
Carbon dioxide (CO₂) emissions	Robust	Medium	High**	Trends in aviation CO ₂ emissions and differences between simplified C-cycle models	Better assessment of uncertainties from multiple models
Short-term ozone increase	Medium	Medium	Medium*	Observed trends of tropospheric ozone and laboratory studies of chemical kinetics, reliance on a large number of model results for aviation emissions	Elevated owing to many more studies
Long-term ozone decrease	Limited	Medium	Low*	Reliance on chemical modelling studies	Not provided previously
Methane decrease	Medium	Medium	Medium*	Observed trends of tropospheric methane and laboratory studies of chemical kinetics, reliance on a large number of model results for aviation emissions	Elevated owing to many more studies
Stratospheric water vapour decrease	Limited	Medium	Low*	Reliance on chemical modelling studies	Not provided previously
Net NO_x	Medium	Limited	Low*	Associated uncertainties with combining above effects	Elevated owing to more studies but lowered in total owing to additional terms and methodological constraints
Water vapor emissions in the stratosphere	Medium	Medium	Medium	Limited studies of perturbation of water vapor budget of UT/LS	Elevated owing to more studies
Aerosol-radiation interactions					
From soot emissions	Limited	Medium	Low	Limited studies and uncertain emission index	More studies
From sulfur emissions	Limited	Medium	Low	Limited studies and uncertain emission index	More studies
Aerosol-cloud interactions					
From sulfur emissions	Limited	Low	Very low	None available; few studies, probably a negative ERF	Not provided previously
From soot emissions	Limited	Low	Very low	None available; few studies, varying in sign and magnitude of ERF constrained by poor understanding of processes	Not provided previously

* This term has the additional uncertainty of the derivation of an effective radiative forcing from a radiative forcing.

** This term differs from 'Very High' level in IPCC (2013) because additional uncertainties are introduced by the assessment of marginal aviation CO₂ emissions and their resultant concentrations in the atmosphere from simplified carbon cycle models.

1297

1298

1299

1300

1301

1302

1303

1 July 2020 Revised

1304 **Table 4b.** Basis for confidence levels in **Table 4a**^a

Medium <i>High agreement</i> <i>Limited evidence</i>	High <i>High agreement</i> <i>Medium evidence</i>	Very High <i>High agreement</i> <i>Robust evidence</i>
Low <i>Medium agreement</i> <i>Limited evidence</i>	Medium <i>Medium agreement</i> <i>Medium evidence</i>	High <i>Medium agreement</i> <i>Robust evidence</i>
Very Low <i>Low agreement</i> <i>Limited evidence</i>	Low <i>Low agreement</i> <i>Medium evidence</i>	Medium <i>Low agreement</i> <i>Robust evidence</i>

1305 ^a The basis for the confidence level is given as a combination of evidence
 1306 (limited, medium, robust) and agreement (low, medium and high) based
 1307 on guidance given by Mastrandrea et al. (2011).

1308

1 July 2020 Revised

1309 **Table 5.** Emission metrics and corresponding CO₂-equivalent emissions for the ERF components of 2018
 1310 aviation emissions and cloudiness

1311 **Metrics**

ERF term	GWP ₂₀	GWP ₅₀	GWP ₁₀₀	GTP ₂₀	GTP ₅₀	GTP ₁₀₀
CO ₂	1	1	1	1	1	1
Contrail cirrus (Tg CO ₂ basis)	2.32	1.09	0.63	0.67	0.11	0.09
Contrail cirrus (km basis)	39	18	11	11	1.8	1.5
Net NO _x	619	205	114	-222	-69	13
Aerosol-radiation						
Soot emissions	4288	2018	1166	1245	195	161
SO ₂ emissions	-832	-392	-226	-241	-38	-31
Water vapor emissions	0.22	0.10	0.06	0.07	0.01	0.008

1312

1313 **CO₂-eq emissions (Tg CO₂ yr⁻¹) for 2018**

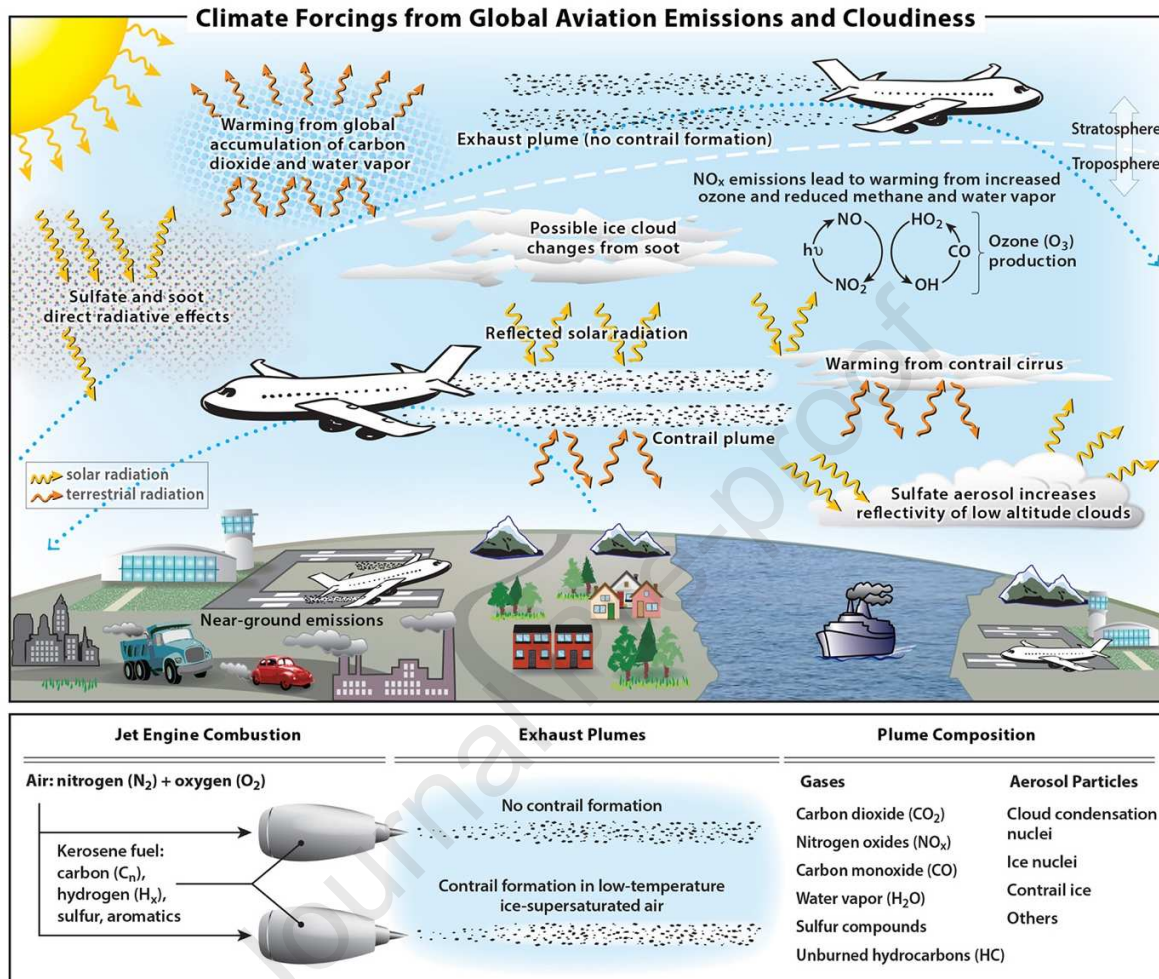
ERF term	GWP ₂₀	GWP ₅₀	GWP ₁₀₀	GTP ₂₀	GTP ₅₀	GTP ₁₀₀	GWP* ₁₀₀ (E* _{CO2e})
CO ₂	1034	1034	1034	1034	1034	1034	1034
Contrail cirrus (Tg CO ₂ basis)	2399	1129	652	695	109	90	1834
Contrail cirrus (km basis)	2395	1127	651	694	109	90	1834
Net NO _x	887	293	163	-318	-99	19	339
Aerosol-radiation							
Soot emissions	40	19	11	12	2	2	20
SO ₂ emissions	-310	-146	-84	-90	-14	-12	-158
Water vapor emissions	83	39	23	27	4	3	42
Total CO ₂ -eq (using km basis)	4128	2366	1797	1358	1035	1135	3111
Total CO ₂ -eq / CO ₂	4.0	2.3	1.7	1.3	1.0	1.1	3.0

1314

1 July 2020 Revised

1315

1316

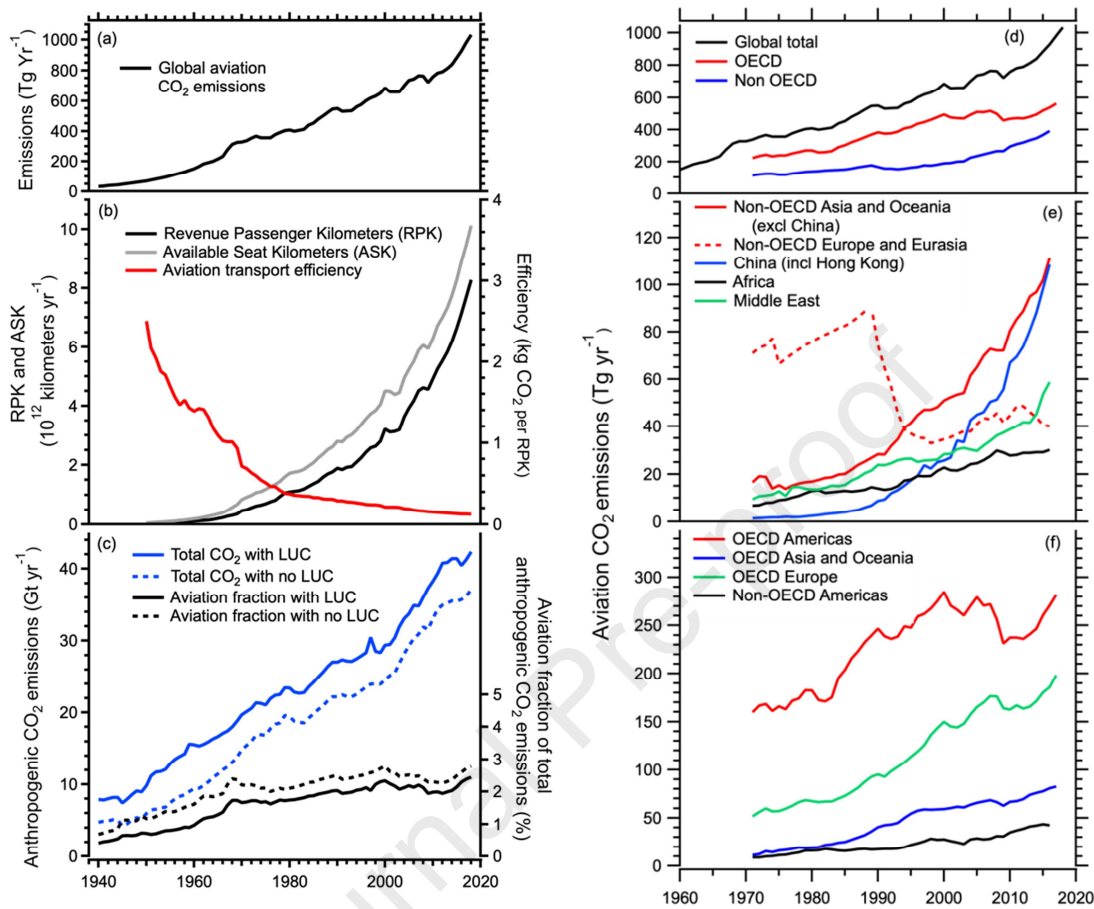


1317 **Figure 1.** Schematic overview of the processes by which aviation emissions and increased cirrus
 1318 cloudiness affect the climate system. Net positive RF (warming) contributions arise from CO₂, water
 1319 vapor, NO_x, and soot emissions, and from contrail cirrus (consisting of linear contrails and the cirrus
 1320 cloudiness arising from them). Negative RF (cooling) contributions arise from sulfate aerosol production.
 1321 Net warming from NO_x emissions is a sum over warming (short-term ozone increase) and cooling
 1322 (decreases in methane and stratospheric water vapor, and a long-term decrease in ozone) terms. Net
 1323 warming from contrail cirrus is a sum over the day/night cycle. These contributions involve a large number
 1324 of chemical, microphysical, transport and, radiative processes in the global atmosphere. The quantitative
 1325 ERF values associated with these processes are shown in **Figure 3** for 2018.

1326

1 July 2020 Revised

1327

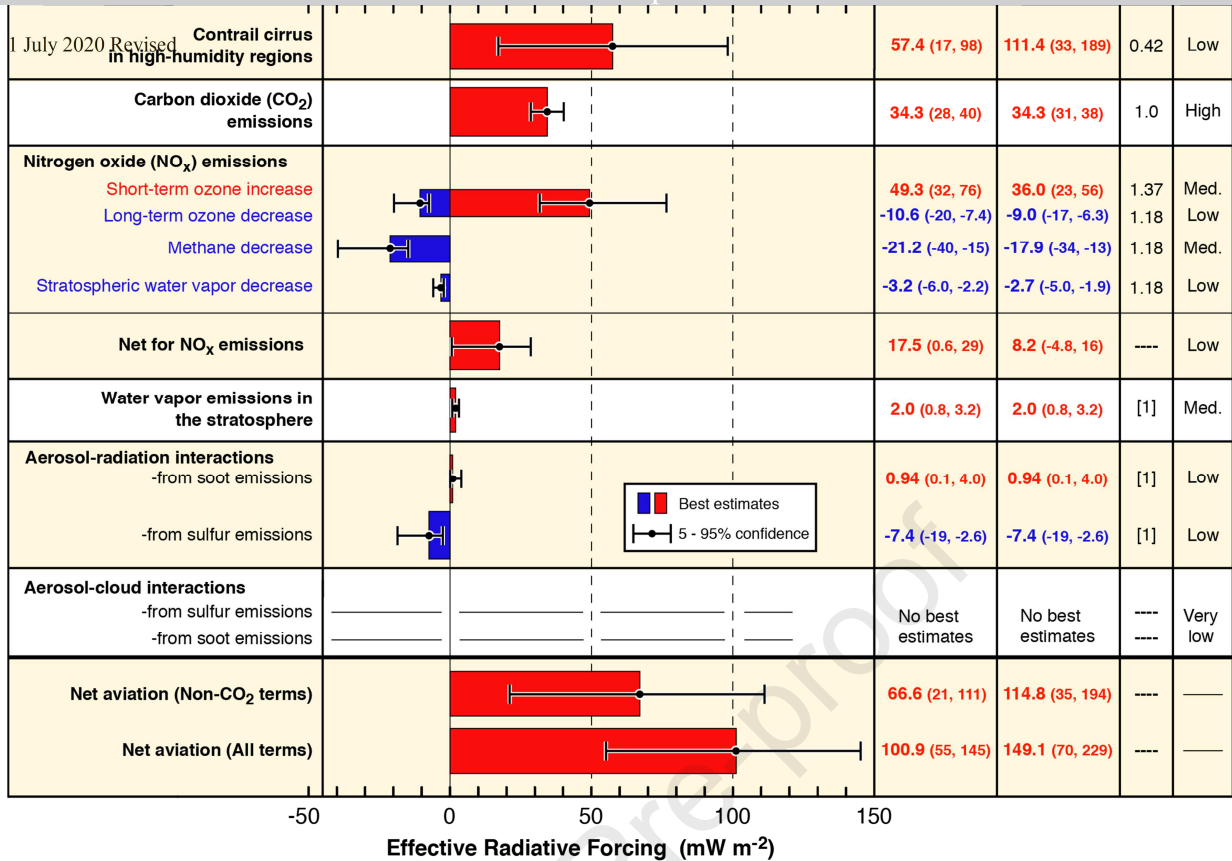


1328

1329 **Figure 2.** Data related to the growth of aviation traffic and CO₂ emissions from 1940 to 2018. Panel (a):
 1330 Global aviation CO₂ emissions. Underlying fuel usage data for 1940 to 1970 are derived from Sausen and
 1331 Schumann (2000) and for 1970–2016 from International Energy Agency (UKDS, 2016) data, which
 1332 include international bunker fuels. For 2017/18, the values are scaled from information from the
 1333 International Air Transport Association (see Appendix A). The average annual increase of global
 1334 emissions from 1960 to 2018 is 15 Tg CO₂ yr⁻¹ and the corresponding decadal average growth rates are 8.0,
 1335 2.2, 3.0, 2.3 and 1.1% yr⁻¹, yielding an overall average of 3.3% yr⁻¹. Panel (b): Global aviation traffic in
 1336 RPK and ASK from Airlines.org (<http://airlines.org/dataset/world-airlines-traffic-and-capacity/>), and the
 1337 transport efficiency of global aviation in kg CO₂ per RPK. The passenger load factor defined as RPK/ASK
 1338 increased from about 60% in 1960 to 82% in 2018. Panel (c): Total anthropogenic CO₂ emissions and the
 1339 aviation fractions of this total with and without the inclusion of CO₂ emissions from land use change
 1340 (LUC) from the Global Carbon Budget 2018 (Le Quéré et al., 2018). Panel (d)–(f): Additional aviation
 1341 emissions data by region and year. The yearly sums of OECD and non-OECD values in (d) equal the
 1342 respective global total values. The regional values in (e) and (f) also sum to equal the yearly global total
 1343 values. Note different vertical scales. (<http://www.oecd.org/about/membersandpartners/>) (UKDS, 2016)
 1344 (Country listings in SD Spreadsheet).

1345

1346



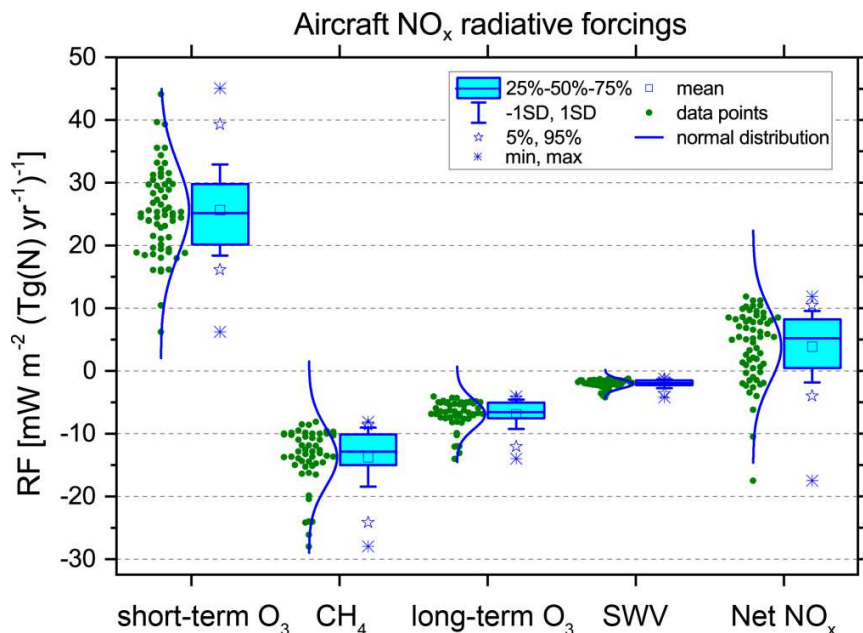
1347

1348

1349 **Figure 3.** Best-estimates for climate forcing terms from global aviation from 1940 to 2018. The bars and
 1350 whiskers show ERF best estimates and the 5–95% confidence intervals, respectively. Red bars indicate
 1351 warming terms and blue bars indicate cooling terms. Numerical ERF and RF values are given in the
 1352 columns with 5–95% confidence intervals along with ERF/RF ratios and confidence levels. ERF and RF
 1353 values are shown for other years in **Tables 2 and 3, Figure 6** and the SD spreadsheet. RF values are
 1354 multiplied by the respective ERF/RF ratio to yield ERF values. ERF/RF values designated as [1] indicate
 1355 that no estimate is available yet. The basis for confidence levels is presented in **Table 4**.

1356

1357

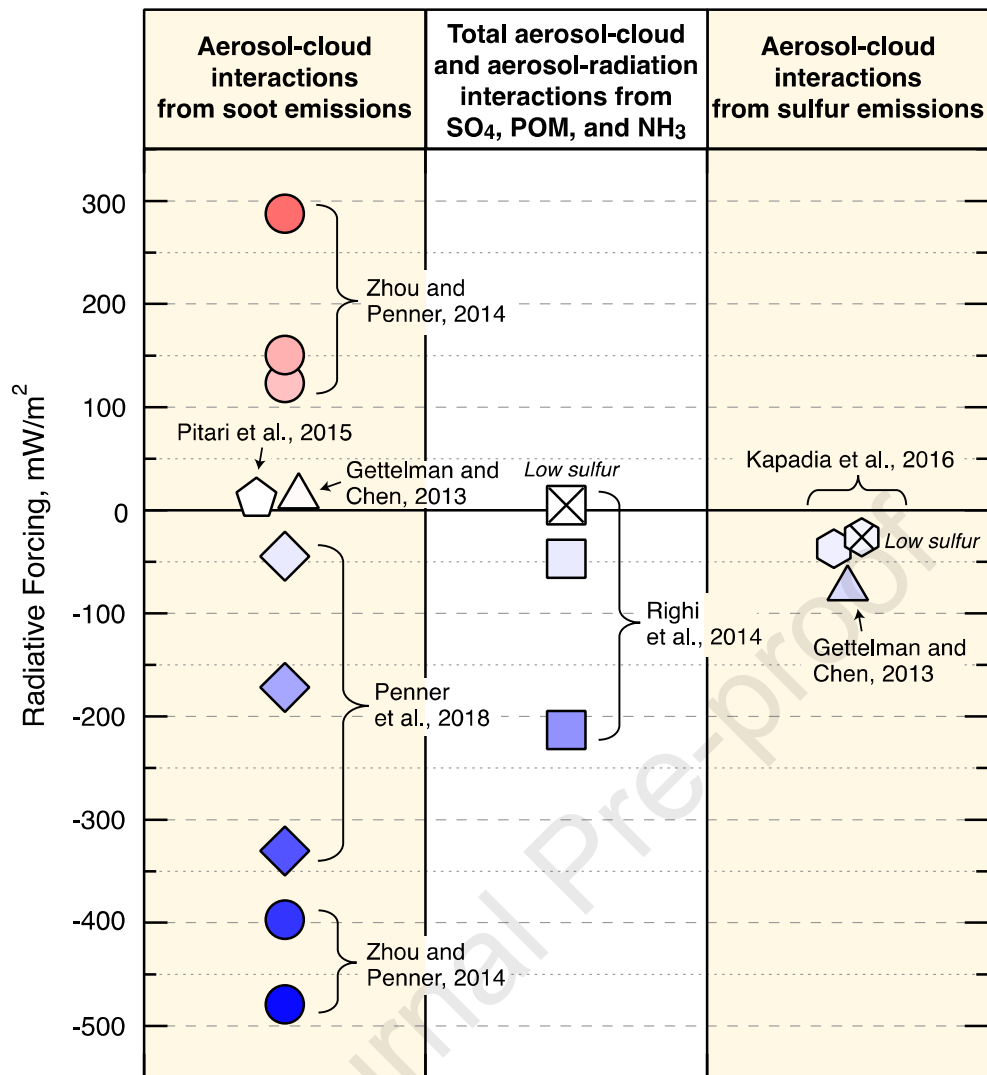


1 July 2020 Revised

1358 **Figure 4.** Results from an ensemble of 18 models from 20 studies for aviation NO_x impacts: short-term O₃
1359 increases; CH₄ reductions, CH₄-induced long-term reductions of O₃, CH₄-induced reductions of
1360 stratospheric water vapor (SWV) and Net NO_x. Each data point represents a value of RF per unit emission
1361 (mW m⁻² (Tg N yr⁻¹)⁻¹) as normalized from a published study (see SD). CH₄-induced O₃ and SWV are
1362 calculated using standardized methodology (see text for details). Note that the displayed values do not
1363 include correction factors to account for the non-steady-state CH₄ responses to NO_x emissions and the new
1364 CH₄ RF parameterization. These adjustments are applied in forming the best estimates as discussed in
1365 Appendix D.

1366

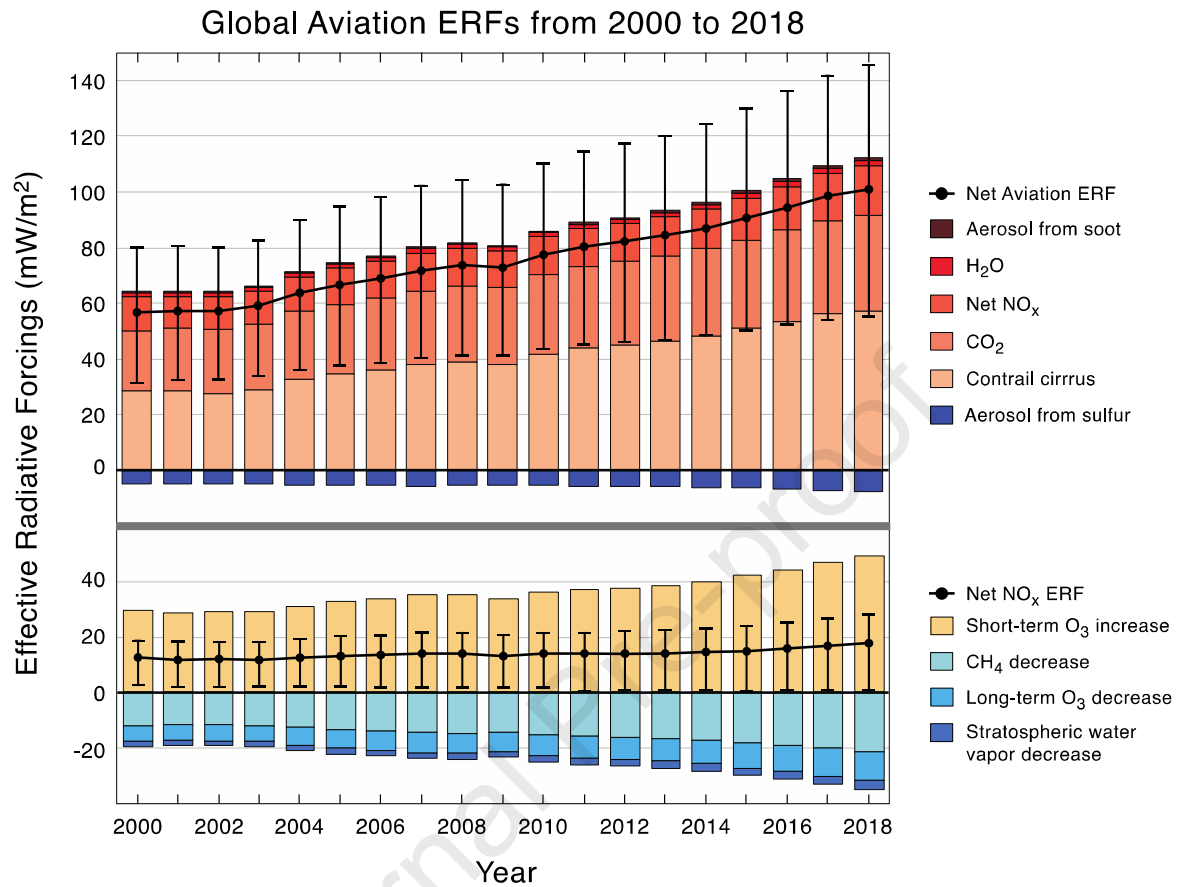
Journal Pre-proof



1367

1368 **Figure 5.** Summary of RF estimates for aerosol-cloud interactions for aviation aerosol as calculated in the
 1369 SD spreadsheet for a variety of published results normalized to 2018 air traffic and 600 ppm fuel sulfur.
 1370 The results are shown for soot; total particulate organic matter (POM), sulfate and ammonia (NH₃); and
 1371 sulfate aerosol from the indicated studies. The color shading gradient in the symbols indicates increasing
 1372 positive or negative magnitudes. No best estimate was derived in the present study for any aerosol-cloud
 1373 effect due to the large uncertainties. In previous studies, the estimates for the soot aerosol-cloud effect are
 1374 associated with particularly large uncertainty in magnitude and uncertainty in the sign of the effect (Penner
 1375 et al., 2009; Zhou and Penner, 2014; Penner et al., 2018). As part of the present study, an author (JEP) re-
 1376 evaluated these earlier studies and it concluded that the Penner et al. (2018) results supersede the earlier
 1377 Penner et al. (2009) and Zhou and Penner (2014) results because of assumptions regarding updraft
 1378 velocities during cloud formation. In addition, a bounding sensitivity case in which all aviation soot acts as
 1379 an IN in Penner et al. (2018) is not included here.

1 July 2020 Revised

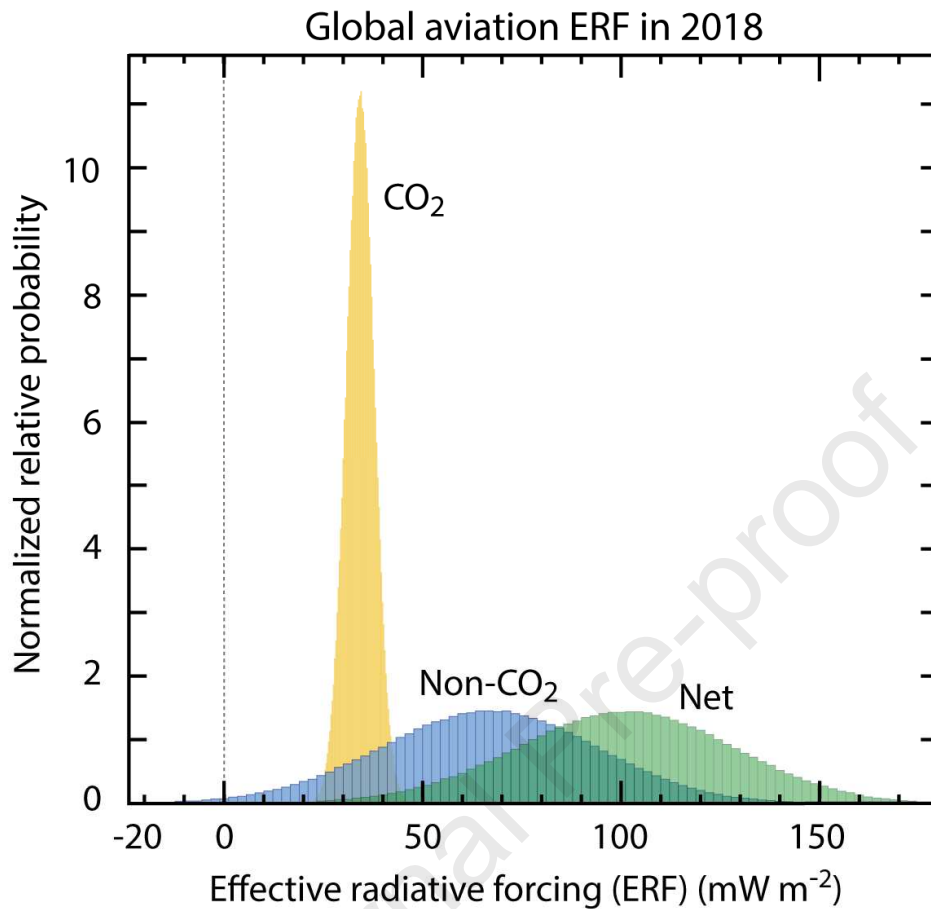


1380

1381 **Figure 6.** Timeseries of calculated ERF values and confidence intervals for annual aviation forcing terms
 1382 from 2000 to 2018. The top panel shows all ERF terms and the bottom panel shows only the NO_x terms
 1383 and net NO_x ERF. All values are available in the SD spreadsheet, in Tables 2 and 3, and in **Figure 3** for
 1384 2018 values. The net values are not arithmetic sums of the annual values because the net ERF, as shown in
 1385 **Figure 3** for 2018, requires a Monte Carlo analysis that properly includes uncertainty distributions and
 1386 correlations (see text).

1387

1 July 2020 Revised



1388

1389 **Figure 7.** Probability distribution functions (PDFs) for aviation ERFs in 2018 based on the results in
1390 **Figure 3** and **Table 2**. PDFs are shown for separately for CO₂, the sum of non-CO₂ terms, and the net
1391 aviation ERF. Since the area of each distribution is normalized to the same value, relative probabilities can
1392 be intercompared. Uncertainties are expressed by a distribution about the best-estimate value that is normal
1393 for CO₂ and contrail cirrus, and lognormal for all other components. A one-million-point Monte Carlo
1394 simulation run was used to calculate all PDFs.

1395

1396 **Appendices**1397 **A. Trends in aviation CO₂ emissions**

1398 Global aviation CO₂ emissions for 1940–1970 were taken from Sausen and Schumann (2000) and for the
 1399 years 1971–2016 were calculated from International Energy Agency (IEA) data on usage of JET-A and
 1400 aviation gasoline, largely from annual ‘Oil Information’ digests (e.g., [https://webstore.iea.org/oil-](https://webstore.iea.org/oil-information-2019)
 1401 [information-2019](https://webstore.iea.org/oil-information-2019)). The regional data are from the same source but accessed online from the IEA Oil
 1402 Information (1960–2017) held at the UK Data Service (IEA, 2019). Note that these data are proprietary
 1403 and must be purchased from IEA. Data were unavailable for 2017 and 2018, so incremental annual
 1404 percentage increases in global aviation fuel usage and, therefore CO₂ emissions, for those years were taken
 1405 from reports of the International Air Transport Association (IATA, 2019). Some uncertainties exist from
 1406 the annual fuel estimations and to a much smaller extent, the emission factors. The IEA does not give
 1407 uncertainties for annual kerosene fuel sales or usage. Sausen and Schumann (2000), from which the 1940
 1408 to 1970 data are based here, estimated that the uncertainty in cumulative fuel consumption from 1940 to
 1409 1995 (their dataset) is 20%. There is a known discrepancy of IEA estimates of aviation fuel usage being
 1410 greater by about 10% than that derived from bottom-up global civil aviation inventories. Actual fuel usage
 1411 is likely to be somewhere between the two estimates: aviation emissions inventories are known to be
 1412 incomplete, with only scheduled traffic being available from some air traffic regions, and fuel usage
 1413 potentially being underestimated from flight routing and cruise altitudes; IEA data on the other hand
 1414 includes military aviation fuel (not included in civil aviation inventories) and a small fraction of kerosene
 1415 not used in aviation, but sold for that purpose (L09). The CO₂ emission factors for aviation fuel on the
 1416 other hand are well determined, and the uncertainty is likely within 1%.

1417 **B. Aviation CO₂ radiative forcings**1418 **Calculation of CO₂ concentrations from emissions—LinClim SCM**

1419 The response of CO₂ concentrations, $C(t)$, to a CO₂ aviation emissions rate, $E(t)$, is modelled using the
 1420 method described in Hasselmann et al., (1997) and is expressed as:

$$1421 \quad \Delta C(t) = \int_{t_0}^t G_C(t-t')E(t')dt' \quad (B.1)$$

1422 where

$$1423 \quad G_C(t) = \sum_{j=0}^5 \alpha_j e^{-t/\tau_j} \quad (B.2)$$

1424 and τ_j is the e-folding time of mode j and the equilibrium response of mode j to a unit emissions of $\alpha_j \tau_j$.

1425 The mode parameters used in this study are presented in Sausen and Schumann (2000) and approximate
 1426 the carbon-cycle model in Meier-Reimer and Hasselmann (1987). The applicability of these parameters in
 1427 the context of aviation response was tested in a model intercomparison exercise (Khodayari et al., 2013).
 1428 For the time horizon of 50-60 years into the future, these were found to compare well with other more
 1429 sophisticated carbon-cycle models such as MAGICC 6.0, which is widely used in the IPCC Fourth
 1430 Assessment Report (IPCC, 2007). Beyond this horizon, aviation CO₂ concentrations begin to have an
 1431 impact on the ocean and biosphere uptake of CO₂ and the non-linearities of the system must be accounted
 1432 for.

1433 **Calculation of CO₂ concentrations from emissions—CICERO-2 SCM**

1434 The CICERO-2 SCM (Fuglestad and Berntsen, 1999; Skeie et al., 2017) uses interconnected process-
 1435 specific IRFs with explicit treatment of air-sea and air-biosphere exchange of CO₂ (Joos et al., 1996;
 1436 Alfsen and Berntsen, 1999) that forms a nonlinear carbon cycle. The ocean and biosphere IRFs in

1 July 2020 Revised

1437 CICERO-2 express how the CO₂ impulse decays within each reservoir. The CO₂ partial pressure in each
 1438 reservoir is calculated as a function of the carbon in that reservoir, and the CO₂ partial pressure in each
 1439 reservoir is related to the CO₂ partial pressure in the atmosphere by explicitly solving for the
 1440 atmosphere/ocean/biosphere CO₂ mass transfer. Therefore, the CICERO-2 carbon cycle takes into account
 1441 the nonlinearity in ocean chemistry and biosphere uptake at high CO₂ partial pressures since it represents
 1442 the atmospheric change in CO₂ as a function of total background.

1443 **Calculation of CO₂ concentrations from emissions—FaIR SCM**

1444 The FaIR SCM is described by Millar et al. (2017) and summarized as follows. FaIR is a modified version
 1445 of the IPCC AR5 four time-constant impulse response function (IRF) model, which represents the
 1446 evolution of atmospheric CO₂ by partitioning emissions of anthropogenic CO₂ between four reservoirs of
 1447 an atmospheric CO₂ concentrations change, following a pulse emission (see Myhre et al., 2013 for more
 1448 details). In more comprehensive models, ocean uptake efficiency declines with accumulated CO₂ in ocean
 1449 sinks (Revelle and Suess, 1957) and uptake of carbon into both terrestrial and marine sinks are reduced by
 1450 warming (Friedlingstein et al., 2006). FAIR captures some of these dynamics within the simple IRF
 1451 structure, mimicking the behaviour of Earth System Models/Earth System Models of Intermediate
 1452 Complexity in response to finite-amplitude CO₂ injections; this is achieved by introducing a state-
 1453 dependent carbon uptake with a single scaling factor, α , to all four of the time constants in the carbon cycle
 1454 of the IPCC AR5 impulse response model used for the calculation of CO₂-equivalence metrics. This
 1455 approach is described in more detail by Millar et al. (2017).

1456 **C. Radiative forcing, efficacy and effective radiative forcing (ERF)**

1457 Radiative forcing (RF) has been introduced as a predictor for the expected equilibrium global mean of the
 1458 (near) surface temperature change ΔT_s that results from the introduction of climate forcers, such as
 1459 additional atmospheric CO₂ or a change in the solar irradiation (e.g., IPCC, 2007):

$$1460 \quad \Delta T_s = \lambda \text{ RF} \quad (\text{C.1})$$

1461 where λ is the climate sensitivity parameter ($\text{K} (\text{W m}^{-2})^{-1}$). Several definitions of RF exist. According to
 1462 the simplest one, the instantaneous RF is the change in the total irradiation (incoming short-wave solar
 1463 radiation minus the outgoing long-wave terrestrial radiation) at the top of the atmosphere over the
 1464 industrial era. However, for most of the climate forcers a better definition (with respect to the linearity of
 1465 Eq. (C.1)) is the stratosphere-adjusted RF at the tropopause. Here, after the introduction of the new climate
 1466 forcer, the temperature of the stratosphere is allowed to reach a new radiative equilibrium, while all other
 1467 atmospheric state variables are kept constant. The stratosphere-adjusted RF at the tropopause was used in
 1468 many of the earlier IPCC reports (IPCC, 1999) and in earlier assessments of aviation climate impacts
 1469 (Sausen et al., 2005; L09).

1470 While Eq. (C.1) is a fairly good approximation for many nearly spatially homogeneously distributed
 1471 climate forcers, such as global increases of CO₂ or CH₄, Eq. (C.1) fails to some extent for many forcers
 1472 that are heterogeneously distributed either horizontally or vertically; such is the case for aviation-induced
 1473 ozone perturbations and contrail cirrus (e.g., Hansen et al., 1997, 2005; Forster and Shine, 1997; Stuber et
 1474 al., 2005). To overcome this problem Hansen and Nazarenko (2004) introduced the efficacy, r_i , into Eq.
 1475 (C.1):

$$1476 \quad \Delta T_s = r_i \lambda_{\text{CO}_2} \text{ RF} = \lambda_i \text{ RF} \text{ with } \lambda_i = r_i \lambda_{\text{CO}_2} \quad (\text{C.2})$$

1477 Here λ_{CO_2} is the climate sensitivity parameter for a CO₂ perturbation. While λ in (C.1) is considered a
 1478 universal constant, which can only be determined by climate models and hence is model dependent, λ_i
 1479 depends on the type of forcing, as does r_i . (While r_{CO_2} is 1 by definition, $r_{\text{linear contrails}}$ is <1 (Ponater, et al.,
 1480 2005; Rap et al., 2010)). Eq. (C.2) can also be expressed differently:

$$1481 \quad T_s = \lambda_{\text{CO}_2} \text{ RF}_i^* \text{ with } \text{RF}_i^* = r_i \text{ RF} \quad (\text{C.3})$$

1482 Here RF_i^* is the forcing modified by the efficacy, which yields a better approximation for the surface
 1483 temperature change than RF. However, the calculation of the RF_i^* is computationally much more
 1484 expensive than the calculation of RF, as it requires the determination of the equilibrium temperature
 1485 change, ΔT_s , with a comprehensive climate model.

1486 As an alternative, the effective radiative forcing (ERF) has been introduced as a more practical indicator of
 1487 the eventual global mean temperature response (IPCC, 2013). While RF_i^* assumes equilibrium climate
 1488 change, ERF only includes all 'fast' atmospheric responses to a given climate forcer. For example, rapid
 1489 adjustments in cloud cover, such as from aerosols, or in properties that respond to changes in water vapor,
 1490 can either increase or decrease the initial RF. In contrast, the instantaneous, stratosphere-adjusted, and
 1491 effective RFs for well-mixed greenhouse gases are nearly equal. In practice, ERF is determined with a
 1492 comprehensive climate model, which calculates a new equilibrium radiative imbalance, while the sea
 1493 surface temperature and/or the global surface temperature is kept constant. As a consequence, an ERF
 1494 value is expected to be somewhere between RF and RF_i^* values and closer to RF_i^* values.

1495 **D. Aviation NO_x radiative forcings**

1496 **Impacts of NO_x emissions on ozone, methane and stratospheric water vapor**

1497 *Model studies.* In this ensemble analysis of the climate forcing from aviation NO_x emissions, the results of
 1498 20 studies published since the IPCC (1999) aviation report were considered: IPCC (1999), Sausen et al.
 1499 (2005), Stordal et al. (2006), Köhler et al. (2008), Hoor et al. (2009), Myhre et al. (2011), Frömming et al.
 1500 (2012), Olivié et al. (2012), Gottschaldt et al. (2013), Köhler et al. (2013), Olsen et al. (2013), Skowron
 1501 et al. (2013), Khodayari et al. (2014a), Khodayari et al. (2014b), Søvde et al. (2014), Skowron et al. (2015),
 1502 Pitari et al. (2015), Kapadia et al. (2016), Pitari et al. (2016), Lund et al. (2017). Three studies that reported
 1503 results from a 100-year integration of a pulse NO_x emission (Wild et al. 2001, Derwent et al. 2001,
 1504 Stevenson et al. 2004) were not included in this analysis, nor has as Unger et al. (2010) which uses a
 1505 different methodology to the aforementioned.

1506 This model ensemble represents various methodologies in calculating and treating the long-term effects; in
 1507 order to avoid gaps and additional uncertainties, standardized RFs for reductions in CH_4 -induced O_3 and
 1508 SWV were adopted, except for one study that calculates the 'real' long-term effects from their 50-yr
 1509 integrations (Pitari et al., 2016):

- 1510 • All analyzed short-term O_3 RFs account for a stratospheric adjustment: Assuming that it reduces the
 1511 instantaneous RF by ~20% (Myhre et al., 2013, Stevenson et al., 1998), a factor of 0.8 was applied to
 1512 any O_3 RF that is an instantaneous RF (e.g., in the cases of Khodayari et al. (2014a,b) and Olsen et al.
 1513 (2013)).
- 1514 • Reductions in CH_4 -induced O_3 and SWV are defined as 50% (Myhre et al., 2013) and 15% (Myhre et
 1515 al., 2007) of reported CH_4 RFs, respectively. This is applicable for studies that either originally did not
 1516 provide CH_4 -induced O_3 and SWV estimates (e.g., IPCC, 1999, Sausen et al., 2005, Olsen et al., 2013)
 1517 or derived these RFs using another assumptions (e.g., Stordal et al., 2006, Köhler et al., 2008, Hoor et
 1518 al., 2009, Gottschaldt et al., 2013, Köhler et al., 2013, Skowron et al., 2013, Khodayari et al., 2014a).

1519 Further assumptions regarding data treatment are:

- 1520 • Frömming et al. (2012), Olivié et al. (2012), Khodayari et al. (2014b) and Kapadia et al. (2016)
 1521 provide the short-term O_3 RFs only and p-TOMCAT in Stordal et al. (2006) calculates just the long-
 1522 term effects; thus, these numbers are included in the respective NO_x variable analysis but do not
 1523 contribute to the net NO_x estimate.
- 1524 • Whenever the same estimate appears repetitively in subsequent studies, it is treated as a single entry:
 1525 this is the case for CAM4 short-term O_3 RF that appears in Khodayari et al. (2014a; b) and Olsen et al.

1 July 2020 Revised

1526 (2013), CAM5 short-term O₃ RF that can be found in Khodayari et al. (2014a; b) and NASA ModelE2
1527 short-term O₃ and CH₄ RFs presented by Unger et al. (2013) and Olsen et al. (2013).

1528 In addition, the ERF estimates for the CH₄ term include shortwave RF (Etminan et al., 2016). The
1529 inclusion of shortwave forcing in the simplified expression increases CH₄ RF from aviation NO_x emissions
1530 by 23% (based on MOZART-3 CTM runs driven for all the aircraft emission inventories represented in the
1531 model ensemble) (**Table D.1**).

1532 **Ensemble values.** This ensemble analysis covers a period of almost two decades; however, none of the RF
1533 per unit of emitted N estimates show any trends over time of publication and the spread in RF per unit of
1534 emitted N values has not changed. The short-term O₃ RF varies from 6.2 to 45.1 mW m⁻² (Tg (N) yr⁻¹)⁻¹,
1535 where these values come from the NASA ModelE2 (Olsen et al., 2013) and p-TOMCAT (Hoor et al.,
1536 2009) models, respectively. The long-term CH₄ RF varies from -27.9 to -8.1 mW m⁻² (Tg (N) yr⁻¹)⁻¹, from
1537 the p-TOMCAT (Köhler et al., 2008) and MOZART3 (Skowron et al., 2015) models, respectively. The
1538 spread of other CH₄-induced long-term effects follows that of CH₄. The net-NO_x RF varies from -17.5 to
1539 11.9 mW m⁻² (Tg (N) yr⁻¹)⁻¹ from ECHAM/MESSy (Gottschaldt et al., 2013) and CAM4 (Khodayari et al.,
1540 2014a), respectively. The results from the mid-1990s CTMs are within the envelope of RFs generated
1541 more recently (**Figure 3**). The numbers from IPCC (1999) and related studies, Sausen et al. (2005) and
1542 L09, where the non-CO₂ effects were originally calibrated to the results from IPCC (1999), do not alter the
1543 best NO_x RF values and their uncertainties (**Table D.2**).

1544 **Correlations.** The correlations between the NO_x RF components are shown in **Figure D.1**. In addition to
1545 the significant negative correlations between the short-term and the long-term aviation RF components,
1546 correlations between the net-NO_x effect and its components are also apparent, especially for the short-term
1547 O₃ and net-NO_x components; however, their strength is around half. The high correlations (p=1, R²=1)
1548 across the long-term effects is expected since CH₄-induced O₃ and SWV are all derived based on CH₄ RFs.
1549 In units of mW m⁻² (Tg(N) yr⁻¹)⁻¹, 49% of this ensemble short-term O₃ RF is concentrated between 20 and
1550 35, 43% of CH₄ RFs is found between -14 and -10, 41% of CH₄-induced O₃ RFs is between -7 and -5 and
1551 45% of SWV RFs vary from -2.5 to -1.5. Of the normalized net-NO_x RFs resulting from this ensemble,
1552 44% are observed between 5 and 10 mW m⁻² (Tg(N) yr⁻¹)⁻¹.

1553 **Transient vs. equilibrium.** In calculating the CH₄ RF response to aviation NO_x emissions, the lack of steady-
1554 state conditions is an important consideration. Since methane (CH₄) has a lifetime of the order 8–12 years
1555 (largely model-dependent) any NO_x perturbation takes on the order ~40 years to come within 2% of the
1556 steady state solution. Moreover, the timescale of removal of CH₄ from the atmosphere is made longer
1557 through a positive chemical feedback (Prather et al. 1994). In order to overcome the necessity to run a
1558 global chemical transport model (CTM) with full chemistry for such long integrations, a parameterization
1559 to account for this perturbation was originally developed by Fuglested et al. (1999) and has been widely
1560 adopted since then. However, with the significant annual increases in aviation NO_x emissions over the last
1561 several decades (**Figure D.2a**) the CH₄ response does not reach its steady-state value in any given year of
1562 emissions, so the steady-state solution generally overstates the CH₄ response in a particular year from
1563 historical time-evolving emissions. Similar considerations apply to other sectors with substantial NO_x
1564 emissions such as shipping (Myhre et al., 2011). If steady-state conditions are utilized, there is a
1565 conceptual and quantitative mismatch when comparing the NO_x RF from aviation with other RF terms,
1566 since RF represents a particular condition at a point in time, not the steady-state conditions. To remedy this
1567 mismatch, Myhre et al. (2011) suggested that a factor accounting for the non-steady-state condition of CH₄
1568 be introduced, thereby modifying the CH₄ impact for a given year of interest, and further suggested that for
1569 the aviation RF in the year 2000 the CH₄ term be reduced by approximately 35% for aircraft emissions
1570 using a simplified estimation derived from Grewe and Stenke (2008).

1571 Here, we present an updated methodology to calculate the non-steady-state aviation-NO_x-induced CH₄
1572 perturbation for the specific year of 2018. The method relies on transient and steady-state runs of the

1 July 2020 Revised

1573 TROPOS 2D CTM. The results of the steady-state runs using constant emissions for a given year are
1574 compared with those of transient runs using background historical surface emissions from anthropogenic
1575 activities and the corresponding aviation NO_x emissions. The latter requires full implementation of time-
1576 varying CH_4 emissions into the model simulation, a requirement that is not a standard set-up for many of
1577 the CTM/GCMs currently in use where CH_4 conditions are defined from observations as fixed
1578 concentrations with relaxation terms introduced to accommodate perturbations to these concentrations. The
1579 use of CTM runs explicitly accounts for changing background atmospheric conditions over the integration
1580 period as well as the change in emission rate dependence of the O_3 and CH_4 responses.

1581 *Method.* In order to compare these two methods, two types of experiments were performed:

- 1582 • Transient experiment: a long-term simulation with anthropogenic (surface and aviation) emissions
1583 evolving over time covering the period 1950–2050, using historical data up to 2000 and the RCP-4.5
1584 scenario after 2000 (**Figure D.2a**),
- 1585 • Steady-state experiment: a 100-year simulation with constant anthropogenic (surface and aviation)
1586 emissions representing the year 2000, 2018 or 2050 (**Figure D.2a**); the steady-state CH_4 response starts
1587 to be observed 60–70 years into the run.

1588 Each of these experiments was run twice, with and without aviation emissions, and the difference between
1589 these two results defined as the aircraft response (e.g., **Figure D.2d-f**). The initial concentrations of CH_4
1590 were set using the observations from NOAA surface stations (Montzka et al., 2000) for 1950 and 2000; for
1591 the year 2050 the CH_4 concentrations are taken from projections of the MAGICC model (Meinshausen et
1592 al., 2011). The background anthropogenic emissions of CO , CH_4 , NO_x , N_2O , and non-methane volatile
1593 organic carbon (NMVOC) compounds, as well as aircraft NO_x emissions, evolve during the period 1950-
1594 2050 (Lamarque et al., 2010; Clarke et al., 2007) (**Figure D.2a**). The natural emissions from soils and
1595 oceans were kept constant and represent the year 2000 (Prather et al., 2001).

1596 The TROPOS CTM is a latitudinally-averaged, two-dimensional Eulerian global tropospheric chemistry
1597 model extensively evaluated by Hough (1989; 1991). The model's domain extends from pole-to-pole (24
1598 latitudinal grid cells) and from the surface to an altitude of 24 km (12 vertical layers). TROPOS is driven
1599 by chemistry, emissions, transport, removal processes and upper boundary conditions. There are 56
1600 chemical species in the chemical mechanism of the model, which consists of 91 thermal reactions, 27
1601 photolytic reactions and 7 more reactions, which include night-time NO_3 chemistry. The reaction rates and
1602 cross sections were updated to the evaluation of Sander et al. (2006) (see Skowron et. al, 2009). There are
1603 no fixed concentrations within the model domain other than the upper boundary conditions, which are
1604 specified for long-lived species and for gases that have stratospheric sources. This 2D CTM has the
1605 disadvantage of zonal symmetry but has the advantage of an adequate chemical scheme and computational
1606 efficiency, such that long-term integrations can be reasonably performed. Owing to the aforementioned
1607 reasons, the O_3 response in TROPOS is overestimated by a factor of ~ 2 by comparison with a range of up-
1608 to-date 3D models. As a consequence, the CH_4 results in **Figures. D.2d-f** were reduced accordingly. This
1609 modification of the original TROPOS responses does not affect the core result of this study, which is the
1610 *relative* difference of CH_4 responses between transient and equilibrium methods.

1611 *Results.* **Figure D.2b** shows the evolution of the global CH_4 burden over the period 1950–2050 in the
1612 transient TROPOS simulation. There is a steady growth in the atmospheric CH_4 burden, with a small
1613 decline over the period 1997–2007 in response to the decrease in CH_4 emissions over the period 1990–
1614 2000. The steady-state simulations for the year 2000 and 2050 agree well (within 1%) with transient CH_4
1615 responses for the respective years. A similar agreement is observed for modelled transient and steady-state
1616 CH_4 lifetimes in **Figure D.2c**. Most of the CH_4 loss in the atmosphere is driven by OH and the oxidative
1617 capacity of the atmosphere changes over time (thus CH_4 lifetime as well), influenced by emissions of CO ,
1618 NO_x , NMVOC or CH_4 .

1 July 2020 Revised

1619 **Figure D.2c** shows the evolution of global CH₄ lifetime (LT) over the period 1950–2050: there is a
1620 decrease in the CH₄ lifetime between 1950 and 2000 (until around 2007), whilst under the RCP-4.5
1621 scenario the opposite is observed, with the CH₄ lifetime increasing by 3.5% by the end of 2050 compared
1622 with 2000. The TROPOS CH₄ lifetimes agree relatively well with other studies (e.g., Holmes et al., 2013;
1623 Voulgarakis et al.; 2013, Dalsøren et al., 2016) not only in terms of absolute numbers but also the rate of
1624 changes; a detailed comparison is presented in **Table D.3**. The perturbation lifetime of CH₄ in TROPOS is
1625 37% longer than its global lifetime and the sensitivity coefficient $s = \partial \ln(\text{LT}) / \partial \ln(\text{CH}_4)$ is 0.27, placing
1626 these estimates in the middle of model ranges (e.g., Prather 2001, Holmes et al. 2011). These terms were
1627 calculated using a 5% increase of CH₄ global levels for the year 2000. There is no need to apply the
1628 feedback factor (1.37) to the TROPOS CH₄ estimates as it is already included in the observed responses;
1629 TROPOS does not have a fixed boundary conditions, so CH₄ and OH can *freely* interact.

1630 Aircraft NO_x emissions, via the chemical coupling to OH and HO₂, enhance OH, which reduces the global
1631 CH₄ lifetime. **Figure D.2d** shows the evolution of the CH₄ lifetime reduction in the transient 1950–2050
1632 simulation and in steady-state runs for conditions representing the years 2000 and 2050. In the transient
1633 run, there is a steady decrease of global CH₄ lifetime as a consequence of a constant increase of aviation
1634 NO_x emissions during the period 1950–2050. The agreement in 2000 and 2050 between the transient and
1635 steady-state CH₄ lifetime reductions is within 6% (on a global scale) (see **Table D.3**). These relatively
1636 small differences in CH₄ lifetime lead to much more pronounced differences in the associated global CH₄
1637 burdens as shown in **Figure D.2e**. In contrast to the lifetime results, the CH₄ burden response in the
1638 transient run lags behind the steady-state CH₄ response with differences of 27% in the year 2000 and 20%
1639 in the year 2050. Similarly, the calculations for 2018 emissions yield a multiplicative correction factor of
1640 0.79 (**Figure D.2f**), which has been incorporated into the ERF values of CH₄, long-term O₃ and SWV
1641 shown in **Figure 5**.

1642 The CH₄ results contrast with O₃ changes from aircraft NO_x emissions, which agree within 3% between
1643 transient and steady-state experiments with aircraft O₃ burdens of 10.3 and 10.6 Tg (O₃), respectively, in
1644 the year 2000. These TROPOS O₃ magnitudes are at the upper limit of model ranges, as present-day
1645 aircraft O₃ perturbations found in the literature vary from 3 to 11 Tg (O₃) (e.g., Hoor et al., 2009; Holmes
1646 et al., 2011; Khodayari et al., 2014a). The aircraft O₃ burden increases by 41% in 2050, reaching 17.2 and
1647 18.0 Tg(O₃) for transient and steady-state experiments, respectively. This agrees with other studies (e.g.,
1648 Olsen et al., 2013) that report a multi-model average increase of 44% in O₃ burden from future aircraft
1649 NO_x emissions under the RCP-4.5 scenario.

1650 The present approach is in general agreement with that presented by Grewe and Stenke (G&S) (2008),
1651 which accounts for CH₄ concentrations not being in steady-state with OH changes in the year of
1652 simulation. The present CTM results further demonstrate the importance of explicitly calculating CH₄
1653 changes in response to time-dependent aviation NO_x emissions rather than assuming constant emissions.
1654 The difference between transient and steady-state CH₄ for the year 2000 found with TROPOS is smaller
1655 than that resulting from the G&S approach (Myhre et al., 2011) (27% and 35%, respectively). **Table D.4**
1656 presents a further comparison of CH₄ correction factors derived in this study. The systematic differences
1657 are likely due to the G&S values being based on a simplified chemistry/climate model (AirClim) and the
1658 present TROPOS simulations having a different experimental setup (all our emissions (surface + aircraft)
1659 are time-varying) and a full chemical reaction scheme with explicit calculations performed on time-
1660 varying emissions. Indeed, if TROPOS is run with constant background emissions representing the year
1661 2000 in a similar manner using G&S methodology, the difference between transient and steady-state CH₄
1662 for the year 2000 increases from 27% to 31%. This change shows that background emissions modify the
1663 CH₄ correction factor and further emphasizes the need to have surface and aircraft emissions that
1664 simultaneously follow historical pathways. In other studies using the G&S methodology, CH₄ correction
1665 factors vary from 0.74 to 1.15 depending on the investigated year (2025 or 2050) and aircraft emission

1 July 2020 Revised

1666 scenario (SRES A1B, B1 and B1 ACARE) (the factor can be larger than 1 if the aircraft emissions are
1667 assumed to decrease in the preceding years) (Hodnebrog et al., 2011; 2012).

1668 Uncertainties in the CH₄ correction factor are associated mainly with inter-model differences and the
1669 applied emission scenarios; the correction factor is sensitive, within ~10%, to inter-model differences
1670 (based on two models, TROPOS and AirClim) and it can vary by another $\pm 10\%$ depending on emission
1671 scenario (based on a range of RCP projections up to 2050). Given that the uncertainties of the CH₄
1672 correction factor on the net-NO_x RF are rather small, especially when compared with overall uncertainties,
1673 we do not include in the estimated uncertainty of the net-NO_x RF value a separate uncertainty due to the
1674 correction factor.

1675 E. Contrail cirrus

1676 The global contrail cirrus RF is calculated by homogenizing existing estimates through the use of specific
1677 scaling factors. The factors relate to the choice of air traffic inventory and its basis year; the use of the full
1678 3D flight distance; the use of hourly air traffic data; the feedback of natural clouds; and correcting for
1679 weaknesses in the radiative transfer calculations. The corrections and scaling actions are:

- 1680 • The estimate of Chen and Gettelman (2013) was corrected by redoing the CAM simulation using a
1681 lower ice crystal radius of 7 μm and a larger contrail cross-sectional area of 0.09 km² for the
1682 initialization of contrails at an age of about 15–20 minutes, in agreement with observations (Schumann
1683 et al., 2017b). The resulting change in cirrus cloudiness including the adjustment in cloudiness due to
1684 the presence of contrail cirrus leads to a radiative forcing of 57 mW m⁻².
- 1685 • A scaling S₁ of 1.4 is applied for estimates based on the AERO2k inventory for the year 2002 instead
1686 of the AEDT inventory for the year 2006 (Bock and Burkhardt, 2016);
- 1687 • A scaling S₂ of 1.14 is applied to estimates that are based on track distance instead of slant distance
1688 (Bock and Burkhardt, 2016). The ‘slant’ air traffic distance is the full flight distance and not the ground
1689 projected ‘track’ distance.
- 1690 • A scaling S₃ of 0.87 is applied to estimates that used monthly instead of hourly resolved air traffic
1691 data. This scaling is based on an estimate for the impact of the temporal resolution of the air traffic data
1692 of -25% to -30% within CAM (Chen et al., 2012) and one of no significant change in ECHAM4-
1693 CCMod.
- 1694 • A scaling S₄ of 1.15 is applied to account for the underestimation of RF in radiative transfer
1695 calculations that use frequency bands instead of line by line calculations (Myhre et al. 2009).

1696 The study details and scaling results are shown in **Table E.1**. Weighting each estimate equally, the best
1697 estimate of global contrail cirrus RF is approximately 66 mW m⁻². As noted in the main text, the Chen and
1698 Gettelman (2013) calculation is interpreted as being closer to an ERF than an RF, so was excluded from
1699 this averaging. This mean RF estimate does not include the RF due to contrails forming within natural
1700 cirrus. Uncertainty due to scalings S₃–S₄ is included in the uncertainty discussion below, whereas
1701 uncertainty in scalings S₁–S₂, namely updating the ECHAM4-CCMod estimates using sensitivities from
1702 ECHAM5-CCMod, is neglected.

1703 The statistical uncertainty of global contrail cirrus RF cannot be estimated from the small number of
1704 available studies. Uncertainties affecting our contrail cirrus estimates are, on the one hand, due to (A)
1705 uncertainties in the radiative response to the presence of contrail cirrus and, on the other hand, (B)
1706 uncertainties in the upper tropospheric water budget and the contrail cirrus scheme. In most cases, we can
1707 only infer very rough estimates for the uncertainties related to specific processes.

1708 (A) Uncertainties associated with the radiative response to contrail cirrus are:

1 July 2020 Revised

- 1709 A1. Uncertainty related to the model's radiative transfer scheme of approximately 35% (Myhre et al.,
1710 2009).
- 1711 A2. Uncertainty in the inhomogeneity of ice clouds within a grid box of a climate model (Carlin et al.,
1712 2002; Pomroy and Illingworth, 2000), the vertical cloud overlap, and the use of plane parallel geometry
1713 as compared to full 3D radiative transfer (Gounou and Hogan, 2007), which together amount to
1714 approximately 35%.
- 1715 A3. Uncertainty estimating radiative transfer in a global climate model in the presence of very small ice
1716 crystals within young contrails, which may amount to about 10% (Bock and Burkhardt, 2016). The
1717 uncertainty is dependent on the contrail cirrus ice water content.
- 1718 A4. Uncertainty due to the ice crystal habit is approximately 20% according to Markowicz and Witek
1719 (2011).
- 1720 A5. Uncertainty in the radiative transfer due to soot cores within the contrail cirrus ice crystals is
1721 thought to be large, as the change in the shortwave (SW) albedo is large (Liou et al., 2013). The soot
1722 impact on contrail cirrus RF has not yet been quantified.
- 1723 Overall, uncertainty in the radiative response to contrail cirrus (excluding A3) is estimated to be about
1724 55%, assuming independence of different uncertainties and excluding the impact of ice crystal soot cores.
1725 The uncertainty A3 is included in the uncertainty estimate under (B) because A3 and B2 are dependent
1726 uncertainties.
- 1727 (B) Uncertainty in contrail cirrus RF associated with the upper-tropospheric water budget and the contrail
1728 cirrus scheme are:
- 1729 B1. Uncertainty in contrail cirrus RF associated with the uncertainty in upper-tropospheric ice
1730 supersaturation. This results from a lack of knowledge in ambient conditions due to the low vertical
1731 resolution of satellite instruments (Lamquin et al., 2012) and to the ability of models to reproduce the
1732 observed statistics of ice supersaturation. This contributes about 20% to uncertainty.
- 1733 B2. There is uncertainty related to ice crystal number densities within young contrails. Ice nucleation
1734 within the plume can vary drastically depending on the water supersaturation reached within the plume
1735 and on the soot emissions (Kärcher et al., 2015; 2018). This dependency on the atmospheric state leads
1736 to a reduction in the number of nucleated ice crystals in particular in the tropics and at lower flight
1737 levels (Bier and Burkhardt, 2019) leading to a large uncertainty in the impact of tropical and subtropical
1738 air traffic. Depending on the atmospheric state and ice crystal numbers, a varying fraction of ice crystals
1739 can be lost in the contrail vortex phase (Unterstrasser, 2014). We assume an uncertainty in average
1740 contrail ice crystal numbers after the vortex phase of about 50% leading to an uncertainty in contrail
1741 cirrus RF of about 20%. This estimate of the sensitivity of contrail cirrus RF to ice crystal numbers in
1742 newly formed contrails is based on simulations with ECHAM5-CCMod (Burkhardt et al., 2018).
- 1743 B3. The uncertainty in the lifetime of contrail cirrus, affecting the day-/night-time contrail cover, has
1744 only a small impact on the estimated contrail cirrus RF (Chen and Gettelman, 2013; Newinger and
1745 Burkhardt, 2012). We estimate the associated uncertainty to be 5–10%.
- 1746 B4. From the sensitivity of the contrail cirrus RF to the temporal resolution in the air traffic dataset in
1747 ECHAM5 and CAM, we deduce an uncertainty of about 10%.
- 1748 B5. The estimate of the feedback of natural clouds, due to contrail cirrus changing the water and heat
1749 budget of the upper troposphere, is very uncertain and has not been properly quantified yet (Burkhardt
1750 and Kärcher, 2011; Schumann et al., 2015). We assume here the uncertainty related to this estimate to
1751 be only slightly smaller than the estimate itself, or about 15%.

1 July 2020 Revised

1752 B6. Uncertainty in the RF estimate of Chen and Gettelman (2013) to assumptions in the initial ice-
1753 crystal radii and contrail cross-sectional areas is about 33%.

1754 We assume independence of the uncertainties except for the dependence of A3 and B3 on the uncertainty
1755 in B2. The overall uncertainty due to the water budget and the contrail cirrus scheme (including
1756 uncertainty A3) is about 40% and more than 50% in the case of the Chen and Gettelman (2013). From the
1757 two different sources of uncertainty (list A, radiative, and list B, contrail cirrus properties, above) we
1758 calculate an overall contrail cirrus RF uncertainty of about 70%, assuming independence of the overall
1759 uncertainties described in A and B.

1760 Note that we do not attempt to infer an estimate for the uncertainty of the factor ERF/RF. When
1761 calculating the contrail cirrus ERF, the error range given refers to the error range of contrail cirrus RF and
1762 not ERF.

1763 F. Emission metrics calculations

1764 We calculate the AGWP and AGTP, and corresponding GWPs and GTPs, for aviation CO₂, NO_x (which
1765 encompasses the ERF of short-term O₃, CH₄, CH₄-induced O₃ and SWV), soot, SO₂, and contrail cirrus.
1766 The methodology and analytical expressions for the emissions metrics are described in detail in previous
1767 literature (e.g., Fuglestedt et al. 2010; Myhre et al. 2013). The impulse response function (IRF) that
1768 describes the atmospheric decay of CO₂ upon emission is taken from Joos et al. (2013). For the other
1769 species, the atmospheric decay is given by a constant e-folding time taken as the ‘perturbation lifetime’.
1770 The lifetimes used here are broadly consistent with Fuglestedt et al. (2010). The radiative efficiency (RE)
1771 for CO₂ is calculated using year 2018 background concentrations of 407 ppm (annual mean, from monthly
1772 mean observed concentrations from NOAA GMD -
1773 ftp://aftp.cmdl.noaa.gov/products/trends/co2/co2_mm_gl.txt). This yields a RE of $1.68 \times 10^{-15} \text{ W m}^{-2} \text{ kg}^{-1}$,
1774 4% lower than used in the IPCC Fifth Assessment report (AR5) (Myhre et al., 2013). The climate response
1775 IRF is taken from Boucher and Reddy (2008). The latter has an inherent equilibrium climate sensitivity
1776 (ECS) of $1.06\text{K (W m}^{-2}\text{)}^{-1}$, equivalent to a 3.9K equilibrium response to a doubling of CO₂.

1777 For the calculation of the average rate of CO₂-warming-equivalent emissions for aviation non-CO₂ forcings
1778 ($E_{\text{CO}_2\text{e}^*}$) under the GWP* metric in **Table 5**, we use the relationship between recent changes in effective
1779 RF and CO₂-equivalent emissions from Allen et al. (2018) (or Equation (1) with $\alpha = 0$),

$$1780 \quad E_{\text{CO}_2\text{e}^*} = [\Delta F / \Delta t] \times [H / \text{AGWP}_{\text{H}(\text{CO}_2)}] \quad (\text{F.1})$$

1781 where ΔF is the change in ERF over the recent period, Δt , and $\text{AGWP}_{\text{H}(\text{CO}_2)}$ is the absolute global warming
1782 potential of CO₂ at time horizon H. We use updated $\text{AGWP}_{\text{H}(\text{CO}_2)}$ values incorporating the updated
1783 radiative efficiency of CO₂ as described in the previous paragraph. Allen et al. (2018) used a backward-
1784 looking period of 20 years as Δt , whereas here we use a backward-looking 18-yr period as our time series
1785 of ERF components only extends back to 2000.

1786 G. List of Acronyms and abbreviations used in tables and figures of the Appendices

1787 ACARE—Advisory Council for Aeronautical Research in Europe
1788 ACCMIP—Atmospheric Chemistry and Climate Model Intercomparison Project
1789 AEDT—Aviation Environmental Design Tool
1790 AEM—Advanced Emission Model
1791 AERO2K—Global aircraft emissions data project for climate impacts evaluation
1792 AGAGE—Advanced Global Atmospheric Gases Experiment
1793 CAM—Community Atmosphere Model
1794 CCMoD—Contrail Cirrus Module
1795 CH₃CCl₃—Methyl chloroform
1796 COCIP—Contrail Cirrus Prediction Tool

1 July 2020 Revised

1797 CTM—Chemical Transport Model
1798 ECHAM—European Centre/Hamburg Model
1799 IPCC—Intergovernmental Panel on Climate Change
1800 MAGICC—Model for the Assessment of Greenhouse Gas Induced Climate Change
1801 MOZART—Model for OZone And Related chemical Tracers
1802 NOAA—National Oceanic and Atmospheric Administration
1803 QUANTIFY—Quantifying the Climate Impact of Global and European Transport System
1804 REACT4C—Reducing Emissions from Aviation by Changing Trajectories for the benefit of Climate
1805 RCP—Representative Concentration Pathway
1806 SRES—Special Report on Emission Scenarios
1807 TAR—Third Assessment Report
1808 TRADEOFF—Aircraft emissions: contribution of different climate components to changes in radiative
1809 forcing—tradeoff to reduce atmospheric impact
1810 TROPOS—2D global TROPOSpheric model
1811 WDCGG—World Data Centre for Greenhouse Gases

1 July 2020 Revised

1812 **Table D.1.** The CH₄ RFs derived for all the aircraft emission
 1813 inventories that are present in the model ensemble.^a

Inventories	CH ₄ RF, mW m ⁻²	
	Old	New
AEDT	-6.67	-8.22
AEM	-6.82	-8.41
AERO2K	-7.09	-8.74
REACT4C	-6.97	-8.59
QUANTIFY	-6.96	-8.58
TRADEOFF	-7.11	-8.76

1814 ^a Values are those represented in the model ensemble based on MOZART-3
 1815 CTM simulations (Old) and recalculated values using a revised simplified
 1816 expression for the CH₄ RF (New) as presented by Etmnan et al. (2016). The
 1817 NO_x emissions of each inventory are normalized so that all RFs are scaled to
 1818 the same global total emissions (0.71 Tg(N) yr⁻¹) as in the REACT4C model.

1819

1820 **Table D.2.** The best NO_x RFs per unit emission derived for datasets that include and exclude late 1990s
 1821 numbers and related estimates, see text for details.

Components	Value	Uncertainty*	Value	Uncertainty*
	(mW m ⁻² (Tg (N) yr ⁻¹) ⁻¹)			
	with IPCC (1999)		without IPCC (1999)	
Short-term O ₃	25.6	±7.3	25.1	±7.2
CH ₄	-13.8	±4.7	-13.4	±4.5
CH ₄ -induced O ₃	-6.9	±2.3	-6.7	±2.3
SWV	-2.1	±0.7	-2.0	±0.7
Net NO _x	3.9	±5.7	4.0	±5.8

1822 *Stated uncertainties are one standard deviation (68% confidence interval).

1823

1 July 2020 Revised

1824 **Table D.3.** Methane response in TROPOS and other studies

Variable	Year	2D CTM, TROPOS		Study	Literature		Variable estimate/change
		Transient	Steady-state ^a		Ref	Model/Years	
CH ₄ burden, Tg	2000	4770.8	4785.1	IPCC TAR	1998	4850 Tg	
				Voulgarakis et al 2013	ACCMIP	4750 ^d Tg	
				Dalsøren et al 2016	Oslo CTM3	4560 ^d Tg	
				Dalsøren et al 2016		+15 %	
				This study ^c	1970–2012	+13 %	
	2050	5051.6	5081.4	Voulgarakis et al 2013	ACCMIP	5000 ^d Tg	
			Voulgarakis et al 2013		+5.3 ^d %		
			This study ^c	2000–2050	+5.9 %		
CH ₄ abundance, ppb	2000	1784.2	1787.5	Observations	NOAA AGAGE WDCGG	1773 ppb 1774 ppb 1783 ppb	
	2050	1886.2	1897.6	Meinshausen et al 2011	MAGICC	1833 ppb	
CH ₄ lifetime (τ _{CH₄+OH}) ^b , yr	2000	10.6	10.5	Prather et al 2012	CH ₃ CCl ₃ -based	11.2 ± 1.3 yr	
				Voulgarakis et al 2013	ACCMIP	9.8 ± 1.6 yr	
				Holmes et al 2013	1980/85–2000/05	-2.2 ± 1.8 %	
				This study ^c		-2.06 %	
				Voulgarakis et al 2013	1980–2000	-4 %	
	This study ^c		-2 %				
2050	11.0	11.0	Voulgarakis et al 2013	2000–2050	+1.0 ^d %		
			This study ^c		+3.5 %		
aircraft CH ₄ lifetime (τ _{CH₄+OH}), yr	2000	-0.137	-0.145	Hoor et al 2009	AERO2K	-1.55 % Tg(N) ⁻¹	
				Myhre et al 2011	QUANTIFY	-1.46 % Tg(N) ⁻¹	
				Holmes et al 2011	Model ensemble	-1.77 % Tg(N) ⁻¹	
				Søvde et al 2014	REACT4C	-1.36 % Tg(N) ⁻¹	
				This study ^c	dE _{NO_x} =QUANTIFY	-1.48 % Tg(N) ⁻¹	
	2050	-0.293	-0.311	Hodnebrog et al 2011	SRES B1	-1.61 % Tg(N) ⁻¹	
					B1 ACARE	-1.48 % Tg(N) ⁻¹	
				Hodnebrog et al 2012	SRES A1B	-1.22 % Tg(N) ⁻¹	
				Khodayari et al 2014a	AEDT Scenario1	-1.88 % Tg(N) ⁻¹	
				This study ^c	AEDT Baseline RCP45	-1.59 % Tg(N) ⁻¹ -1.36 % Tg(N) ⁻¹	

1825

1826

1 July 2020 Revised

1827 **Table D.4.** Calculated CH₄ correction factors

Aviation emissions year	CH ₄ correction factors	
	This study	Grewe and Stenke (2008) methodology
2000	0.73	0.65
2005	0.75	0.73
2011	0.78	0.81
2018	0.79	0.86

1828

1829 **Table E.1.** Scaling of contrail cirrus RF and ERF results ^a

Model	Inventory	Representation of flight distance	RF (mW/m ²)	Scalings	Scaled RF (mW/m ²) ^b	Reference
ECHAM4-CCMod	AERO2K 2002	track	38	S ₁ , S ₂ , S ₄	70	Burkhardt and Kärcher (2011)
ECHAM5-CCMod	AEDT 2006	slant	56	S ₃ , S ₄	56	Bock and Burkhardt (2016)
COCIP	AEDT 2006	flight vectors	63	S ₄	72	Schumann et al. (2015)
CAM5	AEDT 2006	slant	13 [57] ^c	S ₃ , S ₄	57	Chen and Gettelman (2013)
Best estimate					66 ^d	

1830 ^a Adapted from Table 1 of Bock and Burkhardt (2016).1831 ^b RF that would be expected in 2006 when using slant distance from the AEDT inventory with hourly resolution.1832 ^c An updated simulation (see text) yielded 57 mW m⁻².1833 ^d The best estimate is of RFs, and excludes the Chen and Gettelman (2013) results since this is closer to an ERF
1834 (see main text).

1835

1836

1837

1 July 2020 Revised

1838 **Table F.1a.** Emission metrics and corresponding CO₂-equivalent emissions for the ERF components of
 1839 2018 aviation emissions and cloudiness using CO₂ IRF without C-cycle feedbacks from Gasser et al.
 1840 (2017), and climate IRF from Boucher and Reddy (2008).

1841 **Metrics**

ERF term	GWP ₂₀	GWP ₅₀	GWP ₁₀₀	GTP ₂₀	GTP ₅₀	GTP ₁₀₀
CO ₂	1	1	1	1	1	1
Contrail cirrus (Tg CO ₂ basis)	2.39	1.15	0.68	0.70	0.11	0.10
Contrail cirrus (km basis)	40	19	11	12	1.9	1.6
Net NO _x	637	216	122	-231	-75	14
Aerosol-radiation						
Soot emissions	4409	2125	1252	1295	210	177
SO ₂ emissions	-856	-412	-243	-251	-41	-34
Water vapor emissions	0.22	0.11	0.06	0.07	0.01	0.009

1842

1843 **Table F.1b.** Emission metrics and corresponding CO₂-equivalent emissions for the ERF components of
 1844 2018 aviation emissions and cloudiness using CO₂ IRF without C-cycle feedbacks, and climate IRF from
 1845 Gasser et al. (2017).

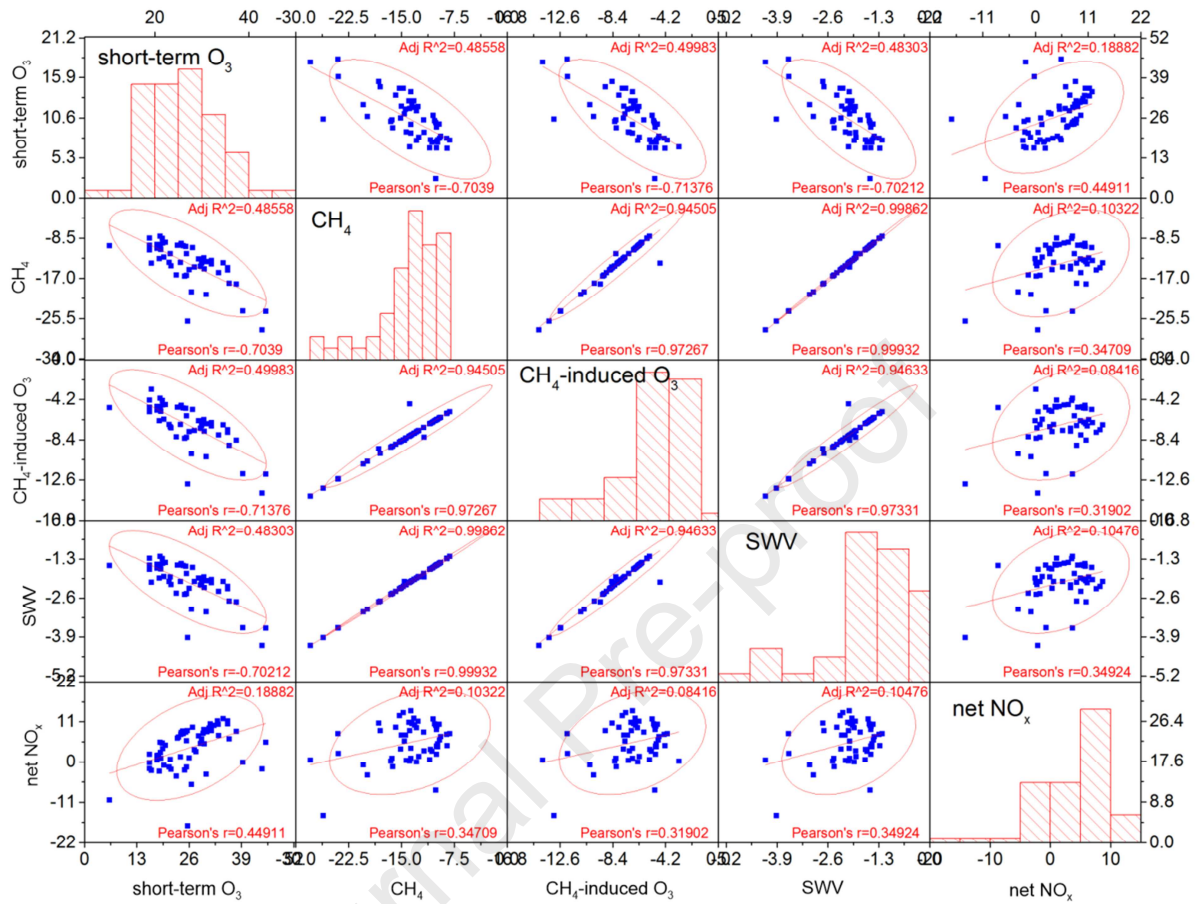
1846 **Metrics**

ERF term	GWP ₂₀	GWP ₅₀	GWP ₁₀₀	GTP ₂₀	GTP ₅₀	GTP ₁₀₀
CO ₂	1	1	1	1	1	1
Contrail cirrus (Tg CO ₂ basis)	2.39	1.15	0.68	0.3	0.19	0.15
Contrail cirrus (km basis)	40	19	11	4	3.3	2.6
Net NO _x	637	216	122	-420	-18	22
Aerosol-radiation						
Soot emissions	4409	2125	1252	466	360	284
SO ₂ emissions	-856	-412	-243	-90	-70	-55
Water vapor emissions	0.22	0.11	0.06	0.03	0.018	0.014

1847

1 July 2020 Revised

1848

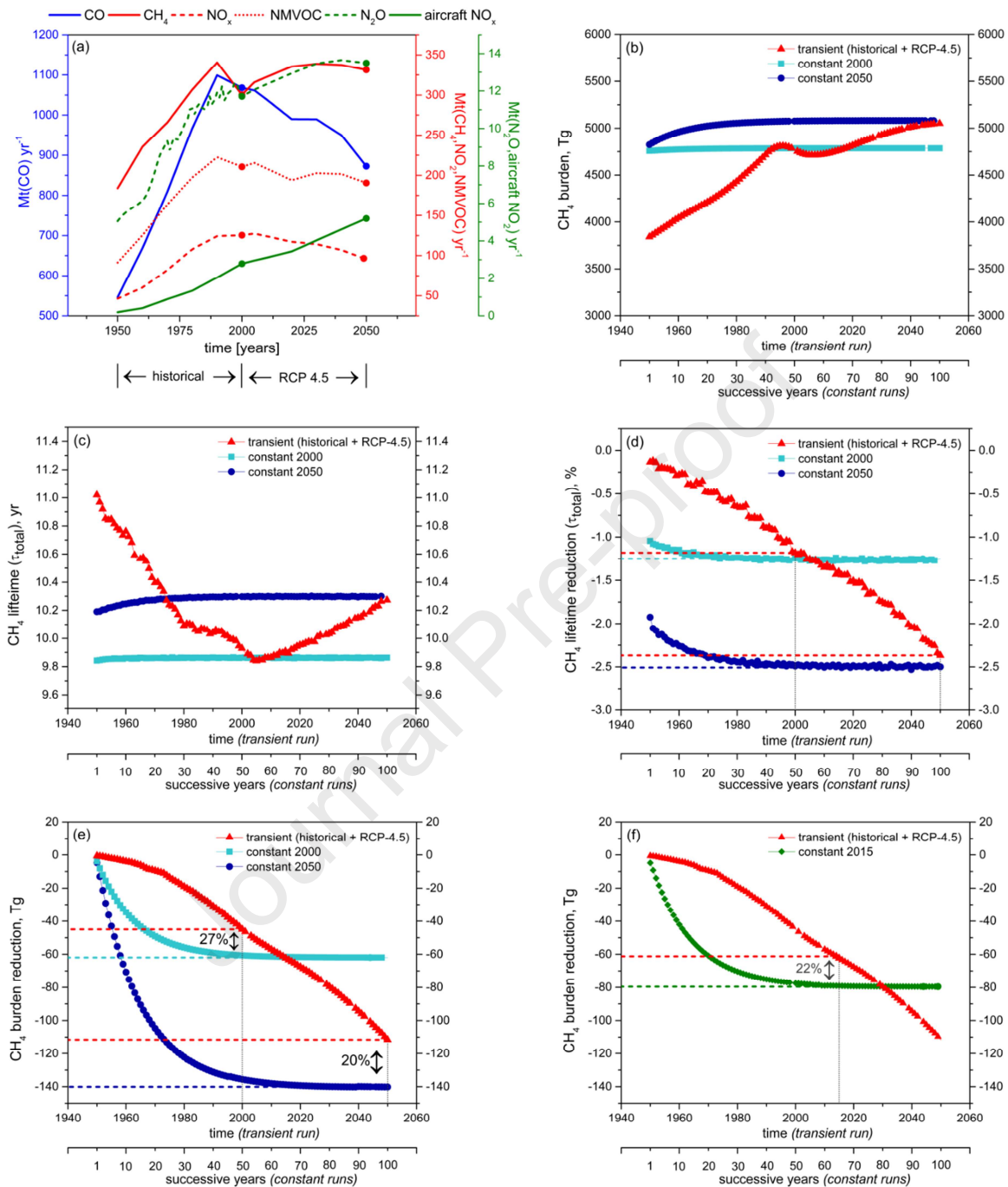


1849

1850 **Figure D.1.** Matrix of pair-wise scatter plots of RF values from NO_x terms: short-term O₃, CH₄, CH₄-
 1851 induced O₃, SWV and net NO_x (i.e., the sum of all 4 components), all represented as normalized RFs
 1852 (mW m⁻² (Tg(N)yr⁻¹)⁻¹) from the ensemble studies (see details in text). The red line is the linear fit, the
 1853 ellipse shows the 95% confidence level and histograms present frequencies.

1854

1 July 2020 Revised



1855

1856 **Figure D.2.** (a) Past and future anthropogenic emissions of CO, CH₄, NO_x, NMVOC, N₂O and aircraft
 1857 NO_x (IIASA RCP Database: <http://www.iiasa.ac.at/web-apps/tnt/RcpDb/>). Dots represent conditions for
 1858 'constant 2000' and 'constant 2050' simulations.

1859 (b) Evolution of the global CH₄ burden in TROPOS for transient aircraft NO_x emissions combining
 1860 historical emissions (1950–2000) and RCP-4.5 emissions (2000–2050); and constant emissions for the
 1861 years 2000 and 2050.

1 July 2020 Revised

1862 (c) Global CH₄ lifetime due to aircraft NO_x emissions in TROPOS for transient emissions combining
1863 historical emissions (1950–2000) and RCP-4.5 emissions (2000–2050); and constant emissions for the
1864 years 2000 and 2050.

1865 (d) Global CH₄ lifetime reduction due to aircraft NO_x emissions in TROPOS for transient emissions
1866 combining historical emissions (1950–2000) and RCP-4.5 emissions (2000–2050); and constant
1867 emissions for the years 2000 and 2050. The dashed lines represent 2000 and 2050 equilibrium values
1868 (light and dark blue) and 2000 and 2050 transient values (red).

1869 (e) Global CH₄ burden reduction due to aircraft NO_x emissions in TROPOS for transient emissions
1870 combining historical emissions (1950–2000) and RCP-4.5 emissions (2000–2050); and constant
1871 emissions for the years 2000 and 2050. The dashed lines represent 2000 and 2050 equilibrium values
1872 (light and dark blue) and 2000 and 2050 transient values (red).

1873 (f) Global CH₄ burden reduction due to aircraft NO_x emissions in TROPOS for transient emissions
1874 combining historical emissions (1950–2000) and RCP-4.5 emissions (2000–2050); and constant
1875 emissions for the year 2018. The dashed lines represent 2018 equilibrium (green) and transient values
1876 (red).

1877

Highlights

- Global aviation warms Earth's surface through both CO₂ and net non-CO₂ contributions.
- Global aviation contributes a few percent to anthropogenic radiative forcing.
- Non-CO₂ impacts comprise about 2/3 of the net radiative forcing.
- Comprehensive and quantitative calculations of aviation effects are presented.
- Data are made available to analyze past, present and future aviation climate forcing.

Journal Pre-proof

Declaration of competing interest

The authors* declare that they have no known competing financial interests or personal relationships that could have appeared to influence the work reported in this paper.

Authors* **D. S. Lee, D. W. Fahey, A. Skowron, M. R. Allen, U. Burkhardt, Q. Chen, S. J. Doherty, S. Freeman, P.M. Forster, J. Fuglestedt, A. Gettelman, R. R. De León, L. L. Lim, M. T. Lund, R. J. Millar, B. Owen, J. E. Penner, G. Pitari, M. J. Prather, R. Sausen, L. J. Wilcox**